DOCTORAL (PhD) DISSERTATION

University of Sopron

Roth Gyula Doctoral School of Forestry and Game Management

Geospatial Assessment of Vegetation Recovery, Climate Variability, and Ecosystem Services in Conflict-Displaced Landscapes

By:
Abdalrahman Ahmed Abdalrahman

Supervisors:
Dr. Kornel Czimber

Sopron
2026

Geospatial Assessment of Vegetation Recovery, Climate Variability, and Ecosystem Services in Conflict-Displaced Landscapes

Written by in order to obtain Doctoral (PhD) degree:

Abdalrahman Ahmed Abdalrahman

Prepared by the University of Sopron
ROTH GYULA DOCTORAL SCHOOL

Supervisor(s): Dr. Kornel Czimber

Acceptance recommended (yes / no)

____
(signature)

I propose to accept the dissertation as a reviewer (yes / no)

1st Reviewer (Dr _____________________) yes / no _______________ (signature)

2nd Reviewer (Dr _____________________) yes / no _______________ (signature)

(Opt. 3rd Reviewer (Dr _____________________) yes / no) _______________ (signature)

Result of the public dissertation defense: ____________%

Sopron, ____day ___________month ______ year

____
Chairman of the Public Defence Committee

Qualification of the doctoral (PhD) diploma _______________

____
Chairman of the UDHC

DECLARATION

I, the undersigned **Abdalrahman Ahmed Abdalrahman** by signing this declaration declare that my PhD thesis entitled **Geospatial Assessment of Vegetation Recovery, Climate Variability, and Ecosystem Services in Conflict-Displaced Landscapes** was my own work; during the dissertation I complied with the LXXVI and the rules of the doctoral dissertation prescribed by the Roth Gyula Doctoral School, especially regarding references and citations.[1]

Furthermore, I declare that during the preparation of the dissertation I did not mislead my supervisor(s) or the programme leader with regard to the independent research work.

By signing this declaration, I acknowledge that if it can be proved that the dissertation is not self-made or the author of a copyright infringement is related to the dissertation, the University of Sopron is entitled to refuse the acceptance of the dissertation.

I further declare that I am not in the process of obtaining a doctoral degree in the same discipline, that I am not in the process of having my doctoral degree revoked, and that I have not had a previously awarded doctoral degree revoked within 5 years.

Refusing to accept a dissertation does not affect any other (legal, civil law, misdemeanour law, criminal law) consequences of copyright infringement.

Sopron, 20....year…………………………….month……………. day

…………………………………..

PhD candidate

[1] **Act LXXVI of 1999** Article 34 (1) Anyone is entitled to quote details of the work, to the extent justified by the nature and purpose of the recipient work, by designating the source and the author specified therein.

Article 36 (1) Details of publicly lectures and other similar works, as well as political speeches, may be freely used for the purpose of information to the extent justified by the purpose. For such use, the source, along with the name of the author, shall be indicated, unless this is impossible.

Acknowledgements

First, I extend my deepest gratitude to Allah Almighty for granting me the strength, resilience, and clarity to undertake and complete this research project.

My sincere appreciation goes to my academic supervisor, Kornel Czimber, for his guidance, encouragement, and invaluable insights throughout this study. Your critical feedback has greatly enriched the quality of this work.

I am grateful to the faculty and staff at the University of Sopron, particularly the Institute of Geomatics and Civil Engineering, Faculty of Forestry, for their logistical and academic support during the various phases of this study.

Special thanks to PlanetScope, ESRI, GEE, QGIS, R-Programing, MODIS, FAO, and NASA, whose open-access datasets and repositories provided the foundational data used in this research.

To my friends and fellow PhD candidates, your intellectual companionship and motivation were vital sources of encouragement during difficult times.

Finally, my heartfelt thanks to my family for their unwavering support and prayers. I especially thank my wife Suaad, my son Mowafag, and my daughter Ola. You have been my greatest source of inspiration.

Contents

List of Figures

List of Tables

Abstract

The Darfur region of Sudan is one of the most ecologically and politically complex landscapes in sub-Saharan Africa, where environmental degradation, climate variability, and conflict-induced human displacement intersect. This study investigates the long-term spatiotemporal patterns of Land Use and Land Cover (LULC) change, vegetation dynamics, drought patterns, and the environmental impacts of Internally Displaced Persons (IDPs) in Darfur between 1981 and 2024, using predictive modeling extending to 2034. A multi-source remote sensing framework was employed, incorporating MODIS NDVI/EVI, Sentinel-2, and PlanetScope imagery, alongside climate data processed using the Standardized Precipitation Evapotranspiration Index (SPEI). Ecosystem Service Valuation (ESV) was conducted using benefit transfer methods to quantify changes in ecological functions.

The findings revealed a net increase in vegetation cover since 2010, particularly in Central and West Darfur, attributed to improved rainfall distribution, reforestation programs, land abandonment in conflict-affected zones, and community-driven agroforestry initiatives. Forest cover increased by more than 100% in some regions, while a notable reduction in bareland and non-vegetated zones reflected ongoing ecological recovery. The SPEI-based drought analysis identified a significant reduction in drought frequency and severity post-2000, especially in West Darfur (R^2 = 0.34), which is consistent with broader Sahelian climatic trends.

Projected LULC changes under a business-as-usual (BAU) scenario indicate the continued expansion of forest, grassland, and built-up areas, accompanied by a decrease in cropland. Patch-based landscape analysis showed an increase in the Largest Patch Index (LPI) and reduced patch density, implying improved landscape connectivity and a decline in ecological fragmentation.

The ESV analysis showed a modest increase in the total ecosystem service value from USD 1.23 billion in 2017 to USD 1.27 billion by 2034 primarily driven by gains in regulating and supporting services due to forest regeneration and vegetation densification. However, a decline in provisioning services from Cropland signals a potential threat to the local food security.

Overall, the results demonstrate that despite persistent conflict and socio-political instability, Darfur is experiencing pockets of environmental recovery, largely driven by climate improvements, adaptive land use, and community-based interventions. However, these positive trends remain vulnerable to renewed displacement, the unsustainable exploitation of natural resources, and governance breakdowns. This study underscores the urgent need for integrated land-use planning, climate-resilient restoration strategies, and conflict-sensitive environmental governance to achieve long-term sustainability in the Darfur and similar fragile ecosystems.

List of Acronyms and Abbreviations

ADF	Augmented Dickey-Fuller
AI	Artificial Intelligence
AIC	Akaike Information Criterion
ARIMA	Autoregressive Integrated Moving Average
BAU	Business As Usual
BFAST	Breaks For Additive Seasonal and Trend
BIC	Bayesian Information Criterion
CA	Cellular Automata
CHIRPS	Climate Hazards Group InfraRed Precipitation with Station
CNNs	Convolutional-Neural Network
DEM	Digital Elevation Model
ES	Ecosystem Services
ESRI	Environmental Systems Research Institute
ESV	Ecosystem Services Valuation
ESVD	Ecosystem Services Valuation Database
ETS	Exponential Smoothing
EVI	Enhanced Vegetation Index
FAO	Food and Agriculture Organization
FCC	Forest Cover Change
FNC	Forest National Corporation
GIS	Geographic Information System
GIS	Geographic Information Systems
HAC	Humanitarian Aid Commission
HECS	Human-Environment-Climate Security
IDP	Internally Displaced Persons
IPCC	Intergovernmental Panel on Climate Change
ITA	Innovative Trend Analysis
KNN	K-Nearest Neighbor
LCM	Land Change Modeler
LPG	liquefied petroleum gas
LPI	Largest Patch Index
MERRA-2	Modern-Era Retrospective analysis for Research and Applications, Version 2
ML	Machine Learning
MODIS	Moderate Resolution Imaging Spectroradiometer
NDBI	Normalized Difference Built-up Index
NDMI	Normalized Difference Moisture Index
NDVI	Normalized Difference Vegetation Index
OA	Overall Accuracy
PA	Producer's Accuracy
PD	Patch Density
PET	Potential Evapotranspiration
RCP	Representative Concentration Pathways

REDD+	Reducing Emissions from Deforestation and forest Degradation, Plus
RF	Random Forest
RS	Remote Sensing
RSF	Rapid Support Forces
SAF	Sudanese Armed Forces
SDGs	Sustainable Development Goals
SPEI	Standardized Precipitation Evapotranspiration Index
SPI	Standardized Precipitation Index
SSTs	Atlantic Sea Surface Temperatures
SSTs	Atlantic Sea Surface Temperatures
SVM	Support Vector Machine
UA	User's Accuracy
ULC	Land Use and Land Cover
UNEP	United Nations Environment Program
VC	Value Coefficients
ViTs	Vision Transformers

CHAPTER 1

INTRODUCTION

1.1 Background

1.1.1 Conflict Background

The Darfur region of western Sudan Figure 1, has been a focal point of conflict and humanitarian crises since the early 2000s. Driven primarily by ethnic tensions, political marginalization, and competition over scarce resources, the conflict has displaced millions and caused profound environmental degradation (N. Solomon et al., 2018). Often described as the "first genocide of the twenty-first century," the Darfur conflict since 2003 has led to mass displacement, with hundreds of thousands seeking refuge within Sudan and neighboring Chad (Behrends, 2024).

The roots of this violence are deeply embedded in socio-political dynamics, notably the deliberate targeting of essential resources, such as food and water, as tools of war and displacement (Hagan & Kaiser, 2011). Janjaweed militias, supported by elements of the Sudanese government, have been implicated in systematic attacks on civilian populations, contributing to the displacement of approximately 2.7 million individuals (Birech, 2009). The resulting sociopolitical instability has amplified vulnerabilities, leading to unsustainable resource management practices, as displaced communities increasingly depend on the overexploitation of local natural environments (Young & Ismail, 2019).

1.1.2 Impact on Internally Displaced Persons (IDPs)

IDPs in Darfur remain among the most vulnerable groups globally, facing acute protection gaps due to the absence of binding international legal frameworks (Islam, 2006). Unlike refugees, IDPs lack safeguards enshrined in international refugee law, leaving their welfare largely contingent on national capacity and political will.

Conflict-induced displacement has directly accelerated environmental degradation across Darfur. Extensive research has indicated that warfare-driven land cover changes contribute to increased desertification, deforestation, and soil erosion (Brendan, 2008). Violence frequently results in the destruction of agricultural fields and the decimation of livestock populations, undermining food security and altering local ecological equilibria (FAO, 2023). Remote sensing analyses have captured significant shifts in land use patterns, highlighting the conversion of former agricultural zones into barren or scrubland ecosystems (Kyrpychova et al., 2024).

As of 2024, Sudan is home to one of the world's largest IDP populations, exceeding 10.4 million people which is exacerbated by the resurgence of conflict and environmental stresses (ACAP, 2023; OCHA, 2024). The current displacement crisis, claiming more than 5,000 lives, has heightened anthropogenic pressure around IDP camps, with dense population concentrations accelerating vegetation loss and resource depletion (Hagenlocher et al., 2012). Persistent droughts, rainfall variability, and socioeconomic instability are critical global hotspots for land degradation and the environment (Akasha, 2013; Almulhim et al., 2024; Hardt & Brief, 2019; Younis et al., 2022).

Furthermore, the degradation of natural resources exacerbates competition among displaced and host communities, reinforcing cycles of violence and undermining efforts toward durable peace (OCHA, 2023; X. Xie et al., 2024). Thus, understanding the dynamic interplay between vegetation loss, climate variability, and conflict-induced displacement is essential for effective humanitarian and environmental interventions.

Despite international efforts, including the Juba Peace Agreement, durable peace remains elusive. The international community's response has been criticized as insufficient, with peacekeeping missions operating below authorized capacities and financial resources often falling short (Barltrop, 2010; Foerstel, 2010; Samah, 2022). Geopolitical considerations, including the strategic interests of international actors such as China, further complicate this situation (Foerstel, 2010).

1.1.3 Prospects for Peace and Reconciliation

Resolving Darfur conflict requires an integrated approach that balances justice, reconciliation, and sustainable development. Traditional conflict resolution mechanisms, that emphasize community-based dialogue and trust-building, have been proposed to facilitate the voluntary return or local integration of displaced people (Birech, 2009). However, persistent insecurity continues to impede these initiatives.

Recent escalations, notably the April 2023 conflict between the Sudanese Armed Forces (SAF) and Rapid Support Forces (RSF), have further displaced more than eight million individuals internally, alongside 3.9 million refugees seeking safety abroad (USCRI, 2025). This unprecedented displacement underscores the urgent need for durable solutions that incorporate the perspectives of the affected populations. Studies indicate that many IDPs express a preference for local resettlement over returning to their places of origin, reflecting the complex considerations of security, livelihoods, and social cohesion (Yagub, 2019). Therefore, a comprehensive peace framework must consider not only political settlements but also environmental recovery and livelihood restoration as foundational pillars for long-term stability.

1.1.4 Climate Change and Environmental Stressors

Climate change has emerged as a fundamental driver exacerbating existing vulnerabilities in conflict-affected regions. It has profound impacts on ecosystems, agriculture, water availability, and human health, particularly in developing countries that already have socio-economic and institutional weaknesses (Füssel, 2009; Kikstra et al., 2022; S. Solomon et al., 2007).

Africa, particularly the Sahel region, is on the frontline of climate change. Rising temperatures, declining precipitation, frequent droughts, and increasing desertification are projected to intensify, and the Intergovernmental Panel on Climate Change (IPCC) forecasts that temperature increases in the Sahel will exceed global averages (Osman et al., 2021; Yvonne et al., 2020).

Sudan's exposure to these climatic risks is compounded by endemic poverty, weak governance structures, limited adaptive capacities, and ongoing conflicts (Hamadalnel et al., 2022). These challenges significantly constrain the resilience of the local populations and ecosystems. Recent studies have demonstrated that strategic land management interventions and shifts in precipitation patterns can support vegetation regeneration and ecological restoration in degraded landscapes (Elhag & Walker, 2009; Nzabarinda et al., 2021). Therefore, understanding the interconnectedness between climate variability, land use changes, and ecological recovery is critical for designing integrated approaches for building resilience, sustainable development, and post-conflict reconstruction.

1.2 Problem Statement

Darfur faces the complex and interlinked challenges of environmental degradation, climate variability, and prolonged conflict. However, the environmental impacts of these drivers, particularly those linked to displacement, remain underexplored. There is a critical need for a holistic understanding of how human displacement, climatic stress, and land-use pressure shape vegetation dynamics and ecosystem services.

1.3 Research gab

While several studies have examined climate and land-use change in Sudan, few have integrated high resolution satellite data with drought indices, ecosystem service valuation, and IDP-related land pressure. There is a lack of predictive modeling that connects environmental degradation with socio-political displacement trends in semi-arid zones. This study addresses these gaps by applying remote sensing, statistical trend analysis, and ecosystem valuation to Darfur's evolving landscapes.

1.4 Research objectives

1. To quantify and analyze land use and land cover (LULC) changes in Darfur using multi-sensor remote sensing data.

2. To evaluate the spatial and temporal dynamics of vegetation cover using the NDVI/EVI time-series and their relationships with climate trends.

3. To assess the impact of IDPs on vegetation dynamics and land use transitions using spatial overlays.

4. To analyze drought patterns and their influence on vegetation and ecosystem resilience using Standardized Precipitation Evapotranspiration Index (SPEI-6 and SPEI-12) timescales.

5. To forecast future land cover changes under business-as-usual (BAU) scenarios using CA-Markov modeling.

6. Estimate ecosystem service values (ESVs) across different LULC classes and evaluate the impact of LULC changes on service provisioning.

1.5 Research question

1. What are the major land use and land cover changes that occurred in Darfur?

2. How have vegetation patterns evolved in response to climate variability and displacement-driven land pressures?

3. What is the spatial impact of IDP settlements on the surrounding vegetation and land use change?

4. How have drought patterns influenced environmental degradation and vegetation recovery in Darfur?

5. What are the projected LULC changes under BAU scenarios by 2034?

6. How have changes in LULC affected ESVs over time?

7. What sustainable strategies can enhance vegetation recovery and ecological resilience in Darfur?

CHAPTER 2

Literature Review

2.1 Chapter overview

Environmental degradation in conflict-prone regions such as the Sahel is a result of complex interactions between anthropogenic pressures, climate variability, displacement, and institutional fragility. Darfur represents a microcosm of these dynamics, where land use, vegetation health, and ecosystem functionality are continuously shaped by sociopolitical disruptions and ecological stressors. This chapter provides a comprehensive review of the relevant literature to contextualize the current research and underscore its contribution to academic and applied discourse.

Section 2.2: explores the nexus between conflict and environmental degradation by drawing on regional evidence from the Sahel and case-specific examples from Darfur. This highlights how recurrent violence, governance breakdowns, and militarized land access accelerate ecological decline, particularly in forested and pastoral zones.

Section 2.3: focuses on the role of IDPs in altering land use patterns. The literature demonstrates how displacement-driven resettlement increases pressure on natural resources, leading to deforestation, informal expansion of cultivation zones, and competition for ecosystem services in host areas.

In Section 2.4: attention is shifted to climate change and environmental recovery, particularly in post-conflict zones. While conflict exacerbates environmental stress, improved rainfall patterns and targeted interventions can foster natural regeneration, which is increasingly being documented across the Sahelian belt.

Section 2.5 and 2.6: delve into the use of remote sensing technologies in conflict-affected landscapes. These sections highlight the evolution of satellite-based tools for detecting land cover changes, vegetation trends, and drought episodes using indices, such as NDVI, EVI, and SPEI. The literature confirms that remote sensing provides a cost-effective, scalable, and non-intrusive means of environmental assessment in insecure areas.

Section 2.7: reviews the global evidence on Ecosystem Services (ES) and their relationship with LULC. Drawing from foundational and contemporary frameworks, this section evaluates how ESVs are quantified and how shifts in land cover influence provisioning, regulating, supporting, and cultural services.

Finally, Section 2.8: examines Forest Cover Change (FCC), deforestation trends, and modelling approaches used to project land transitions. This highlights the growing use of tools such as CA–Markov, Land Change Modeler (LCM), and machine learning-based classifiers in predicting forest loss and recovery, with a focus on semi-arid and politically fragile contexts.

Collectively, this literature review identifies the knowledge gaps that this study addresses particularly the limited integration of spatial modelling, remote sensing, ecosystem service valuation, and post-conflict recovery analysis in the context of Darfur. This chapter sets the stage for the methodological approach and analytical frameworks employed in subsequent sections of this dissertation.

2.2 Conflict and Environmental Degradation in the Sahel and Darfur

Environmental degradation has emerged as a critical contributor to conflict dynamics in the Sahel and Darfur regions, where ecological vulnerability and sociopolitical instability interact in complex ways. In Darfur, prolonged desertification, soil degradation, and diminishing water resources have been cited as structural stressors that exacerbate the competition between nomadic pastoralists and sedentary farmers (Benjaminsen, 2016; Khan, 2015; Sachs, 2007). The United Nations Environment Program (UNEP) has identified climate change and land degradation as significant, although not exclusive, drivers of the Darfur conflict (Sachs, 2007).

In the broader Sahel, climate variability intensifies the existing socio-ecological tensions. Rising temperatures, declining rainfall, and extreme weather events such as droughts and floods contribute to reduced agricultural yields, further straining already scarce resources (Mbaye, 2020; Sakr, 2023). These environmental stressors are compounded by weak governance, political marginalization, and social inequalities, creating a web of multidimensional conflict drivers (Macauley, 2016; Schwarz et al., 2022).

Darfur exemplifies a region in which an ecological crisis is deeply entangled with conflict history. Studies suggest that extreme poverty, population pressure, and declining access to water have amplified vulnerability and fueled violent disputes over land and grazing rights (Thornton et al., 2006). Similarly, in the Sahel, religious extremism, weak institutions, and ethnic fragmentation converge, with the environmental degradation of fuel-protracted violence (Olumba et al., 2022). The concept of "eco-violence" encapsulates these interlinkages, emphasizing that both social injustices and ecological stressors must be addressed in peacebuilding (Mbaye, 2020).

The environmental footprint of the displacement has also become increasingly visible. Remote sensing analyses in Darfur revealed significant land cover transformation, including deforestation and vegetative decline, in proximity to the IDPs settlements (Ahmed, Rotich, Kipkulei, et al., 2025). The ecological pressure resulting from concentrated human activities in fragile environments highlights the urgent need for integrated land management and conflict-sensitive environmental policy.

Therefore, comprehensive responses to conflict in the Sahel and Darfur must be aligned with climate adaptation, environmental rehabilitation, and political stability. Environmental programming must be mainstreamed into humanitarian and reconstruction agendas, and transboundary cooperation and adherence to international environmental norms are essential for sustainable peace (Jude, 2009; Macauley, 2016).

2.3 Internally Displaced Persons and Land Use Pressure

The environmental impacts of internal displacement are profound, particularly in fragile ecosystems. IDPs forced from their homes by violence yet remaining within national borders create localized but intense pressure on land use and resource systems (Bríd, 2022; Schimmel, 2022). As IDPs establish semi-permanent settlements, they often exploit the surrounding natural resources for shelter, fuel, and subsistence agriculture, triggering measurable land-cover transformations (Gorsevski et al., 2012; Rome, 2007)

In Darfur's Kas locality, Ahmed et al., (2024) reported a 35.33% decrease in vegetative cover over six years in areas surrounding IDP camps, driven by agricultural expansion and biomass extraction. Similar patterns have been documented in Sierra Leone, where post-conflict urban expansion by IDPs has led to significant deforestation and landscape fragmentation, particularly in the Western Area (Gbanie et al., 2018; Wadsworth & Lebbie, 2019). The reluctance of IDPs to return to rural areas has further intensified land demand on urban fringes, undermining forest conservation efforts and biodiversity.

In northeastern Nigeria, over two million displaced persons have exacerbated environmental degradation, with reported impacts including deforestation for firewood and conflicts over limited water sources (Kamta et al., 2020; Ogbue et al., 2024). In the Taraba and Borno States, these resource pressures have directly led to the deterioration of water quality and loss of vegetative cover (Ifeanyichukwu et al., 2022). (Kashim & Kashim, 2020) emphasized the urgent need for environmentally sensitive IDP policy frameworks that account for ecological sustainability and community resilience.

2.4 Climate Change and Environmental Recovery in Post-Conflict Zones

Climate change functions as both a risk multiplier and critical factor influencing post-conflict environmental trajectories. In vulnerable and recently stabilized regions, climatic disruptions can act as catalysts for renewed conflicts or impede the recovery of ecosystems and livelihoods (Abrahams, 2021; Peters, 2021). In Karamoja and, Uganda, erratic weather patterns and prolonged droughts have altered pastoral migration and land use, thereby reinforcing cycles of violence and vulnerability.

Environmental recovery is often underprioritized in post-conflict reconstructions. In Colombia, the return of displaced populations without coordinated land use planning has intensified deforestation and land tenure conflicts (Suarez et al., 2018). Somalia, also, demonstrates how climate-induced disasters undermine peacebuilding efforts and sustainable development, particularly SDG 13 (Dirie et al., 2024).

Governance and institutional capacity are pivotal. As Daoudy, (2021) illustrated in Sudan and Syria, the ecological impacts of climate change are often exacerbated by state neglect or mismanagement. The Human-Environment-Climate Security (HECS) framework posits that many conflict-related environmental crises stem more from poor governance than from direct climate phenomena (Corbera et al., 2019; Okpara et al., 2018).

Conversely, post-conflict transition offers opportunities for "green recovery." Ukraine's reconstruction has been framed as a vehicle for sustainable energy transition and ecological justice, a concept embedded in the emerging paradigm of post-growth peacebuilding (Kopytsia, 2024; Simangan, 2024). Such approaches are becoming increasingly critical for shaping climate-resilient futures in fragile regions.

2.5 Remote Sensing Applications in Conflict-Affected Regions

Remote sensing has become indispensable for analyzing conflict-affected environments, offering high-resolution, real-time data where traditional access is limited or unsafe (Karongo et al., 2024; Zwijnenburg & Ballinger, 2023). The utility of satellite imagery extends to conflict monitoring, damage assessment, vegetation tracking, and resource allocation for humanitarian responses (Avtar et al., 2021; Kaplan et al., 2022).

In Syria, satellite-derived data have enhanced early warning systems by identifying the spatial patterns of conflict escalation (Racek et al., 2024). In Ukraine, high-resolution imagery

revealed extensive destruction in Mariupol, enabling the quantification of urban damage and supporting international legal documentation efforts (Huang et al., 2023).
Vegetation indices such as NDVI have proven effective in monitoring ecological damage and recovery in conflict zones (Molikevych et al., 2023). Furthermore, remote sensing can detect unreported violence, for example, by analyzing fire anomalies to identify destroyed settlements (Naghizadeh, 2025).
Recent advances in Artificial Intelligence (AI) have expanded remote sensing capabilities. Deep learning models, such as Convolutional-Neural Network (CNNs) and Vision Transformers (ViTs), have significantly improved classification accuracy in post-conflict zones, particularly when combined with big data sources such as nighttime lights and open-source intelligence (Levin et al., 2018; Pushkarenko & Zaslavskyi, 2024).
Remote sensing platforms integrated into web mapping applications allow for hybrid analysis workflows and balance manual expertise with automated change detections. In Darfur, these approaches enhance the target detection accuracy and resource allocation for damage assessments (Knoth et al., 2018).

2.6 Importance of Remote Sensing for Drought Monitoring

Drought is one of the most destructive climate hazards in semi-arid and conflict-affected regions. Its insidious onset and widespread impact make early detection critical, especially in data-scarce environments where ground-based monitoring is compromised. Remote sensing provides spatially consistent near real-time coverage, making it an indispensable tool for drought assessment (Ejaz et al., 2023; Kocaaslan et al., 2021).
The SPEI has emerged as a preferred meteorological drought indicator owing to its incorporation of both precipitation and temperature-driven evapotranspiration (Vicente-Serrano, Beguería, et al., 2010). Unlike the Standardized Precipitation Index (SPI), which excludes temperature, the SPEI reflects the growing influence of warming on drought intensity (Ahmadalipour et al., 2017; Diffenbaugh et al., 2015). In regions such as Darfur, where temperature variability is significant, the SPEI outperforms the SPI in terms of drought detection accuracy (Gurrapu et al., 2014).
Recent research has leveraged Machine Learning (ML) to estimate or downscale SPEI using satellite derived vegetation, soil moisture, and land surface temperature (Fu et al., 2022; Xu et al., 2024). Random forests, ensemble models, and neural networks have demonstrated high correlations with ground-based indices, enabling field-scale drought monitoring, even in inaccessible areas.
In this study, we applied the Breaks For Additive Seasonal and Trend (BFAST) method to detect breakpoints and trends in vegetation and climate time series. Unlike other methods, BFAST integrates seasonal components, offering robust insights into the ecological responses to climate variability (He et al., 2021; Verbesselt et al., 2010).
The combined use of high-resolution remote sensing, drought indices, such as SPEI, and advanced time-series analytics presents a powerful framework for monitoring environmental resilience. In conflict-affected landscapes, such as Darfur, these tools are crucial for anticipating ecological tipping points and supporting adaptive land management.

2.7 Ecosystem Services and Land Use Change: A Review of Concepts and Global Evidence

ES are the direct and indirect contributions of ecosystems to human well-being and survival. They encompass essential ecological processes and products that sustain livelihoods, support economic development, and mediate the relationship between nature and society (Costanza et al., 1998; Fisher & Kerry Turner, 2008; Mengist et al., 2022). The Millennium Ecosystem Assessment (2005) provides a widely adopted framework that categorizes ES into four primary types: provisioning services (e.g., food, water, and timber), regulating services (e.g., climate regulation, and flood control), supporting services (e.g., soil formation, nutrient cycling), and cultural services (e.g., spiritual enrichment, recreation, and aesthetic experiences).

These ecosystem functions are interdependent, and the continued delivery of services is contingent on ecological integrity, which is influenced by both natural processes and anthropogenic pressures (Styers et al., 2010). Among the major anthropogenic drivers, changes in the LULC are particularly significant. LULC transitions alter landscape structure and ecosystem composition, thereby modifying ecosystem functions and, consequently, the quantity and quality of services provided (Kipkulei et al., 2025).

LULC changes serves as a critical proxy for assessing ecosystem service trends over time and space. These transformations driven by agriculture, urbanization, deforestation, or conservation can enhance or degrade ecosystem services depending on their scale and context. For instance, forest expansion typically increases regulation and support services, whereas cropland expansion may improve provisioning services at the expense of others (Costanza et al., 2014; de Groot et al., 2012; Kindu et al., 2013).

Researchers have developed ESV methods to assess these changes quantitatively. ESVs assign monetary or otherwise economic values to both the use and non-use benefits of ecosystems. These include market-based approaches (e.g., direct valuation of goods) and non-market techniques, such as contingent valuation, benefit transfer, and replacement cost methods (Brander et al., 2024; Costanza et al., 1997; Mengist et al., 2020).

Numerous global studies have applied ESV methods to assess the impacts of LULC changes on ecosystem services. In Africa, research in Ethiopia and Kenya (Arowolo et al., 2018; Gashaw et al., 2018) has demonstrated strong correlations between deforestation and ESV decline, while studies in Asia (Sharma et al., 2019; G. Xie et al., 2017; Yuan et al., 2019), Europe (Cabral et al., 2016; Quintas-Soriano et al., 2016), and South America (Mendoza-González et al., 2012; Zilio et al., 2022) have confirmed similar trends. In North America, works by (Lawler et al., 2014; Polasky et al., 2011), and (Kreuter et al., 2001) highlighted the trade-offs and synergies in ecosystem management, particularly within multifunctional landscapes.

The growing corpus of ESV research underscores its value in decision-making and planning, particularly in data-scarce regions where benefit transfer methods provide useful approximations for local valuation (Costanza et al., 2014). However, scholars emphasize the need for localized valuation studies to enhance accuracy and account for biophysical and socio-cultural variability (Mengist et al., 2022; Wang et al., 2022)

The literature demonstrates that ecosystem service valuation is not only critical for understanding environmental change but also indispensable for guiding sustainable land management, particularly in ecologically sensitive and conflict-affected regions such as Darfur.

2.8 Forest Cover Change (FCC), Deforestation Dynamics, and Modelling Approaches

Deforestation, forest degradation, and forest fragmentation are critical global challenges that directly undermine biodiversity, carbon sequestration, and ESV. Understanding the drivers, extent, and patterns of FCC is vital for designing evidence-based forest conservation and restoration strategies, especially for ecologically vulnerable and politically fragile landscapes (Agariga et al., 2021; Reddy et al., 2013). Historical and temporal analyses of forest structure and extent provide a foundation for forecasting future FCC trajectories and informing sustainable forest management policies (Karahalil et al., 2009).

Modern forest monitoring has benefited significantly from the integration of Remote Sensing (RS), Geographic Information Systems (GIS), and LULC change modeling. These technologies enable cost-effective, repeatable, and scalable analyses of forest dynamics at both the macro and micro scales. Among the most widely used simulation and prediction tools are CA models, which simulate spatially explicit land dynamics based on neighborhood effects (Kamusoko et al., 2013), Markov Chain Analysis, which models the probability of LULC transitions over time (Kumar et al., 2014), and CA–Markov models, which integrate spatial and temporal dynamics and are particularly powerful in projecting future forest scenarios (Mengist et al., 2021; Mwabumba et al., 2022; Tadese et al., 2021; Yue et al., 2024), LCM, which is popular for its intuitive interface and suitability for biodiversity-related landscape studies (Armenteras et al., 2019; Munsi et al., 2012), STCHOICE and GEOMOD, which allow for simulation under various land-use decision-making scenarios (Giriraj et al., 2008; Reddy et al., 2017; Sakieh & Salmanmahiny, 2016). These tools have proven invaluable in identifying deforestation hotspots, transition zones, and future risk areas, particularly when combined with socio-environmental datasets. They enhance decision-making for conservation planning, reforestation, and Reducing Emissions from Deforestation and forest Degradation, plus (REDD+) implementation, providing timely and spatially explicit information that traditional field surveys alone cannot deliver (Abad-Segura et al., 2020; Dewan et al., 2012)

The urgency of such modeling efforts is underscored by alarming trends in land-use conversion. According to the (MacDicken, 2015), forests continue to be cleared at accelerating rates to meet the demands of agriculture, urban expansion, and energy, driven primarily by population growth and food security imperatives. A multi-decadal satellite-based land cover study across seven East African countries Tanzania, Ethiopia, Kenya, Uganda, Zambia, Malawi, and Rwanda revealed a loss of over 189,400 km² of naturally vegetated areas, including forests, grasslands, and wetlands between 1985 and 2015 (Bullock et al., 2021). Such trends pose profound threats to ecological resilience, hydrological cycles, and regional climate systems.

In summary, the convergence of RS-GIS tools and advanced modeling techniques offers indispensable capabilities for monitoring, forecasting, and managing forest cover dynamics. In contexts such as Darfur, where conflict and displacement intersect with environmental change, these tools are particularly crucial for designing adaptive and sustainable land-use interventions.

CHPTER 3

Methodology

3.1 Introduction

This chapter presents the comprehensive methodological framework employed to assess vegetation recovery, land degradation, and climate ecosystem interactions in the conflict-affected Darfur region. The study integrates multi-source RS, climatic datasets, spatial simulation models, and ESV to evaluate environmental transformations between 1981 and 2024, with predictive modelling extending to 2034.

The methodological framework includes data acquisition, preprocessing, classification, accuracy assessment, vegetation and drought analysis, CA-Markov modelling, and ecosystem service valuation. To improve clarity, this chapter is structured into concise subsections focusing on satellite data, climatic inputs, platforms, modelling methods, and validation techniques.

3.2 Study Area and Sampling Site

3.2.1 The Darfur Region

The Darfur region, situated in western Sudan (latitude 9°00′-18°56′ N, longitude 23°54′-27°02′ E), spans approximately 531,304 km^2 and shares international borders with Chad, Libya, South Sudan, and the Central African Republic (Vehnämäki, 2006). It comprises five federal states: North, South, Central, East, and West Darfur (Nweke, 2021). Ecologically, the region transitions from hyper-arid desert zones in the north to savanna woodlands in the south, reflecting steep gradients in rainfall and vegetation cover.

Darfur's climatic regime is characterized by high spatial and temporal variability, with a short rainy season from June to September. The annual precipitation ranges from less than 100 mm in the northern desert to more than 600 mm in the southern savannahs (Eltahir et al., 2023). Dry season temperatures often exceed 40°C, compounding water stress and evapotranspiration. The Jebel Marra massif, rising to 3,000 meters above sea level, plays a critical role in shaping microclimates, supporting montane forests and localized biodiversity hotspots (Ahmed et al., 2020; Hegazy et al., 2018).

Socio-ecologically, Darfur is one of the most fragile regions in the Sahel, grappling with prolonged conflict, land degradation, displacement, and climate-induced vulnerability (Attaalmannan, 2019). Rain-fed agriculture, transhumant pastoralism, and dependence on forest-based resources dominate rural livelihoods, making the region highly sensitive to both anthropogenic pressure and environmental fluctuations (Elamin, 2018).

3.2.2 Case Study Zones

To balance macro- and micro-scale analyses, five nested sampling areas were selected across Darfur based on ecological gradients, population pressure, and data availability. These include zones with high IDP concentrations, diverse land use dynamics, and contrasting vegetation-climate interactions. The selection of five focal sites was strategic, capturing ecological heterogeneity and socio-political contrasts across Darfur.

1. Kas Locality (South Darfur)

The Kas lies between 12°23′-12°36′ N and 24°9′-24°26′ E, with an area of ~1,007 km² and an elevation of approximately 400 m asl. The area is characterized by an annual rainfall of ~519 mm and a mean temperature of 26°C. The locality hosts over 365,000 people, including 76,843 IDPs. The vegetation is dominated by Acacia woodland and is vital for fuelwood, grazing, and non-timber forest products (HAC, 2017). This is the site for high-resolution Sentinel-2A-based LULC studies.

2. El-Salam IDP Camp

Located between 11°53′-12°0′ N, and 24°51′-25°4′ E, El-Salam Camp spans ~24,437 ha. Established in 2004, it has grown into a large semi-urban enclave for displaced populations that engage in smallholder agriculture (Salih et al., 2017a). The LULC mosaic includes bareland, Wadi sand, cultivated fields, and vegetated patches, examined using PlanetScope data for vegetation-climate interaction studies.

3. West Darfur

West Darfur (12°0′-15°0′ N, 23°0′-24°0′ E) covers ~22,798 km². The state experiences 200–700 mm of rainfall annually and daily temperatures between 25°C and 32°C, with ecosystems ranging from semi-arid woodlands to savannahs (Darfur, 2024). Due to recurrent violence, the region hosts numerous IDP camps and is the focus of climate-vegetation interaction research using MODIS NDVI time-series and SPEI-based drought indicators.

4. Central Darfur

Central Darfur (11°0′-13°0′ N, and 23°0′-25°0′ E) covers ~3,715,324.45 ha. The state experiences 700-800 mm of rainfall annually and daily temperatures between 25°C and 30°C.

5. Entire Darfur Region

Used for macro scale MODIS-EVI trend (2000-2023). This large-scale analysis facilitated climate-vegetation coupling studies, detection of drought impacts, and identification of regreening hotspots across the region.

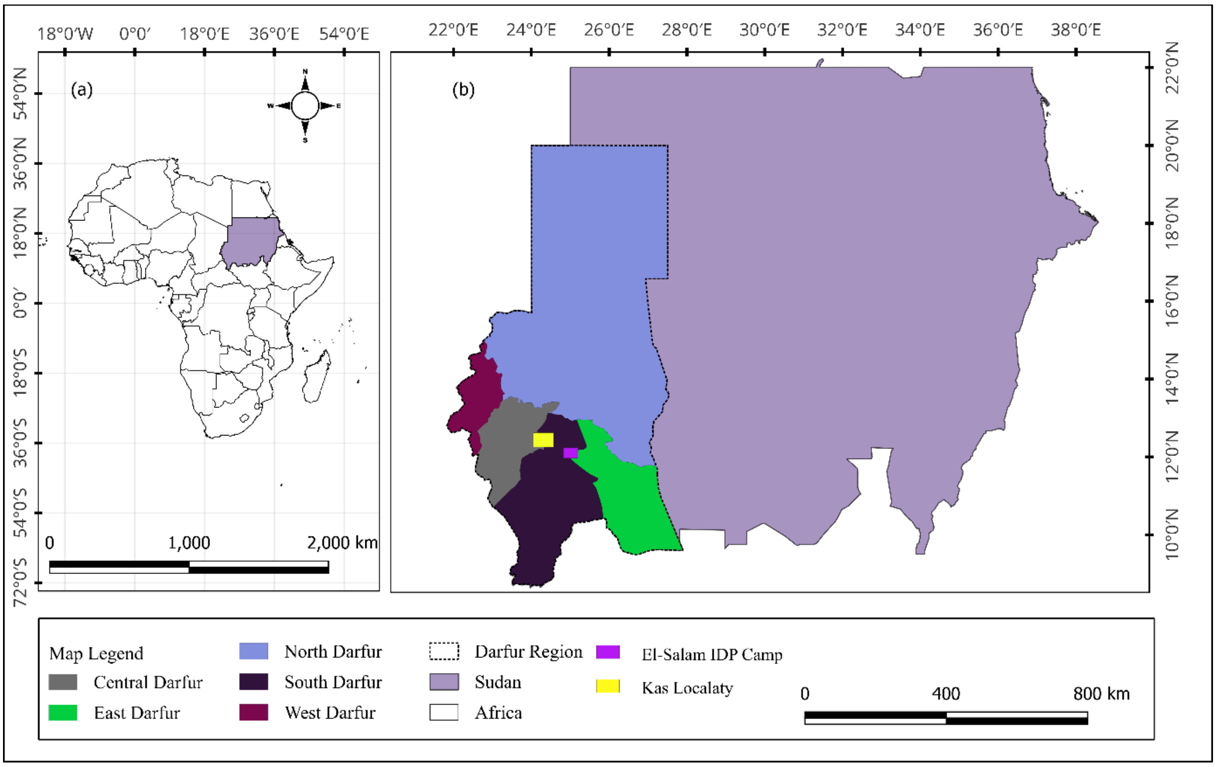

Figure 1. Study Area Map (a) depict Sudan location within Africa, and (b) depict Darfur location within Sudan.

3.3 Workflow Visualizations

To enhance workflow transparency and provide a comprehensive overview of the methodological sequence, the following figures illustrate the integrated process: Figure 2 Generalized Workflow Diagram of the entire research process illustrates the alignment between the research objectives and corresponding data sources, analytical tools, and methodological approaches. This highlights the integration of high-resolution satellite imagery, climate datasets, forecasting models, and GIS-based simulations to comprehensively analyze vegetation dynamics and land-use change in conflict-displaced communities in Darfur. Figure 3 illustrates the data processing pipeline for the NASA POWER (Macpherson et al., 2021; Stackhouse et al., 2023) and station-based weather datasets, detailing extraction, and correlation stages. Figure 4 highlights the conceptual framework showing the theoretical linkage between conflict, land degradation, vegetation recovery, and ecosystem services, thus guiding the analytical architecture of the study. These visual representations serve as both instructional tools and validation checkpoints to support transparency and scalability for future research.

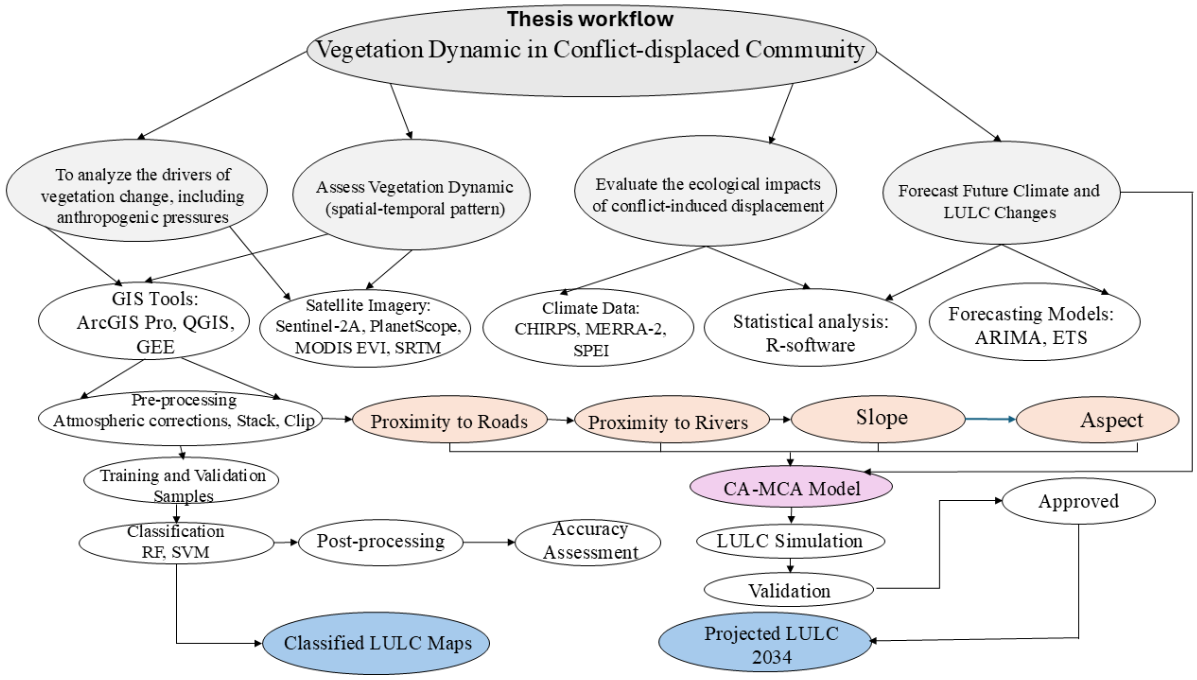

Figure 2. Methodology Framework.

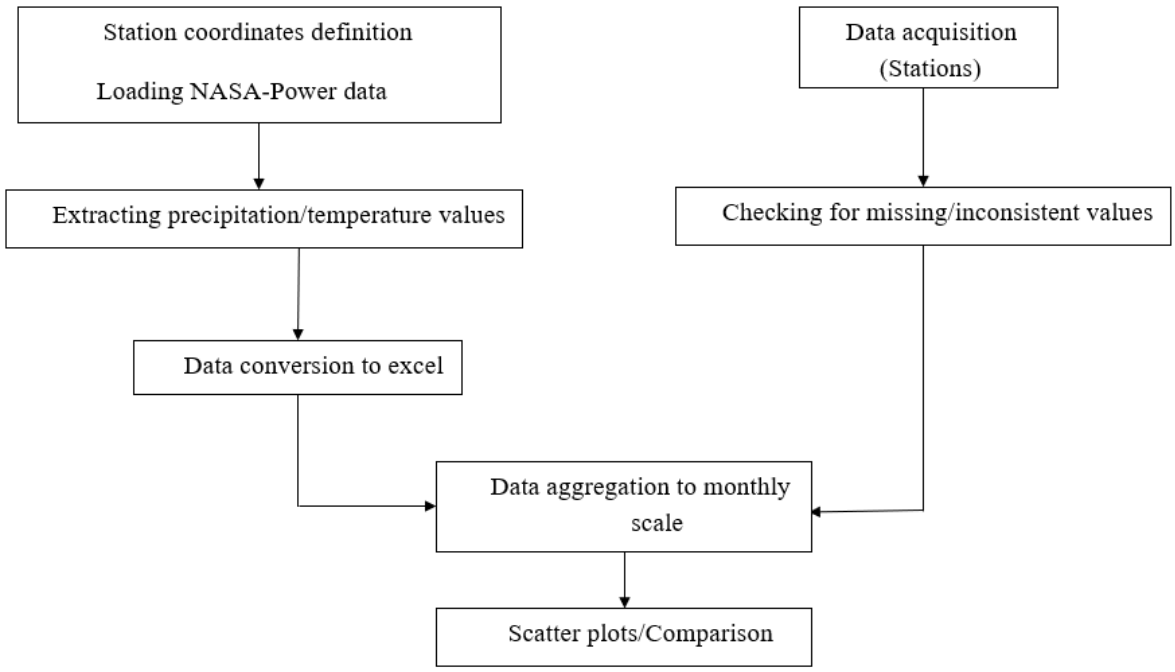

Figure 3. Processing workflow for NASA POWER data and Station data.

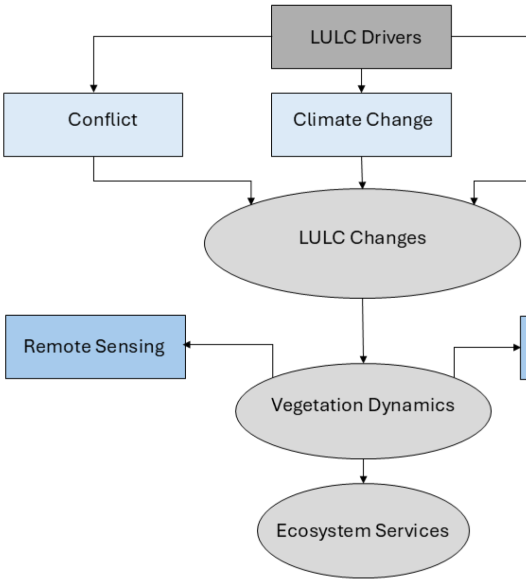

Figure 4. Conceptual model shows the interlink between conflict, climate, LULC, and ecosystem services.

3.4 Satellite Imagery and Land Cover Data

The study utilized multi-resolution satellite data tailored to different spatial and temporal scales of analysis. Selection criteria included spatial resolution, revisit frequency, spectral coverage, data continuity, and suitability for detecting environmental change in semi-arid regions. Sentinel-2A/B and PlanetScope data supported localized studies in IDP-affected zones, while MODIS provided long-term regional monitoring. All datasets underwent rigorous pre-processing to ensure spatial, temporal, and thematic consistency across the scales (Table 1).

3.4.1 Rationale for Sentinel-2A/B Use

Both Sentinel-2A and 2B were employed post-2017 to enhance temporal density and reduce cloud interference. Earlier data (pre-2016) were excluded due to limited availability and inconsistent quality. The sensors' 10 m resolution and 13-band spectral range offer optimal detail for vegetation and land-use mapping in fragmented landscapes.

3.4.2 Value of Sentinel-2 vs. ESRI Land Cover

While the ESRI Land Cover dataset offers globally standardized, deep-learning derived maps with consistent annual coverage at 10 m resolution, Sentinel-2 imagery provides superior thematic precision, flexibility in training data selection, and the capacity for localized validation. This distinction is critical for analyzing micro-scale, human-influenced landscapes such as Kas Locality and El-Salam Camp, where environmental dynamics are strongly shaped by the IDP settlements, smallholder cultivation, and recurrent degradation regeneration cycles. The decision to employ different methodological approaches across study zones was therefore guided by both scientific rationale and data-context considerations.

In highly dynamic areas (Kas, El-Salam), custom classification of Sentinel-2 and PlanetScope imagery using RF and SVM algorithms allowed for precise detection of fine-scale transitions and short-term vegetation fluctuations that global products often overlook.

In contrast, for broader and less temporally volatile regions such as Central Darfur, ESRI Land Cover maps were used. Their standardized, AI-based annual classification ensures temporal consistency, minimizes user bias, and supports CA-Markov land-use simulations and long-term regional trend analysis.

This complementary use of both datasets thus balances spatial detail and temporal continuity, enabling a comprehensive, multi-scale understanding of land-system transformations in Darfur.

Table 1. Summary of Datasets and Sources Used in the Study

Dataset / Variable	Source / Provider	Spatial Resolution	Temporal Resolution / Frequency	Coverage Period	Primary Application
MODIS NDVI/EVI	NASA LPDAAC (MOD13Q1, MYD13Q1)	250 m	16-day composite	2000-2023	Long-term vegetation trend and drought–vegetation correlation
Sentinel-2A/B MSI	ESA Copernicus Open Access Hub	10 m	5-day revisit	2017-2024	High-resolution LULC mapping, vegetation classification
PlanetScope	Planet Labs, Inc.	3 m	Daily	2017-2023	Fine-scale land use dynamics, IDP settlement analysis
ESRI Land Cover (Sentinel-based)	Esri, Microsoft & Impact Observatory	10 m	Annual	2017-2024	Regional-scale LULC classification, model validation
CHIRPS Precipitation	Climate Hazards Group (UCSB)	0.05° (~5 km)	Monthly	1981-2024	Rainfall analysis, SPEI computation
MERRA-2 Temperature / PET	NASA GMAO	0.5° × 0.625°	Monthly	1981-2024	Temperature trends, evapotranspiration, drought analysis
SPEI Drought Index	Computed from CHIRPS & MERRA-2	Derived	6- & 12-month scale	1981-2024	Drought pattern detection
FAO–UNESCO Digital Soil Map	FAO & UNESCO	1 km	Static	Global coverage	Soil classification and vegetation productivity assessment
NASA POWER Data	NASA POWER Project	0.5° × 0.5°	Monthly	1981-2024	Validation of climate variables, PET computation
Google Earth Pro Imagery	Google LLC	<1 m (variable)	Periodic	2016-2024	Visual validation and training sample extraction
Topographic Data (SRTM DEM)	NASA JPL	30 m	Static	2000	Slope, elevation, and aspect derivation for CA-Markov model

3.5 Data Preprocessing

Comprehensive data preprocessing was conducted to ensure comparability, spatial consistency, and analytical integrity of all satellite and climatic datasets used in this study. The workflow involved atmospheric correction, geometric alignment, cloud masking, spectral normalization, and resampling. All datasets were harmonized to a 10-meter spatial resolution and reprojected to the WGS 84 / UTM Zone 35N coordinate system to facilitate integrated spatial analysis.

3.5.1 Satellite Data Processing

3.5.1.1 Sentinel-2A/B MSI

Level-2A (Drusch et al., 2012) surface reflectance products were used, as they are preprocessed through Sen2Cor atmospheric correction algorithms. Cloud masking was applied using both the QA60 band and the Scene Classification Layer (SCL), effectively filtering clouds, cirrus, and shadow pixels (<5% cloud threshold per image). Vegetation indices (NDVI and EVI) were computed using reflectance values in the red (B4) and near-infrared (B8) bands. A median composite was generated for each study year to minimize the impact of residual atmospheric noise and data gaps.

Sentinel 2A data were used to analyze LULC changes in the Kas locality in South Darfur. A supervised classification was conducted using RF, SVM, and KNN algorithms using the Dzetsaka Plugin in QGIS 3.34.3 (integrated with Scikit-learn 1.0.1). Model parameters include Ntree = 100, Mtry = √n_features, and Training/Validation Split = 50:50 to avoid over training the data.

3.5.1.2 PlanetScope

PlanetScope imagery (Acharki, 2022; Pham-Duc et al., 2024) was atmospherically corrected to surface reflectance using vendor-provided coefficients. Cloud and haze were masked using the scene classification layer, and the data were spectrally normalized to Sentinel-2 band equivalents to maintain cross-sensor consistency. These datasets were primarily used for fine-scale LULC mapping in IDP-influenced zones such as El-Salam Camp.

3.5.1.3 MODIS NDVI/EVI

MODIS (Didan et al., 2015) vegetation indices (MOD13Q1) were accessed and processed via Google Earth Engine (GEE). Atmospheric corrections were applied, and the time series were smoothed using the Savitzky-Golay filter (Deng et al., 2013) to reduce noise while preserving temporal vegetation dynamics. Monthly and annual composites were derived to facilitate long-term trend and correlation analyses.

3.5.1.4 ESRI Land Cover

The ESRI (Venter et al., 2022) Sentinel-based global land cover dataset (2017-2024) was imported directly into ArcGIS Pro 3.2 (Karra et al., 2021). Classes were reclassified into six standardized categories Forest, Grassland, Cropland, Built-up, Bareland, and Water (Table 2) to ensure comparability across all data sources. This standardization supported regional

LULC change detection and validation of Sentinel-2 classifications. The ESRI Land Cover dataset was used to analyze the annual LULC transitions for Central Darfur.

Using a global ground truth dataset with a minimum mapping unit of 250 m^2, (Venter et al., 2022) found that the Esri Land Cover product achieved the highest overall accuracy (75%) when compared to Dynamic World (72%) and WorldCover (65%). Among all global land cover classes, water bodies were mapped with the highest accuracy (92%), followed by built-up areas (83%), tree cover (81%), and cropland (78%) particularly in biomes characterized by temperate and boreal forests. Independent validation by Karra et al. (2021) and the Impact Observatory reported mean global accuracies between 86-89%, while Africa-specific validations indicated accuracy ranging from 84-87% across major land cover types, including cropland, forest, grassland, and bareland.

These results collectively demonstrate that the Esri Land Cover dataset offers a high degree of spatial and thematic reliability, particularly in semi-arid and data-scarce regions such as Darfur. The consistent annual coverage, fine spatial resolution (10 m), and machine learning based classification makes it a robust tool for regional monitoring. Its integration into this study was therefore strategically justified to enhance temporal continuity, minimize processing demands, and improve the accuracy and consistency of LULC change detection for Central Darfur, especially in areas influenced by conflict, displacement, and environmental recovery dynamics.

Table 2. LULC Classification Scheme

Class Name	**Description**
Forest	Natural or semi-natural vegetation >10% tree cover
Grassland	Non-woody vegetation (shrubs, grasses) with sparse tree cover
Crops	Cultivated annual and perennial agricultural lands
Bare ground	Areas with no vegetation, including rocky surfaces and exposed soil
Built Areas	Settlements, roads, urban features, and IDP camp infrastructure
Water	Rivers, lakes, ponds, and seasonal Wadis

3.5.2 Climate Data Preprocessing

3.5.2.1 CHIRPS Precipitation

Daily rainfall data from CHIRPS were aggregated to monthly totals using R and Google Earth Engine. Temporal smoothing was applied, and seasonal and decadal means were extracted to assess rainfall variability. These data served as input for drought (SPEI) and rainfall–vegetation correlation analyses.

3.5.2.2 MERRA-2 Temperature and PET

MERRA-2 datasets (Bingkun et al., 2020; Qiao et al., 2023) were processed for both near-surface air temperature and potential evapotranspiration (PET). PET was calculated using the Thornthwaite method, which considers mean temperature and daylight duration. Outputs were aggregated to monthly averages, aligning temporally with the CHIRPS rainfall series.

3.5.2.3 SPEI Drought Index

The SPEI was computed using the R-SPEI package for both 6-month (SPEI-6) and 12-month (SPEI-12) time scales. SPEI-6 represents short-term agricultural drought conditions, while SPEI-12 captures long-term hydrological drought. SPEI was selected as the primary index because of its ability to incorporate both precipitation and Potential Evapotranspiration (PET), making it more sensitive to climate change than precipitation-only indices such as SPI.

Advantages of SPEI: Integrates both moisture input (rainfall) and atmospheric demand PET, captures short, medium, and long-term droughts (1-24 months), and is well-suited for semi-arid and arid environments (Vicente-Serrano, S. M., et al., 2010). The following widely accepted thresholds (Cai et al., 2024) were applied (Table 3).

Table 3. SPEI Classification Thresholds

SPEI Value	Drought Severity
> 2.0	Extremely wet
1.0 to 1.99	Moderately to very wet
-0.99 to 0.99	Near normal
-1.0 to -1.49	Moderate drought
-1.5 to -1.99	Severe drought
< -2.0	Extreme drought

3.5.3 Data Validation and Harmonization

Validation against in-situ meteorological stations produced correlation coefficients of r = 0.53 for rainfall (CHIRPS vs. observed) and r = 0.47 for temperature (MERRA-2 vs. observed). These values are consistent with validation studies by Dinku et al. (2018) and Zambrano-Bigiarini et al. (2017), confirming the suitability of CHIRPS and MERRA-2 datasets for climate assessment in data-scarce, conflict-affected regions.

All datasets were finally mosaicked, spatially aligned, and temporally synchronized for use in subsequent analyses including LULC classification, vegetation trend detection, CA-Markov simulations, and ecosystem service valuation. The standardized preprocessing workflow ensured high data fidelity, temporal coherence, and analytical comparability across multiple satellite platforms.

3.5.4 Modelling Platforms and Analytical Tools

GEE for time-series vegetation and drought analysis. ArcGIS Pro 3.4 for visualization and zonal statistics. QGIS 3.34.3 for spatial analysis, classification, and metric computation. R (v4.3) and Python (Scikit-learn 1.0.1) for time series analysis BFAST, drought index calculation SPEI, and trend modeling. MOLUSCE Plugin (QGIS) for CA-Markov land-use simulation.

3.5.5 Accuracy Assessment

An accuracy assessment performed to determine the performance of the RF, SVM, and KNN classifiers in characterizing the LULC classification. In this study we applied various accuracy metrics, including the User Accuracy (UA), Producer Accuracy (PA), Kappa coefficient (K) and Overall Accuracy (OA). Over 200 validation points were randomly distributed across the different LULC classes using stratified random sampling methods.

3.5.5.1 User accuracy

The UA determines the proportion of corrected classified pixels in each LULC category to the total number of reference pixels in that category (row). To calculate the UA for a specific class, the number of correctly classified pixels in the corresponding column (true positives) is divided by the total number of pixels in that column from the confusion matrix, then multiplied by 100 as shown in equation 1 (Wahelo et al., 2024).

$$AU = \frac{Correctly\ classified\ samples}{P} \times 100 \qquad (1)$$

Where: p refers to the total number of points in each class that agree with the classified map

3.5.5.2 Producer's accuracy

The PA determines the proportion of correctly classified pixels in each LULC category to the total number of pixels in that category (column) (Becker et al., 2021). The PA is calculated by dividing the number of correctly classified pixels by the sum of the row totals and multiplied by 100 equation 2.

$$PA = \frac{Correctly\ classified\ samples}{R} \times 100 \qquad (2)$$

Where: R refers to the total number of reference points in the reference class category

3.5.5.3 Kappa coefficient

The K is a numerical measure of agreement between raters, factoring in the possibility of agreement occurring by chance. It contrasts the actual classification accuracy with the expected accuracy based solely on chance (Congalton, 1991; Congalton & Green, 2019). The K was calculated using equation 3.

$$K = \frac{OA-EA}{1-EA} \qquad (3)$$

Where: K = Kappa coefficient; OA = proportion of actual agreement between raters; EA = proportion of agreement expected by chance.

3.5.5.4 Overall accuracy

Overall Accuracy (OA) is the ratio of the total number of pixels that is correctly classified to the sum of all pixels multiplied by 100 equation 4. It provides an overall assessment of the classification performance (Pal et al., 2013).

$$OA = \frac{Total\ number\ of\ correctly\ classified\ samples}{N} \times 100 \qquad (4)$$

Where: N refers to a total number of samples

3.6 Vegetation Trend Analysis and Climate Correlation

MODIS NDVI/EVI time-series data were decomposed into seasonal, trend, and remainder components by using BFAST. The climate vegetation correlations were computed using the following methods:

- Pearson's r between NDVI and rainfall (CHIRPS), temperature (MERRA-2).
- SPEI for drought sensitivity.
- Breakpoints (e.g., drought years) were statistically identified and mapped to vegetative changes.

Two complementary classification approaches were applied:

(a) Regional Vegetation Density Classification (EVI-based)

MODIS NDVI trends (2000-2023) were used to classify the vegetation cover into four density classes (Table 4) and (Figure 5) based on established NDVI and EVI classification frameworks (Liu et al., 2023). Considering the previous studies in Darfur (Kranz et al., 2015; Lang et al., 2010; Olaf et al., 2016), the analysis used mean EVI values from 2000-2023 to identify vegetation patterns and health across the study area. Changes in the spatial extent of each class were tracked to assess the regional greening or degradation dynamics.

Table 4. EVI-based Vegetation Classification

EVI Range	Vegetation Class	Description
< 0.1	Non-vegetated	Bareland, sand, urban areas
0.1-0.2	Low vegetation	Sparse grasses, or degraded scrub
0.2-0.3	Moderate vegetation	Grass land and mixed savanna vegetation
>0.3	High vegetation	Dense wood land or forest canopy

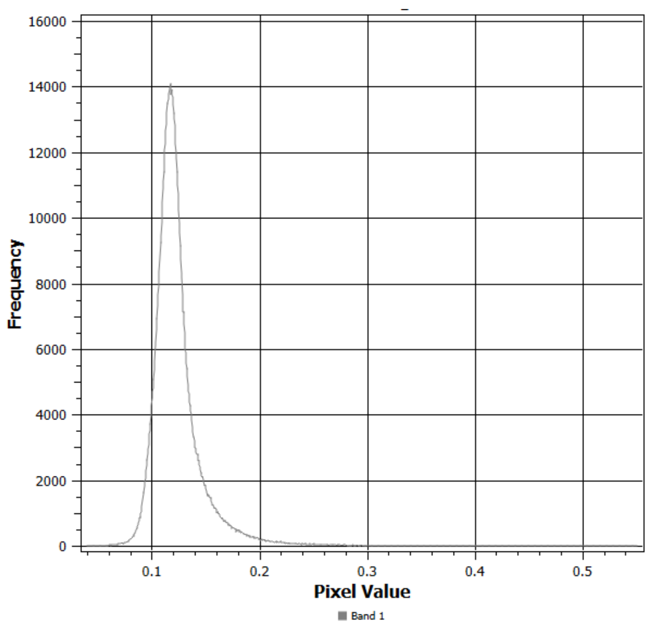

Figure 5. Raster histogram of the EVI classification threshold.

(b) Forest vs. Non-Forest Reclassification (NDVI-based)

For forest cover dynamics, NDVI composites were reclassified into Forest: NDVI > 0.25 Non-Forest: NDVI ≤ 0.25.

The NDVI > 0.25 threshold is widely used to delineate woody vegetation in dryland and savanna ecosystems, including Sudan and the greater Sahel, where forests are predominantly open dry woodlands rather than closed-canopy tropical forests.

To evaluate classification reliability, a stratified random sampling approach was applied for each reference year (2000, 2005, 2010, 2015, 2020, and 2024). A total of 400 validation points per year were generated, proportionally distributed across forest and non-forest classes.

Reference labels were derived through on-screen digitization using high-resolution (0.15 meters) Google Earth Pro imagery, supplemented by expert visual interpretation. Accuracy assessment was performed using the Semi-Automatic Classification Plugin (SCP) in QGIS 3.34, generating confusion matrices and overall accuracy metrics.

3.7 Cellular Automata-Based LULC Simulation

Simulating future LULC changes is essential for forecasting potential environmental and socio-ecological trajectories in fragile landscapes such as Darfur. This study employed a Cellular Automata-Markov chain modeling framework to model spatial transitions under a BAU scenario. The CA-Markov approach is particularly effective for simulating LULC dynamics, in which past trends and spatial dependencies are assumed to continue. It integrates Markov chain analysis, which predicts the probability of change from one LULC class to another over time, and CA, which introduces spatial rules based on neighborhood configuration, ensuring realistic spatial distribution and patch dynamics. This hybrid model provides both temporal and spatial predictive capacity, making it ideal for Darfur's heterogeneous landscapes where anthropogenic drivers (IDP settlements, farming, and reforestation) and natural factors (climate) influence LULC change.

LULC projections up to 2034 were conducted using the Modules for Land Use Change Simulation (MOLUSCE) plugin in QGIS. The drivers included elevation, slope, aspect, proximity to rivers, towns, and roads.

3.7.1 Input Preparation

To simulate LULC for 2034, ESRI-LULC Maps (2017-2024) were used as historical baselines. Spatial drivers, such as elevation, proximity to towns, and slope were standardized to a 10m resolution to match the ESRI layers.

Class re-mapping ensures consistency across years for accurate transition matrix generation in MOLUSCE.

3.7.2 Simulation Parameters

Transition potential was modeled using ANN Multi-Layer Perceptron and Logistic Regression within MOLUSCE.

Simulation: 2034 LULC prediction under BAU conditions.

3.7. 3 Validation and Accuracy Assessment

The Kappa Index was calculated between 2024 predicted and actual classified maps to validate the model performance. The Figure of Merit (FoM) and Overall Agreement were also used to assess classification quality and transition detection accuracy.

3.8 Vegetation Fragmentation and Land Degradation Analysis

Vegetation fragmentation was assessed using landscape metrics derived from classified land use maps for 2017 and 2024. To understand spatial forest dynamics and fragmentation, landscape metrics were calculated using FRAGSTATS and the LecoS plugin in the QGIS (Jung, 2016). The metrics (Table 5) included the following:

Table 5. Landscape Matrix

Metric	Description
Largest Patch Index (LPI)	Indicates dominance of the largest forest patch
Edge Density (ED)	Total length of forest edges per hectare
Number of Patches (NP)	Absolute number of forest patches
Landscape Proportion (LP)	Proportion of land area covered by forest

These metrics allowed for the temporal assessment of forest connectivity, edge effects, and landscape-level ecological integrity from 2017 to 2034 (including simulated scenarios).

3.9 Climate Forecasting ARIMA and ETS

Forecasting future climate conditions is crucial for anticipating vegetation responses, planning adaptive land-use strategies, and assessing future ecosystem vulnerability especially in environmentally and politically fragile regions such as Darfur. In this study, advanced time-series models were employed to project precipitation and temperature trends for the period of 2024-2034. Specifically, Autoregressive Integrated Moving Average (ARIMA) and Exponential Smoothing (ETS) models were used to derive statistically robust forecasts from historical climatic records (1981-2024), providing essential inputs for ecosystem dynamics interpretation and scenario planning.

Forecasting of precipitation and temperature (2024-2034) was performed using ARIMA and ETS. Both variables were aggregated on a zonal basis (North, South, and West Darfur) to account for ecological and climatic heterogeneity.

3.9.1 Forecasting Methodology

A forecasting methodology was developed that included stationary testing, model development, residual diagnostics, and visualization. Prior to model fitting, each time series was subjected to the Augmented Dickey-Fuller (ADF) test to check for stationarity. Where necessary, differences were applied to remove trends and seasonal components to achieve stationarity for the ARIMA modeling.

Conducted using the Box-Jenkins methodology. The optimal parameters (p, d, q) were selected based on Akaike Information Criterion (AIC) and Bayesian Information Criterion (BIC) scores. Seasonal ARIMA was tested when clear annual cycles were observed.

Complemented ARIMA to capture exponential smoothing components (level, trend, and season). It is suitable for capturing the multiplicative or additive seasonal effects on rainfall and temperature patterns.

The residuals of both the ARIMA and ETS models were tested for white noise behavior using Ljung-Box test (Hassani & Yeganegi, 2020), and ACF/PACF plots (Yakubu et al., 2022). This ensured that no significant autocorrelation remained, thus confirming the adequacy of the model. Modeling was implemented in R using the forecast, tseries, and ggplot2 packages. Forecast outputs were visualized as time-series plots, including 95% confidence intervals, to illustrate prediction uncertainty.

3.10 Ecosystem Service Valuation (ESV)

Sensitivity analysis is a crucial methodological step in the valuation of ecosystem services, particularly when employing the benefit transfer method. It helps to assess the reliability of total ESV estimates by measuring the responsiveness of ESV to changes in the Value Coefficients (VCs) assigned to different LULC classes.

Due to the limited availability of primary valuation data in Darfur, this study used global average value coefficients from (Costanza et al., 1997; de Groot et al., 2012). However, given the ecological and socioeconomic differences between global averages and local realities, a sensitivity analysis was carried out to determine how variations in these coefficients would influence the total ESV estimates. The Benefit Transfer Method (BTM) was used to evaluate ecosystem services across seven LULC classes. The Ecosystem Services Valuation Database (ESVD) (Rudolf de Groot, 2020) provides coefficients ($USD/ha/year) aligned with each LULC-biome pairing. The following equations were used to analyze the total ESV for each LULC class, total ESV for each year, total estimated ESV value, and percentage changes in ESV.

A. Total ESV

The total ESV for each LULC type was obtained by multiplying the area of each LULC type by its corresponding value coefficient as shown in equation 5 (Kindu et al., 2016b; Kreuter et al., 2001b)

$$\mathrm{ESV} = \mathrm{Ak} \times \mathrm{VCk} \qquad (5)$$

Where:

ESV = total estimated ecosystem service value

Ak = the area (ha)

VCk = the value coefficient (USD ha^{-1} $year^{-1}$) for LULC type 'k'.

B. Functional ESVs

The total ESVs for each LULC type were then summed to obtain the total ESV for each year, as per equation 6 (Tolessa et al., 2018).

$$\mathrm{ESV} = \Sigma\,(\mathrm{Ak} \times \mathrm{VCk}) \qquad (6)$$

Where:

ESV = total estimated ecosystem service value, A_k = the area (ha) and VC_k = the value coefficient (USD ha^{-1} $year^{-1}$) for LULC type 'k'.

C. Percentage Change

The percentage (%) changes in ESVs were also calculated by comparing the values of the last and first years, as shown in equation 7 (Gashaw et al., 2018)

$$\% \text{ ESV change} = \left(\frac{\text{ESV final year} - \text{ESV initial year}}{\text{ESV initial year}}\right) \times 100 \qquad (7)$$

Where:

ESV = % ecosystem service value rate change

ESV final year = the area of the final year

ESV initial year = the area of the initial year

D. Elasticity (CS)

Elasticity analysis was conducted to assess the relative responsiveness of ESVs to changes in LULC type over the study period. Elasticity, in this context, quantifies the percentage change in total ESV in response to a given percentage change in a specific LULC class, thereby helping to identify the influence of each land use category on the overall value of ecosystem services (Gaglio et al., 2017). To compute elasticity, the VC for a given LULC type was adjusted to ±50%, while the coefficients of all other LULC types were held constant. This analysis prioritized the importance of each LULC type in influencing the total natural capital value, rather than testing the robustness of the coefficient transfer method itself (Mengist et al., 2020)

The Coefficient of Sensitivity (CS), which reflects this elasticity, was calculated using the simplified formula of (Aschonitis et al., 2016) as shown in Equation 8.

$$CS = \frac{VC_{ik} \times A_k}{ESV_i} \qquad (8)$$

Where:

CS = Coefficient of Sensitivity

VC_{ik} = Total value of ES provided by the k LULC class at i year (US\$ year^{-1})

A_k = Area of LULC type k (ha) in year i,

ESV_i = Total ESV from all LULC types identified at i year (US\$ year^{-1})

A higher CS value indicates that a particular LULC class has a stronger influence on the total ESV, suggesting its strategic importance in maintaining the ecosystem's economic value. This method allows for the identification of priority areas for conservation or management intervention, especially in landscapes experiencing rapid LULC transitions such as Darfur.

3.11 Data Integration and Spatial Scales

A multi-scalar approach was adopted for scalability to reconcile local and regional ecological dynamics, allowing for robust generalizations across Darfur (Table 6).

Table 6. Integration of Data by Spatial Scale

Scale	Region Focus	Satellite/Resolution	Application	Published DOI
Micro-scale	Kas & El-Salam IDP	PlanetScope (3m), Sentinel-2 (10m)	Fine-scale vegetation analysis	(Ahmed et al., 2024)
Meso-scale	West Darfur	MODIS (250m)	Climate-vegetation analysis	(Ahmed & Czimber, 2025)
Meso-scale	Central Darfur	ESRI LULC (10m)	Annual LULC change monitoring (2017-2024), ecosystem valuation	-
Macro-scale	Entire Darfur	MODIS, Climate data	Trends and forecasting	(Ahmed, Rotich, & Czimber, 2025)

3.12 Soil type classification

To complement vegetation and land use dynamics, detailed soil classification was undertaken across the Darfur region using FAO-UNESCO digital soil data (Adhikari et al., 2014; Hartemink et al., 2013), supported by spatial overlays with land cover and ecological zones. Understanding soil properties is essential in dryland ecosystems, as soil texture, fertility, and structure directly affect vegetation growth, ecosystem services, and vulnerability to land degradation, particularly in conflict-impacted areas where land-use pressures are intense (Bai et al., 2008; Zeng et al., 2022). (Figure 6) presents the spatial distribution of soil types, revealing considerable heterogeneity across the region's ecological gradients. The classification distinguishes between dominant and minor soil types, each with distinct implications for vegetation resilience, agricultural viability, and land recovery potential under climate stress and displacement.

3.12.1 Dominant Soil Types Identified in Darfur

Lithosols (I): Shallow and stony: These soils are confined to hilly or rocky terrains. Owing to their limited water-holding capacity, they support only sparse vegetation, primarily shrubs and hardy grasses.

Cambic Arenosols (Qc): Sandy soils with weak profile development, commonly found in northern and central Darfur. They are erosion-prone and exhibit poor nutrient retention yet are moderately suitable for seasonal cultivation with conservation practices, such as mulching or agroforestry (Mermut & Eswaran, 2001).

Yermosols (Y): Extremely arid soils characterized by low organic matter and nutrient contents are prevalent along desert margins. These soils have very low agricultural potential and are indicative of desertification-prone zones (UNEP, 2008).

Eutric Vertisols (Re): Found in floodplains and low-lying depressions, these fertile clay soils are critical for food production. However, their poor drainage and swelling-shrinking behavior create challenges for year-round cultivation without infrastructure (Montgomery, 2017)

Luvic Arenosols (Qi): Sandy, moderately fertile soils often associated with rain-fed farming systems. Their well-drained nature supports the cultivation of millet and sorghum under appropriate rainfall conditions (Wang et al., 2019).

Haplic Xerosols (Xh): Present in hyper-arid zones, these dry mineral soils are susceptible to salinization and are generally unsuited for crops without substantial input.

Dystric Regosols (Rd): These poorly developed soils with low organic content are widespread in degraded transitional zones. They are strongly correlate with deforested or overgrazed areas (Bai et al., 2008).

Calcaric Fluvisols (Jc): Fertile, calcium-rich soils found along the Wadis and floodplains. Their alluvial origin and high fertility make them highly suitable for irrigated farming and agroforestry, especially in El-Salam and Kas localities.

Ferric Luvisols (Lf): Located in forest–savanna ecotones, these soils exhibit a strong structure and moderate fertility, enabling both natural vegetation regeneration and sustainable cultivation (Kindu et al., 2016).

Rock Debris (Rk): Non-soil surfaces composed of exposed bedrock and coarse lithological material. These areas are ecologically marginal but may be relevant for runoff and erosion modeling.

Pellic Vertisols (Vp): Dark clay soils with high fertility but seasonal cracking, posing risks for root crops and requiring careful water management during cultivation cycles.

3.12.2 Minor Soil Types Identified

Chromic Cambisols (Bc) and Eutric Cambisols (Be): These moderately developed soils offer balanced fertility and are often used for diversified cropping, particularly in peri-urban zones and IDP settlement fringes.

Dunes/Shifting Sands (Ds): Predominant in northern Darfur, these unstable sandy deposits are unsuitable for agriculture and indicate active desert encroachment.

Gleyic Luvisols (Lg): These soils exhibit poor drainage in seasonally saturated areas, making them relevant for wetland vegetation studies and potential agroecological restoration zones.

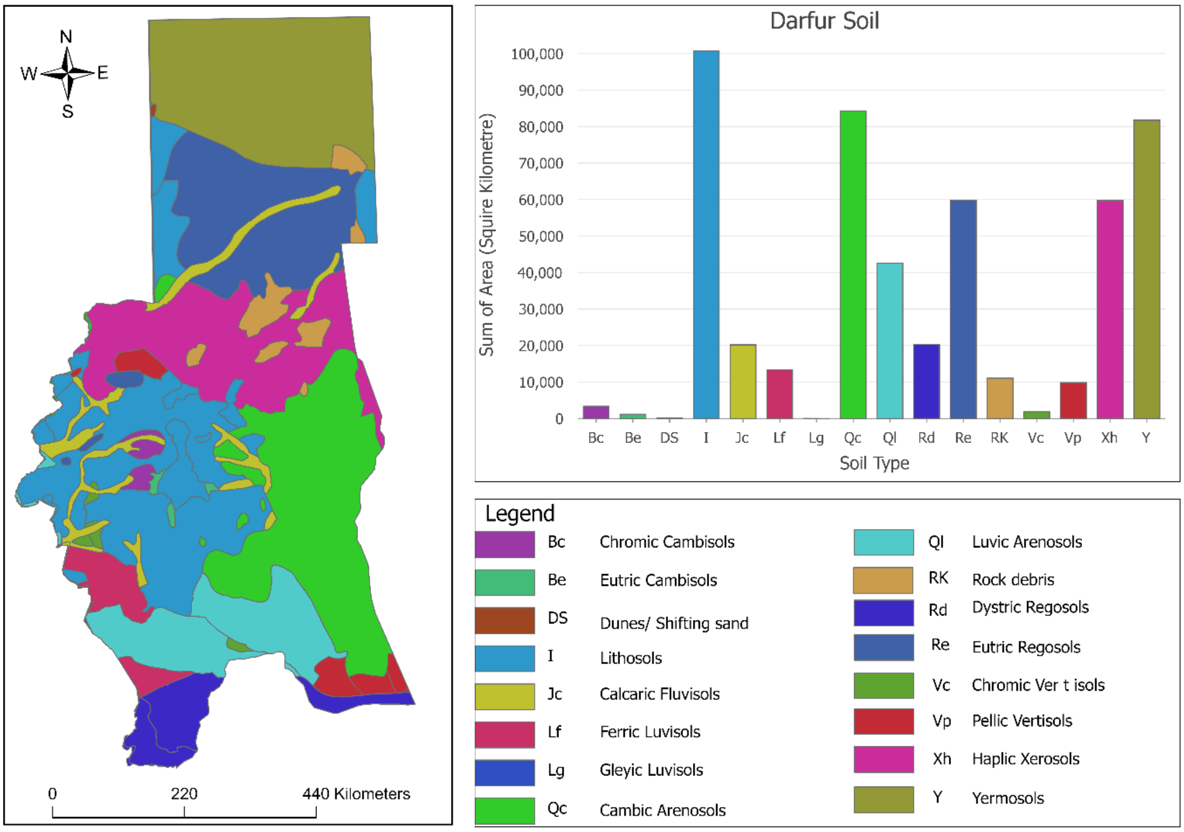

Figure 6. Spatial distribution of soil types in the Darfur region. The map illustrates the diversity and geographic extent of dominant and minor soil classes across varying ecological zones.

This classification reveals that Darfur's soil system is spatially diverse, with substantial portions being constrained by aridity, erosion, and low fertility. However, pockets of fertile soil (e.g., Vertisols and Fluvisols) provide opportunities for sustainable agriculture and ecosystem restoration, particularly when integrated with improved land governance and climate-smart practices (FAO, 2015).

The presence of degraded soils such as Regosols, Arenosols, and Yermosols further supports the NDVI and LULC trends observed in Sections 4.2.1 and 4.2.5, where land degradation correlates strongly with both conflict pressures and unsustainable land use.

In post-conflict recovery planning, soil quality mapping is vital for identifying the zones of agricultural revival, grazing potential, and ecological restoration. The heterogeneity across Darfur soil types reinforces the need for site-specific land management strategies, especially in and around IDP settlements and degraded hotspots.

3.13 Chapter Summary

This chapter details the integrated methodological framework adopted to assess the multi-dimensional environmental transformations occurring in Darfur owing to conflict, climate variability, and displacement dynamics. A multidisciplinary design was employed, incorporating remote sensing technologies, machine learning algorithms, ecosystem service valuation, spatial simulation, and climate forecasting to deliver a comprehensive ecological assessment of the region between 1981 and 2034. Key methodological highlights include:

- High-resolution remote sensing datasets (MODIS, Sentinel-2, PlanetScope, and ESRI LULC) were used to analyze vegetation dynamics and land degradation across scales.

- Deployment of CA-Markov modeling to simulate future LULC changes under a BAU scenario.

- Application of NDVI, EVI, and SPEI to track vegetation-climate interactions and drought trends over time.

- Valuation of ESVs using benefit transfer methods to capture the economic implications of land cover transitions.

- Integration of climate forecasting tools (ARIMA and ETS) to project future rainfall and temperature dynamics.

- Spatial pattern and fragmentation analyses were performed using landscape metrics (LPI, Patch Density, Edge Density) to assess ecological stability and connectivity.

- Sensitivity analysis and model validation techniques were applied to ensure the accuracy and robustness of the models and findings.

- Dominant and minor soil types are based on the FAO-UNESCO classification.

This methodological approach provides a scalable, replicable, and policy-relevant toolkit to study land system changes in conflict-affected ecosystems. The next chapter presents the results derived from these methods, starting with land use and vegetation classification patterns, followed by climatic trends, drought frequency, forest recovery, ecosystem service shifts, and scenario-based land change simulations.

CHAPTER 4

Results and Discussion

4.1 Introduction

This chapter presents and discusses findings derived from a multi-source geospatial analysis of land use and vegetation dynamics across Darfur, Sudan. Through an integrated assessment using high-resolution and moderate-resolution satellite datasets, climate indicators, land cover simulation models, and ecosystem service valuation, this study uncovers spatiotemporal patterns of vegetation change and the ecological consequences of conflict-induced displacement. The discussion is structured around thematic area LULC changes, vegetation trend dynamics, climate-vegetation interactions, future LULC projections, ESV, and land degradation and fragmentation.

4.2 Results

4.2.1 Land Use and Land Cover Change Analysis

4.2.1.1 Kas Locality (Sentinel-2A, 2016-2022)

4.2.1.1.1 Classification Accuracy Assessment and LULC Statistics

Using high-resolution Sentinel-2A satellite data, LULC classification was conducted to analyze the transformation of the Kas locality between 2016 and 2022. Three supervised machine learning algorithms RF, Support Vector Machine (SVM), and K-Nearest Neighbor (KNN) were employed, and their performance was evaluated using confusion matrices, overall accuracy, and Kappa coefficients.

As summarized in Table 7, the RF algorithm exhibited superior performance, achieving an overall accuracy of 86.31% and a Kappa of 0.75 for the 2016 dataset. For the 2022 classification, RF yielded 85.52% accuracy and a Kappa of 0.71. These metrics indicate substantial agreement with the reference data and provide a robust basis for land-cover change detection. By contrast, the KNN and SVM models performed slightly less reliably, with accuracies ranging from 82% to 85%. Given the higher accuracy, the RF classification outputs were used in all subsequent LULC change analyses.

This high classification performance aligns with previous studies that applied RF to LULC in heterogeneous environments, such as the conflict-prone regions of Ethiopia and Nigeria (Arowolo et al., 2018; Kindu et al., 2016). The use of Sentinel-2A's 10-meter spatial resolution further enhanced the detection of finer-scale transitions, especially in agro-ecological mosaics and near IDP settlements.

Table 7. Classification accuracy and Kappa coefficient of Machine Learning (ML) classifiers for Sentinel-2A LULC mapping

Year	Classifier	Overall Accuracy (%)	Kappa Coefficient
2016	RF	86.31	0.76
	SVM	83.67	0.72
	KNN	82.26	0.68
2022	RF	85.52	0.71
	SVM	84.03	0.70
	KNN	85.09	0.69

Throughout both years (Table 8), bareland and vegetation cover classes exhibited the highest accuracy. In 2016, bareland achieved a PA of 96.68% and UA of 95.69%, while vegetation cover reached 93.28% and 92.78%, respectively. By 2022, bareland maintained high accuracy (PA = 97.35%, UA = 93.49%), and vegetation cover remained strong (PA = 87.32%, UA = 97.10%). These values reflect the high separability of these spectral classes in Sentinel-2 imagery due to distinct reflectance characteristics in the red and near-infrared bands.

Built-up areas displayed moderate variability, with accuracy decreasing between 2016 (PA = 91.90%) and 2022 (PA = 72.60%), likely due to the spatial expansion and spectral heterogeneity of settlement structures over time. Similarly, agricultural land and sand classes exhibited higher PA in 2022 (96% and 99.46%, respectively) but lower UA (73.01% and 74.33%), suggesting partial confusion with bareland and vegetation during post-harvest or dry-season conditions.

Overall, the consistency of classification performance across both years supports the reliability of the Random Forest (RF) classifier in distinguishing heterogeneous land cover features under varying environmental conditions. The slight reduction in overall accuracy between 2016 and 2022 can be attributed to increased land-use complexity and mixed pixel effects resulting from the intensification of agricultural and settlement activities in IDP-affected zones. These results meet and exceed the commonly accepted threshold of 85% accuracy for reliable LULC classification (Congalton & Green, 2019), confirming the robustness of the classification process.

Table 8. Classification accuracies for the years 2016 and 2022

LULC Class	PA (2016)	UA (2016)	PA (2022)	UA (2022)
Vegetation Cover	87.32	97.10	93.28	92.78
Bareland	97.35	93.49	96.68	95.69
Built-up	72.60	97.72	91.90	85.30
Agricultural Land	96	73.01	84.57	85.19
Sand	99.46	74.33	83.89	78.71

Note: PA-producer accuracy, UA-user accuracy

4.2.1.1.2 LULC Dynamics and Implications

The classified maps in Figure 7 illustrate the spatial distribution and transitions of the major land cover types of agricultural land, bareland, vegetation, and built-up areas between 2016 and 2022. Agricultural land was the dominant LULC type in both years, expanding from 55.56% in 2016 to 65.32% in 2022, with a net gain of 98.12 km² (17.53%). Bareland declined significantly from 34.97% to 28.33%, whereas vegetation and built-up land experienced minor changes. Built-up land, although still a small fraction of the total area, increased by 5.29 km², representing a 60.53% rise, indicating ongoing peri-urban growth and settlement expansion (Table 9).

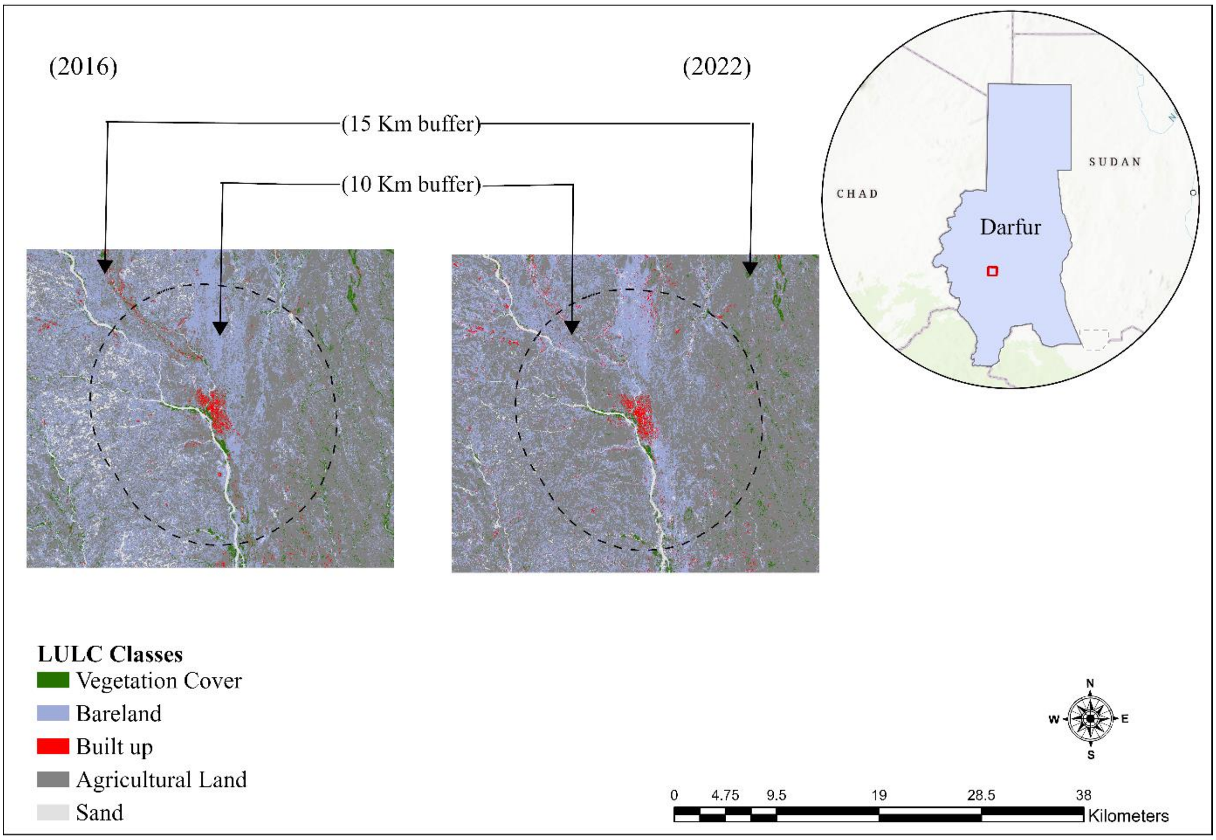

Figure 7. Classified LULC maps of Kas Locality for 2016 and 2022, showing climate change-affected zones (10–15 km = low impact, 0–10 km = high impact) around IDP settlements.

Table 9. LULC Classes areas and percentages

LULC Class	2016		2022	
	Area (km²)	**Percent (%)**	**Area (km²)**	**Percent (%)**
Vegetation Cover	28.87	2.87	18.67	1.85
Bareland	352.21	34.97	285.36	28.33
Built-up	8.74	0.87	14.03	1.39
Agricultural Land	559.63	55.56	657.75	65.32
Sand	57.67	5.73	31.30	3.11
Total	1007.13	100.00	1007.13	100.00

The annual LULC change rates (Figure 8 and Table 10) confirm that agricultural land expanded by 2.92% per year, while bareland declined by 3.16% annually. Vegetation cover has decreased by 5.89% per year, reflecting the pressure on natural ecosystems from land conversion. These transitions suggest increased anthropogenic disturbance linked to IDP resettlement, informal agriculture, and intensified livelihood pressures.

Table 10. LULC Change in Kas Locality, 2016-2022

LULC Class	Total Area Change (km²)	% Change	Annual Change (km²/year)	Annual % Change
Vegetation Cover	-10.20	-35.33%	-1.70	-5.89%
Agricultural Land	+98.12	+17.53%	+16.35	+2.92%
Bareland	-66.85	-18.98%	-11.14	-3.16%
Built-up	+5.29	+60.53%	+0.88	+10.09%
Sand	-26.37	-45.73%	-4.40	-7.62%

**Note: Negative values indicate loss, positive values indicate gain*

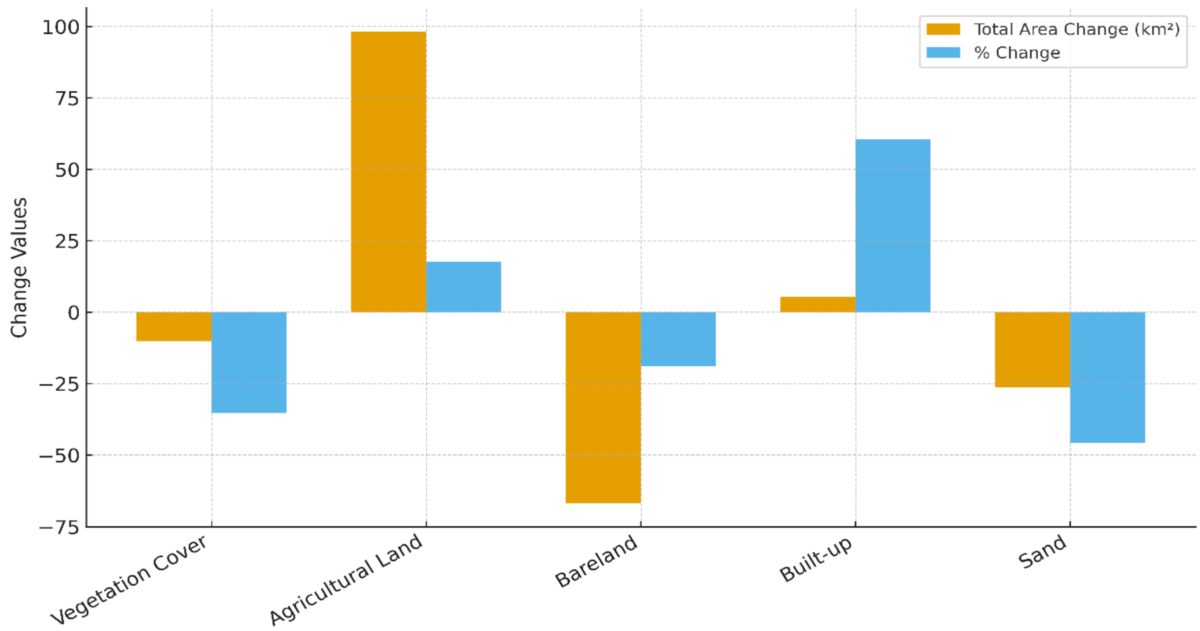

Figure 8. Clustered Bar Chart for LULC change in Kas locality (2016-2022), comparing total area change (km²) and percentage change side by side for each LULC class.

These findings are consistent with the work of Mohamed et al., (2020) and Yousif et al., (2018), who documented similar trends of agricultural expansion and vegetation loss in the displacement-affected zones of South Kordofan and North Darfur. The increase in cultivated land supports the hypothesis that IDPs contribute to land pressure by engaging in survival farming, often in ecologically sensitive zones. Similarly, Gorelick et al., (2020) noted accelerated LULC transitions in areas surrounding refugee and IDP camps, reinforcing the findings in the Kas locality.

Despite the negative trend in vegetation cover, the relatively stable increase in agricultural productivity suggests the potential for recovery if appropriate land management and sustainable agriculture practices are adopted. However, unchecked expansion can lead to land degradation and soil fertility loss, particularly in marginal zones under climatic stress.

In summary, the LULC trends in the Kas locality between 2016 and 2022 highlight the dual narrative of human displacement-driven land transformation and incipient urban expansion, both of which call for targeted interventions in land zoning, reforestation, and agroecological planning.

4.2.1.1.3 IDPs and Climate Change Influences on LULC Patterns

To isolate the effects of IDPs and climate variability on land use patterns, a buffer-based zonal analysis was conducted. The study area was segmented into two impact zones: a highly affected zone (0-10 km radius from IDP clusters) and a lowly affected zone (10-15 km), allowing spatial stratification of LULC changes attributable to settlement proximity.

As shown in Table 11, within the highly affected zone, vegetation cover declined by 42.57%, whereas agricultural land expanded by 17.29% over the study period. The bareland and sandy surfaces also showed notable reductions, suggesting intensified land conversion. Built-up land increased modestly but significantly, indicating informal settlement growth and semi-permanent infrastructure near the IDP camps.

Table 11. LULC Distribution and Changes in IDP/Climate-affected Zones, 2016-2022

	Highly affected (0-10km)					**Lowly affected (10-15km)**				
	2016		**2022**		**2016-2022**	**2016**		**2022**		**2016-2022**
CLASS	**Area (%)**	**Area (km^2)**	**Area (%)**	**Area (km^2)**	**Change (%)**	**Area (%)**	**Area (km^2)**	**Area (%)**	**Area (km^2)**	**Change (%)**
Vegetation Cover	2.32	10.01	1.33	5.80	**-42.57**	3.47	19.87	2.25	12.87	**-35.23**
Bareland	37.81	165.51	31.12	135.32	**-17.69**	32.63	186.71	26.22	150.03	**-19.65**
Built-up	1.29	5.62	1.77	7.71	**37.19**	0.55	3.12	1.10	6.32	**102.56**
Agricultural Land	53.23	231.45	62.43	271.48	**17.29**	57.35	328.19	67.50	386.30	**17.70**
Sand	5.35	23.28	3.35	14.55	**-37.50**	6.00	34.39	2.93	16.76	**-51.26**
Total	**100**	**434.86**	**100**	**434.8**		**100**	**572.28**	**100**	**572.28**	

Note: A decline is indicated by red highlights, and an increase is indicated by green highlights. Between 2016 and 2022, there was a noticeable decline in vegetation, bareland, and sand, and an increase in agricultural land and built-up classes in both highly and lowly affected zones.

In contrast, the lowly affected zone exhibited similar but less intense trends: vegetation loss was 35.23%, bareland was reduced by 19.65%, and sand was reduced by 51.26%. Interestingly, built-up areas more than doubled (+102.56%), signaling outward expansion and possibly resettlement beyond the IDP camp core. Agricultural land increased comparably in both zones.

These results align with prior observations in similar displacement contexts, such as those documented in Northern Nigeria and South Sudan (Annette, 2024; Moyo & Blake, 2024), where displaced populations contribute to land pressure through fuelwood harvesting, emergency farming, and settlement sprawl. The sharp decline in bareland and sand, especially in peripheral zones, also suggests opportunistic land reclamation and cultivation attempts, driven by improved rainfall and livelihood recovery strategies.

Moreover, this spatially disaggregated approach illustrates the gradient of environmental stress from displacement cores, echoing the conclusion of Ahmed & Czimber (2025) that IDP settlements exhibit radiating ecological footprints. However, modest vegetation regrowth, particularly in buffer areas, may indicate the onset of passive recovery due to land abandonment or community-led restoration interventions.

4.2.1.1.4 Vegetation Dynamics Based on NDVI Analysis

As illustrated in Figure 9, the pairwise comparison of NDVI distributions across the study years revealed statistically significant temporal variations in vegetation vigor and greenness. The Mann-Whitney Wilcoxon test indicated highly significant differences ($p < 0.0001$) between the periods 2016-2020, 2020-2022, and 2016-2022, confirming measurable fluctuations in vegetation productivity over time.

These statistically significant changes reflect a marked decline in vegetative biomass and photosynthetic activity, particularly between 2016 and 2022. The trend aligns with LULC transitions observed, where agricultural expansion and settlement growth coincided with a reduction in natural vegetation cover. This reduction suggests the combined influence of anthropogenic pressures, such as increased land conversion for cultivation and fuelwood extraction, alongside climatic stressors, notably rainfall variability and recurrent dry spells.

Overall, the NDVI-based temporal analysis demonstrates a progressive degradation of vegetation health in Kas locality, reinforcing the LULC-derived evidence of ecosystem stress in proximity to IDP settlements and cultivated zones.

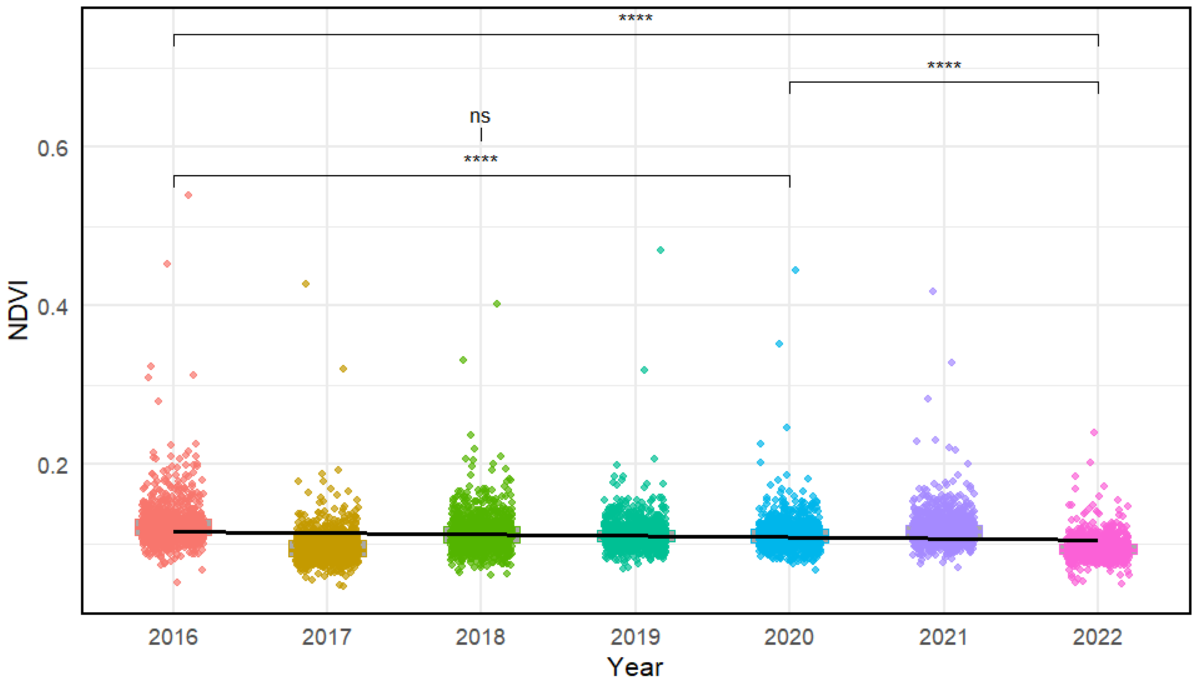

Figure 9. Pairwise comparisons of NDVI distributions between selected years (2016, 2017, 2018, 2019, 2020, 2021, and 2024), based on Mann-Whitney-Wilcoxon test results.

4.2.1.2 El-Salam Camp (PlanetScope, 2017-2023)

4.2.1.2.1 Classification Accuracy and LULC Statistics

LULC classification was conducted Using high-resolution PlanetScope imagery for 2017, 2019, 2021, and 2023. The study employed SVM and RF classifiers to delineate six LULC classes: agricultural land, bareland, vegetation cover, built-up areas, Wadi, and water bodies.

According to Table 12, the SVM classifier consistently outperformed RF, achieving overall classification accuracy of 90.66% and 95.14%, with Kappa coefficients exceeding 0.85. These results demonstrate a high level of thematic and inter-year consistency. RF, while useful, underperformed in later years, particularly in 2023 (accuracy = 78.57%, Kappa = 0.69). Consequently, SVM-derived maps were adopted for trend analysis owing to their superior accuracy and robustness.

Table 12. Accuracy of LULC Classification Maps (2017-2023) for El-Salam Camp Using SVM and RF Algorithms

Year	Classifier	Overall Accuracy (%)	Kappa Coefficient
2017	SVM	92.53	0.89
	RF	88.03	0.83
2019	SVM	95.14	0.93
	RF	95.11	0.93
2021	SVM	92.55	0.87
	RF	88.41	0.82
2023	SVM	90.66	0.86
	RF	78.57	0.69

4.2.1.2.2 Landscape Transformation and Socio-Ecological Drivers

Over the six-year period, the El-Salam Camp exhibited substantial land transformation, as evidenced by the LULC statistics (Table 13). In 2017, agricultural land covered 117.93 km^2 (48.26%), while bareland comprised 46.82%. Other land classes, including built-up areas, vegetation, and wadi areas, comprised smaller shares. By 2023, agricultural land had increased to 133.44 km^2 (54.61%), marking a net gain of over 6.35%, while bareland shrank to 39.31% (Figure 10).

Significantly, the vegetation cover (forest, and shrubs) more than doubled, rising from 0.75% to 1.60%, suggesting a modest but encouraging trend in revegetation and ecological recovery. Built-up land also grew incrementally from 1.41% to 1.50%, indicating slow urbanization or consolidation of settlement structures.

Table 13. LULC Statistics for El-Salam Camp from 2017 to 2023

	2017		**2019**		**2021**		**2023**	
LULC classes	Area (km^2)	Area (%)	Area (km^2)	Area (%)	Area (km^2)	Area (%)	Area (km^2)	Area (%)
Agricultural land	117.93	48.26	117.21	47.96	117.35	48.02	133.44	54.61
Bareland	114.43	46.82	114.50	46.85	112.24	45.93	96.07	39.31
Water bodies	0.002	0.001	0.011	0.005	0.014	0.006	0.033	0.014
Vegetation cover	1.83	0.75	2.34	0.96	2.62	1.07	3.91	1.60
Built up	3.45	1.41	3.48	1.42	3.61	1.48	3.67	1.50
Wadi	6.74	2.76	6.84	2.80	8.53	3.49	7.24	2.96
Total	244.37	100.00	244.37	100.00	244.37	100.00	244.37	100.00

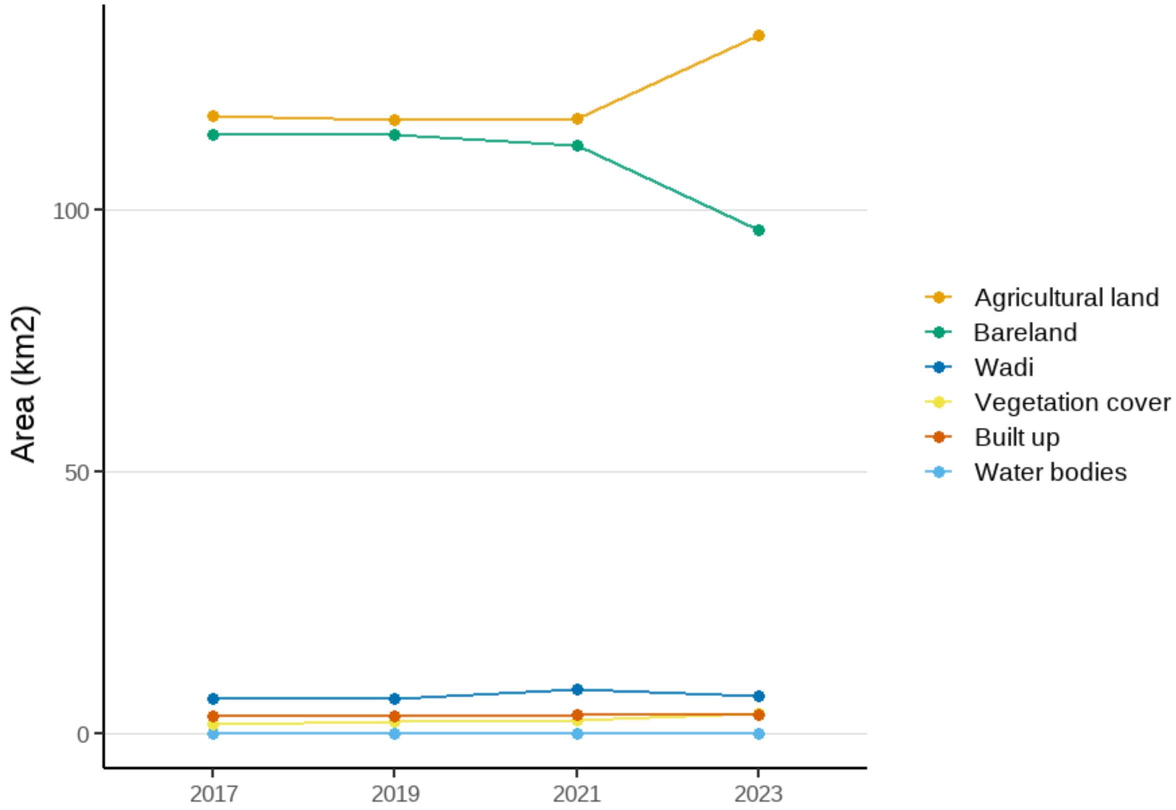

Figure 10. Temporal dynamics of LULC areas of 2017, 2019,2021, and 2023.

These spatial changes are visualized in (Figure 11) mirror observations by Gorelick et al., (2020) and Omer & Abdoun, (2020), who report similar regrowth patterns in camps with stable climatic conditions and minimal conflict resurgences. The increase in vegetation and agricultural land supports the argument that some IDP communities actively engage in land stewardship, reforestation, or agroforestry practices especially when tenure security and rainfall support farming viability.

However, the ongoing reduction in bareland also implies sustained land pressure and reduced fallow cycles, which may risk soil degradation if not counterbalanced by conservation agriculture. While El-Salam exhibits signs of resilience, it remains vulnerable to renewed conflict, governance gaps, and unsustainable expansion.

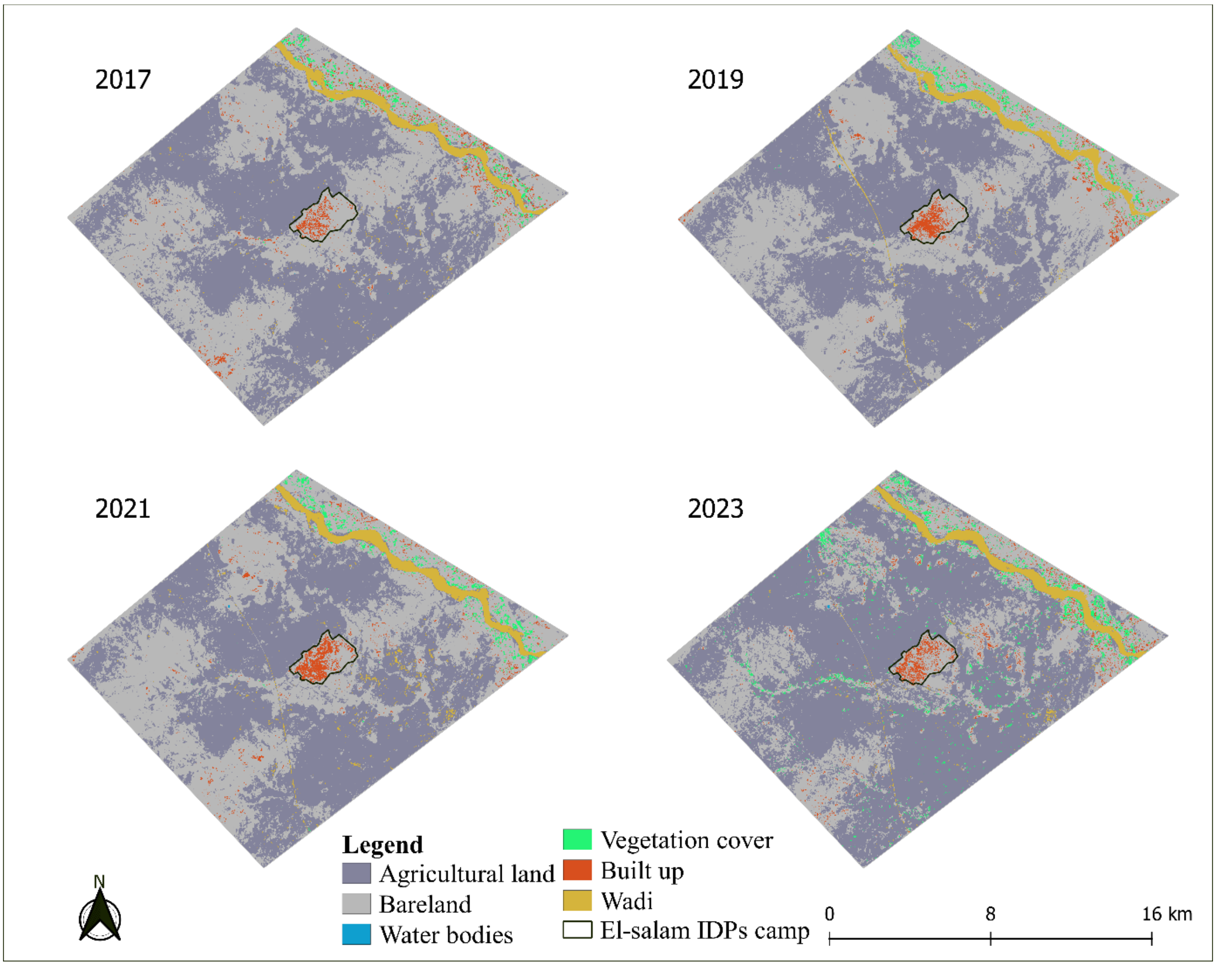

Figure 11. LULC classification maps for El-Salam Camp (2017, 2019, 2021, and 2023), showing spatial distribution of key land cover classes.

4.2.1.2.3 Vegetation Health Condition: Trends and Ecological Interpretation

NDVI was employed to evaluate the temporal evolution of vegetation health in the El-Salam IDP camp and surrounding areas. NDVI is a well-established proxy for photosynthetic vigor, plant density, and overall vegetative productivity and is particularly useful in data-scarce and conflict-affected landscapes.

The NDVI values across the study period (2017-2023) ranged from 0 to +0.82 (Figure 12). This spectrum captured the full range of ecological conditions from non-vegetated and stressed areas to zones of healthy, high-density vegetation.

4.2.1.2.4 Observed Trends and Contributing Factors

Temporal analysis revealed progressive improvement in vegetation health between 2017 and 2023. The spatial extent of the high and moderate NDVI classes increased, whereas the low-NDVI areas (indicative of bare soil, degraded land, or water surfaces) decreased significantly. Several key drivers contribute to this positive ecological trajectory.

1- Increased annual precipitation: Enhanced rainfall patterns, particularly post-2019, improved soil moisture availability, facilitating biomass growth and regreening. These patterns are consistent with the regional climate recovery trends observed in West Darfur and broader Sahelian zones (Abdalla et al., 2020; Siam et al., 2013).

2- Agroforestry expansion: Community-led agroforestry practices have emerged as a dominant land-use innovation. The integration of woody perennials with annual crops and livestock in sustainable silvo-pastoral systems promotes soil stabilization, microclimate regulation, and nutrient cycling to restore vegetation health in degraded lands.

3- Natural regeneration and land-use shifts: Marginal lands previously categorized as bareland or transitional sand zones showed signs of passive vegetation recovery, possibly linked to land abandonment, improved rainfall, and reduced grazing pressures.

This aligns with Herrmann et al., (2005) and Bai et al., (2008), who reported similar regreening episodes in the post-crisis Sahelian regions. The observed trajectory also mirrors the NDVI-climate coupling trends discussed by Duan et al., (2021), emphasizing that climate improvements, coupled with local stewardship, can yield measurable ecological benefits even in conflict-fragile contexts.

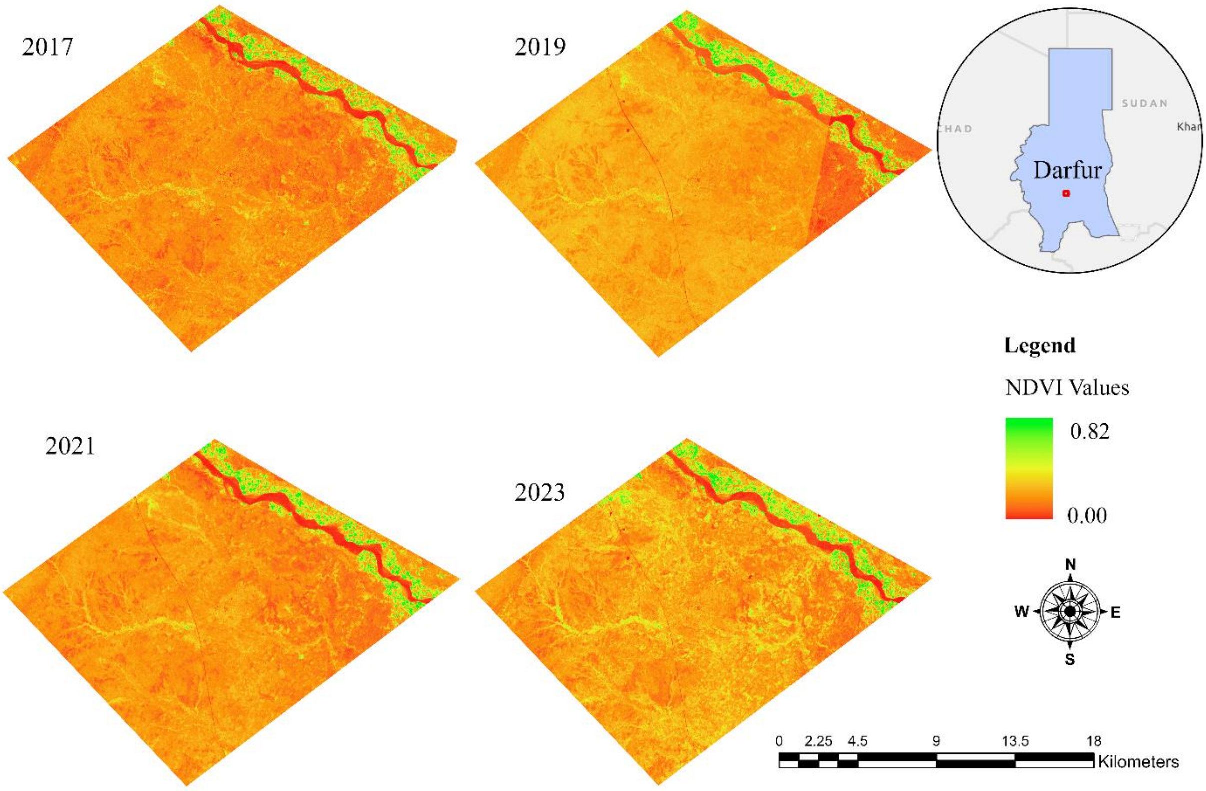

Figure 12. NDVI-derived vegetation health maps for El-Salam Camp (2017, 2019, 2021, 2023), illustrating improvements in greenness and biomass cover.

4.2.1.2.5 Statistical Validation of NDVI Change

As visualized in Figure 13, pairwise comparisons of the NDVI distributions across the study years highlighted statistically meaningful vegetation shifts. The Mann-Whitney-Wilcoxon test showed highly significant differences (****, $p < 0.0001$) between 2017-2021 and 2017-2023.

These differences underscore the marked positive shift in vegetative biomass and productivity over the six-year period. Interestingly, no significant differences were observed between 2017 vs. 2019 and 2021 vs. 2023, suggesting plateaus of relative ecological stability during those intervals.

This implies that while the initial regreening was more gradual, major leaps in vegetative health occurred between 2019 and 2021, coinciding with agroforestry scaling and rainfall recovery. The later plateau (2021-2023) may reflect system stabilization or a shift from expansion to ecological consolidation, where ecosystems are maintained but do not significantly advance vegetative gain.

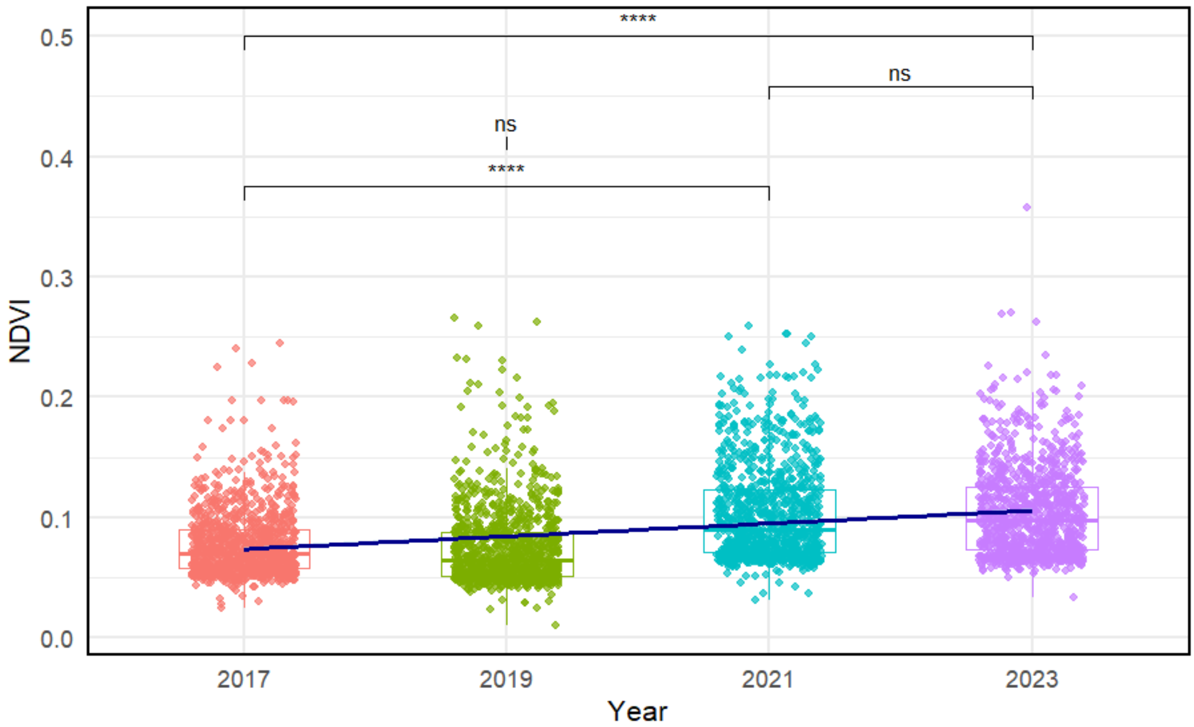

Figure 13. Pairwise comparisons of NDVI distributions between selected years (2017, 2019, 2021, and 2023), based on Mann-Whitney-Wilcoxon test results.

4.2.1.2.6 Implications for Environmental Recovery

These findings collectively highlight the importance of localized adaptation strategies particularly agroecological interventions and passive recovery in shaping post-conflict environmental outcomes. While IDP settlements are often framed as ecological stressors, this study suggests that displaced communities can contribute to land rehabilitation under conducive climatic conditions and minimal conflict relapses.

However, future pressures such as resettlement expansion, food insecurity, and fuelwood demand could reverse these gains. This underscores the need for policy safeguards and continued community-based resource governance to ensure sustainable ecological resilience.

4.2.1.3 West Darfur (MODIS-NDVI, 2000-2024)

4.2.1.3.1 Forest and Non-Forest Dynamics - Trends

Long-term vegetation dynamics in West Darfur were assessed using MODIS-derived NDVI data from 2000 to 2024, focusing on the spatial extent and temporal evolution of forested and non-forested areas. This analysis provides crucial insights into the ecological change trajectories across conflict-affected and drought-prone landscapes. The resulting overall accuracies demonstrate strong and improving classification performance over time 2000 =82.83%, 2005 = 81.17%, 2010 = 82.46%, 2015 = 87.85%, 2020 = 92.17%, and 2024 = 90.75%. The progressive improvement reflects enhanced image quality, better reference data availability, and improved vegetation signal stability in later years.

As illustrated in (Table 14), (Figure 14 and Figure 15), the region experienced two contrasting phases:

4.2.1.3.2 Phase 1 - Decline (2000-2010): Deforestation and Stress Period

During the first decade, forested land declined sharply from 2,578.82 km² in 2000 to 1,657.38 km² in 2010, representing a net loss of 921.44 km², or 35.75%. This deforestation wave aligns with prolonged drought cycles, particularly those affecting the Sahel between the late 1980s and the early 2000s (Dai, 2011; Herrmann et al., 2005).

Conflict-driven displacement, which intensified fuelwood extraction and agricultural encroachment in the absence of regulated land management.

Breakdowns in forest governance and conservation programs due to institutional fragility during civil unrest. This period mirrors patterns observed elsewhere in the Sahel, where socio-political crises compound climate-induced ecological degradation (Nicholson et al., 2013). Classification accuracy for this phase remained stable with overall accuracies exceeding 81%, confirming that observed trends are not artifacts of classification uncertainty.

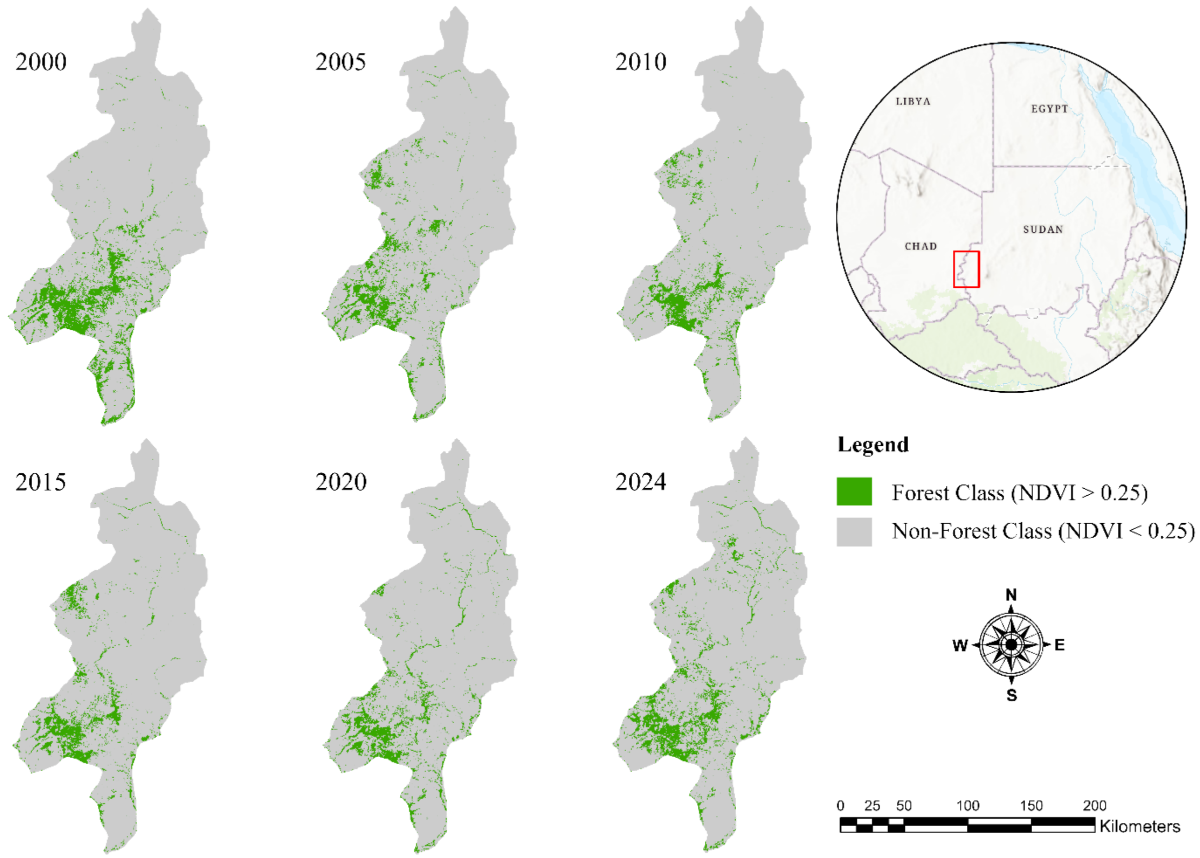

Figure 14. Forest and non land cover classification maps for West Darfur from 2000, 2005, 2010, 2015, 2020, and 2024.

4.2.1.3.3 Phase 2 - Recovery (2010-2024): Reforestation and Regeneration

A notable reversal has occurred post-2010. Between 2015 and 2020, forested areas increased by 5.02%, gaining about 89.35 km², and continued to expand by an additional 31.11% between 2020 and 2024 (Figure 16). Several interacting factors explain this regreening trajectory:

1- Improved precipitation patterns: Following Sahel-wide trends, rainfall increased steadily post-2000, especially in western Sudan (Siam et al., 2013), supporting natural vegetation regeneration.
2- Conflict-related land abandonment: Large areas were left fallow due to displacement and insecurity. This passive reforestation aligns with the ecological rebound documented in abandoned lands across war-torn regions (UNEP, 2017; Yengoh et al., 2015).
3- Reforestation programs and agroforestry: Community-based agroecological interventions, possibly supported by NGOs and local authorities, contributed to vegetation densification, especially in buffer zones around IDP settlements.
4- NDVI-Climate Coupling**:** The strong correlation between NDVI trends and climate recovery ($r > 0.70$) in West Darfur confirms the importance of rain-fed ecological feedback loops, a pattern echoed by (Bai et al., 2008; Duan et al., 2021).

This interpretation is supported by improved classification accuracy in later years, peaking at 92.17% in 2020 and remaining high at 90.75% in 2024.

Table 14. Composition and Percentage Differences of Forest and non-forest Classification

Year Range	Class	Area Start (km²)	Area End (km²)	Change (km²)	% Change
2000-2005	Forest	2,578.82	1,932.59	-646.23	-25.04%
	Non-Forest	20,219.26	20,865.49	+646.23	+3.19%
2005-2010	Forest	1,932.59	1,657.38	-275.21	-14.24%
	Non-Forest	20,865.49	21,140.70	+275.21	+1.31%
2010-2015	Forest	1,657.38	1,779.63	+122.25	+7.37%
	Non-Forest	21,140.70	21,018.45	-122.25	-0.57%
2015-2020	Forest	1,779.63	1,868.98	+89.35	+5.02%
	Non-Forest	21,018.45	20,929.10	-89.35	-0.42%
2020-2024	Forest	1,868.98	2,540.47	+581.49	+31.11%
	Non-Forest	20,929.10	20,347.61	-581.49	-2.77%

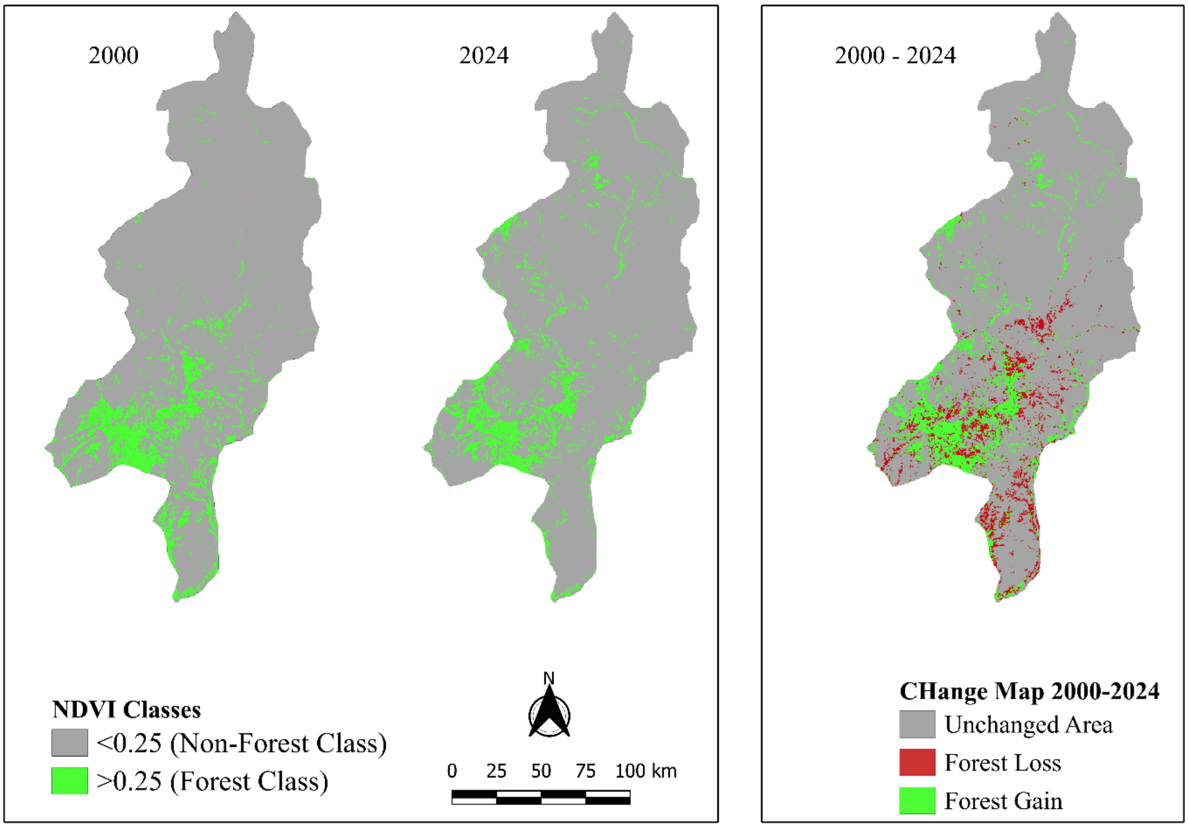

Figure 15. Forest and non-forest land cover classification maps for West Darfur (2000 and 2024), showing distinct periods of degradation and regrowth.

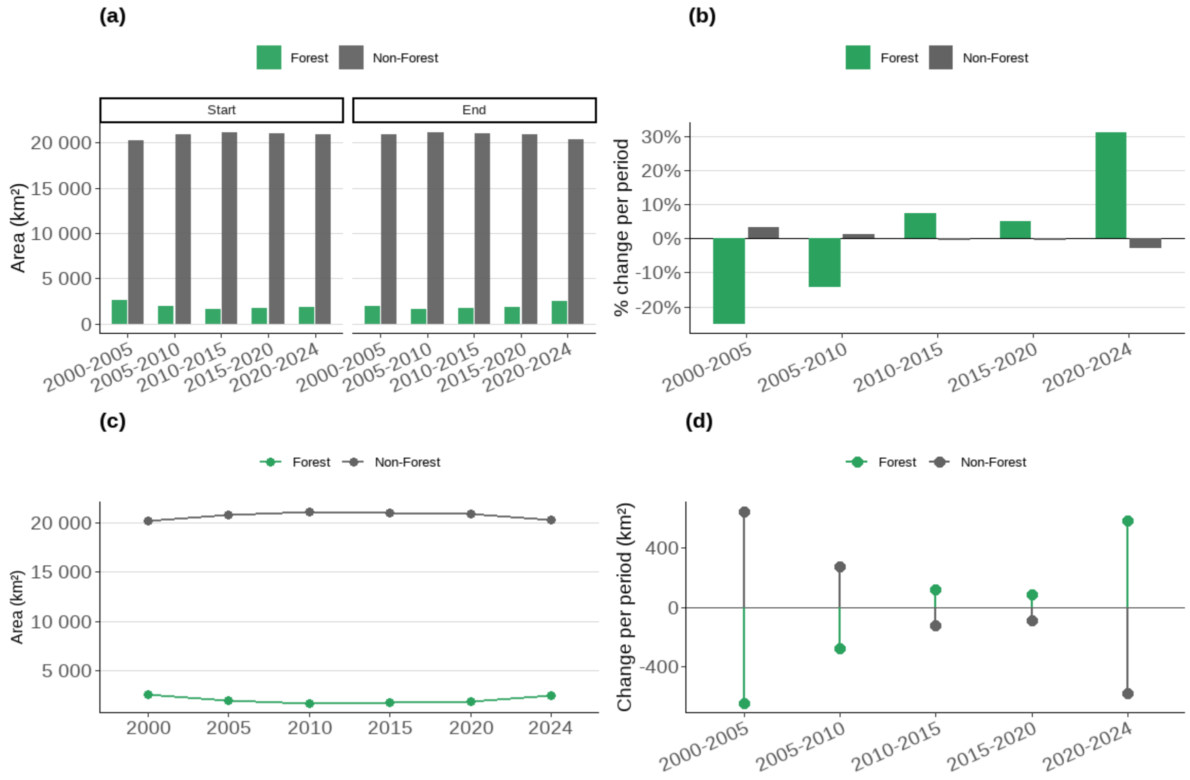

Figure 16. Forest vs non-Forest (a) shows start vs end Area by period, (b) period percentage change, (c) forest vs non-forest area trajectory (2000-2024), and (d) net area change by period.

Non-Forest Dynamics: Inverse Relationship

Non-forested areas expanded in the first decade as forest cover declined. However, post-2010, this trend reversed non-forest land shrank by 10.40%, equaling a loss of 2,001 km², mirroring forest gains. This inverse relationship underscores the landscape-scale shift from degradation to recovery.

4.2.1.3.4 Implications for Regional Ecology and Policy

Despite ongoing instability the net positive forest balance by 2024, is a notable indicator of ecosystem resilience. It suggests that:

- Post-conflict ecological recovery is feasible when rainfall improvement converges with reduced anthropogenic pressures and community-based conservation.
- Forest expansion in West Darfur significantly contributes to ecosystem service restoration, including carbon sequestration, erosion control, and climate regulation.
- However, these benefits remain highly fragile. Renewed displacement, reliance on fuelwood, or returning populations without sustainable land-use plans could reverse this trajectory.

Sustaining these forest gains will require conflict-sensitive land management, investment in alternative energy, and monitoring frameworks to ensure ecological integrity in a rapidly changing socio-political environment.

4.2.1.4 Central Darfur (ESRI Land Cover, 2017-2024)

4.2.1.4.1 Land Cover Changes and Interpretations

To assess LULC transitions in Central Darfur, a high-resolution analysis was conducted using ESRI Land Cover datasets derived from Sentinel-2 imagery at spatial resolution of 10 m. This study focused on the period from 2017 to 2024, capturing evolving spatial patterns across six land cover classes: grassland, forest, cropland, built-up areas, bare ground, and water bodies.

As summarized in Table 15 and visualized in Figure 17 and Figure 18, the landscape remained overwhelmingly grassland-dominated, with 34509.81km^2 (92.89%) in 2017. Forest and cropland covered 5.81% and 0.77%, respectively. Built-up areas and water bodies were negligible, collectively accounting for < 0.1% of the region. However, by 2024, several significant shifts were observed, grassland area decreased by 502.94 km^2, falling from 92.89% to 91.53% of the total land area. While still dominant, this decline reflects increasing land conversion pressure particularly from urban expansion, agricultural intensification, and forest regeneration. This grassland contraction parallels similar transformations across the Sahel where reforestation, agroforestry, and urbanization reconfigure the vegetation matrix (Wang et al., 2022; Yengoh et al., 2015).

Forest cover expanded by 451.79 km^2, representing a 20.92% increase over the seven years. This notable recovery supports the regional regreening narrative observed in West Darfur and is likely driven by the following:

- Improved precipitation and soil moisture availability
- Passive reforestation due to land abandonment in conflict-affected zones
- Community-level agroforestry and afforestation efforts

Forest gains align with the vegetation trends reported by MODIS NDVI and EVI data, suggesting that climatic recovery and reduced land-use pressure in specific zones have enabled natural vegetation regeneration (Funk et al., 2015; Herrmann et al., 2005).

The cropland area increased by 34.17%, reaching 382.81 km^2 in 2024. This trend is consistent with the resettlement of displaced populations, leading to the reactivation of abandoned farmland, smallholder cultivation, and market-oriented agriculture in the peri-urban zones.

This pattern echoes the findings from the Kas locality and El-Salam camp, where IDP-driven agricultural expansion was a dominant landscape driver.

Built-up land surged by 66.72%, increasing from 32.01 km^2 to 53.37 km^2. This explosive growth, though still small in absolute terms, reflects rising settlement densities, IDP camp expansions, and infrastructure development linked to post-conflict rehabilitation and semi-urban transformation. Given Darfur’s history of forced migration and protracted conflict, such patterns signal new socio-spatial dynamics that require land-use planning frameworks.

The bareground declined by 41.50%, shrinking from 163.75 km^2 to 95.80 km^2. This change provides strong evidence of ecological regeneration, possibly aided by the following factors:

- Reduced grazing pressure in conflict-abandoned zones
- Soil stabilization through vegetation recovery
- Enhanced moisture retention and nutrient cycling via reforestation and agroforestry

Such trends reinforce conclusions from climate-vegetation coupling studies, where NDVI recovery is strongly correlated with SPEI-based drought alleviation, especially post-2010.

Although water bodies remained marginal, their area increased by 10.85%, suggesting seasonal water availability improvements, possibly linked to enhanced rainfall, better groundwater recharge, and natural recovery of Wadis and ephemeral wetlands.

Table 15. Land Cover Area Statistics and Changes in Central Darfur (2017-2024)

LULC Class	2017		2024		Change	
	Area (km^2)	Area (%)	Area (km^2)	Area (%)	Change (km^2)	Change (%)
Water	2.35	0.01	2.61	0.01	+0.26	+10.85
Forest	2160.00	5.81	2611.78	7.03	+451.79	+20.92
Crops	285.31	0.77	382.81	1.03	+97.50	+34.17
Built Area	32.01	0.09	53.37	0.14	+21.36	+66.72
Bare Ground	163.75	0.44	95.80	0.26	-67.96	-41.50
Grassland	34509.81	92.89	34006.87	91.53	-502.94	-1.46
Total	37153.24	100.00	37153.24	100.00		

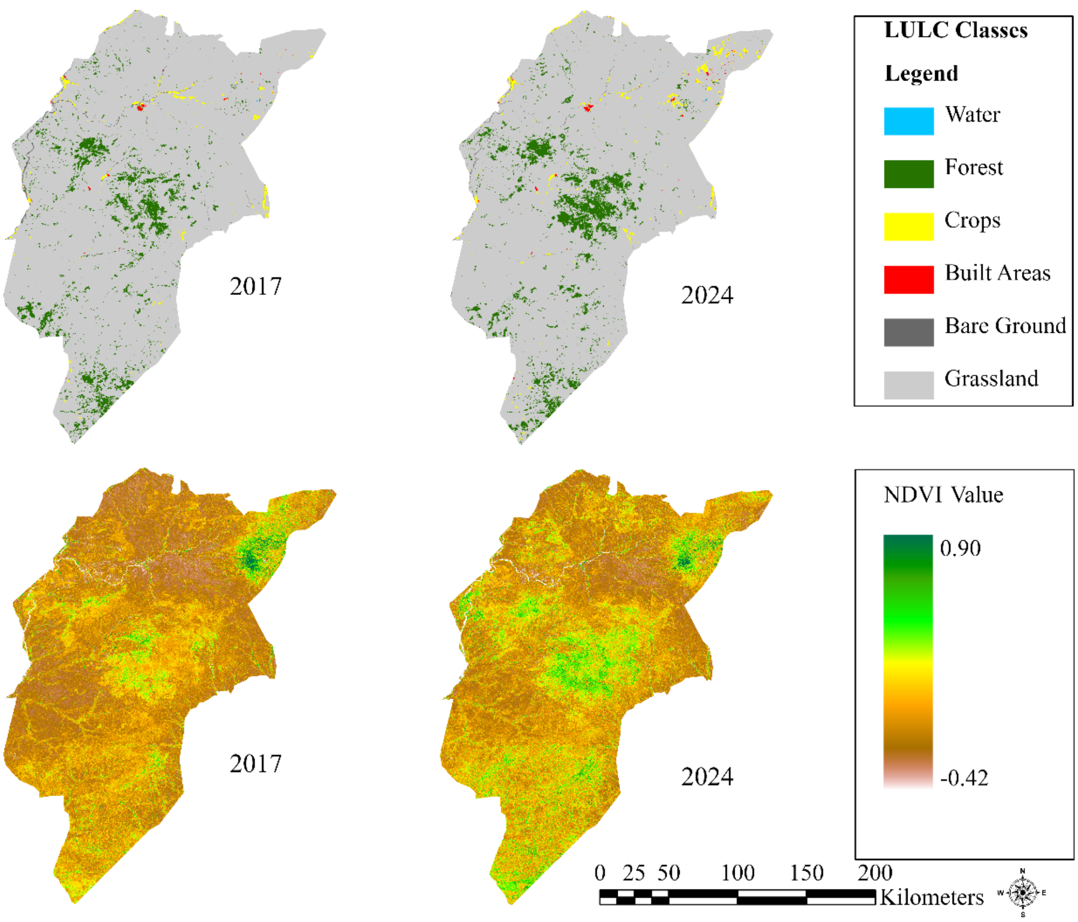

Figure 17. ESRI Sentinel-2-based classified land cover and NDVI Map of Central Darfur for 2017 and 2024, showing dominant grassland distribution, expansion of forest and cropland, and increase in built-up areas over time.

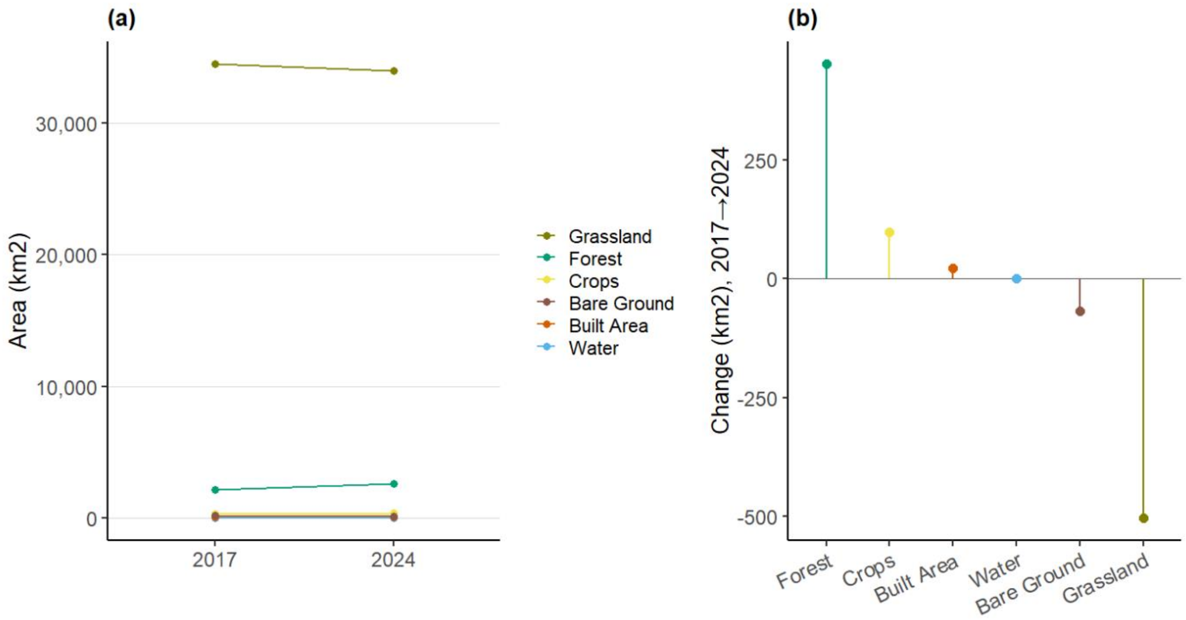

Figure 18. Illustrate (a) change in LULC areas (2017-2024), and (b) net LULC.

Overall, the land cover trajectory of Central Darfur reflects a complex but promising ecological transformation. While grasslands still dominate, the concurrent forest expansion, cropland intensification, and urban spread point to a multi-dimensional recovery shaped by conflict transitions, climate variability, and land-use adaptation.

The sharp decline in bare ground and forest gains mirror broader Sahelian regreening patterns documented by Bai et al., (2008) and (Nicholson et al., 2013). However, these improvements should be interpreted cautiously. Without robust policy instruments and environmental governance, expanding built-up zones and cropland pressure may threaten gains in vegetation and ecosystem services.

This section reinforces the urgent need for conflict-sensitive land-use planning, buffer zoning, and community-led conservation models to sustain recovery in post-conflict landscapes such as Central Darfur.

4.2.1.5 Regional Vegetation Dynamics - Entire Darfur (MODIS-EVI)

4.2.1.5.1 EVI Classification Statistics and Spatial Patterns

To provide a macro-scale assessment of vegetation recovery across Darfur, MODIS-EVI data from 2000 to 2023 were used to classify vegetation into four distinct categories no vegetation, low vegetation, moderate vegetation, and high vegetation. The spatial distribution and temporal progression of these categories are visualized in Figure 19 and Figure 20, and detailed area statistics are provided in (Table 16).

In 2000, nearly half of Darfur's land surface (49.34%) was categorized as having no vegetation, covering approximately 262,131.31 km². By 2023, this figure had dropped to 205,242.44 km² (38.63%), indicating a 21.7% reduction in barren or severely degraded lands. Simultaneously, moderate and high vegetation classes witnessed remarkable expansion: Moderate vegetation increased by 37,682.25 km², rising from 17.97% to 25.06% of the land surface. High vegetation areas more than doubled, growing from 4.90% to 11.35%, with a gain of 34,284 km². These shifts reflected a positive regional trajectory for ecological regeneration and greening.

Table 16. EVI-based Vegetation Cover Statistics in Darfur (2000-2023)

Class	2000 (km²)	2000 (%)	2005 (%)	2010 (%)	2015 (%)	2020 (%)	2023 (km²)	2023 (%)
No Vegetation	262,131.31	49.34	48.85	48.09	49.22	43.93	205,242.44	38.63
Low Vegetation	147,671.25	27.79	25.65	27.47	28.32	28.24	132,593.88	24.96
Moderate Vegetation	95,478.63	17.97	21.42	19.22	18.69	19.80	133,160.88	25.06
High Vegetation	26,023.06	4.90	4.08	5.22	3.77	8.03	60,307.06	11.35
Total Area	531,304.25	100.00	100.00	100.00	100.00	100.00	531,304.25	100.00

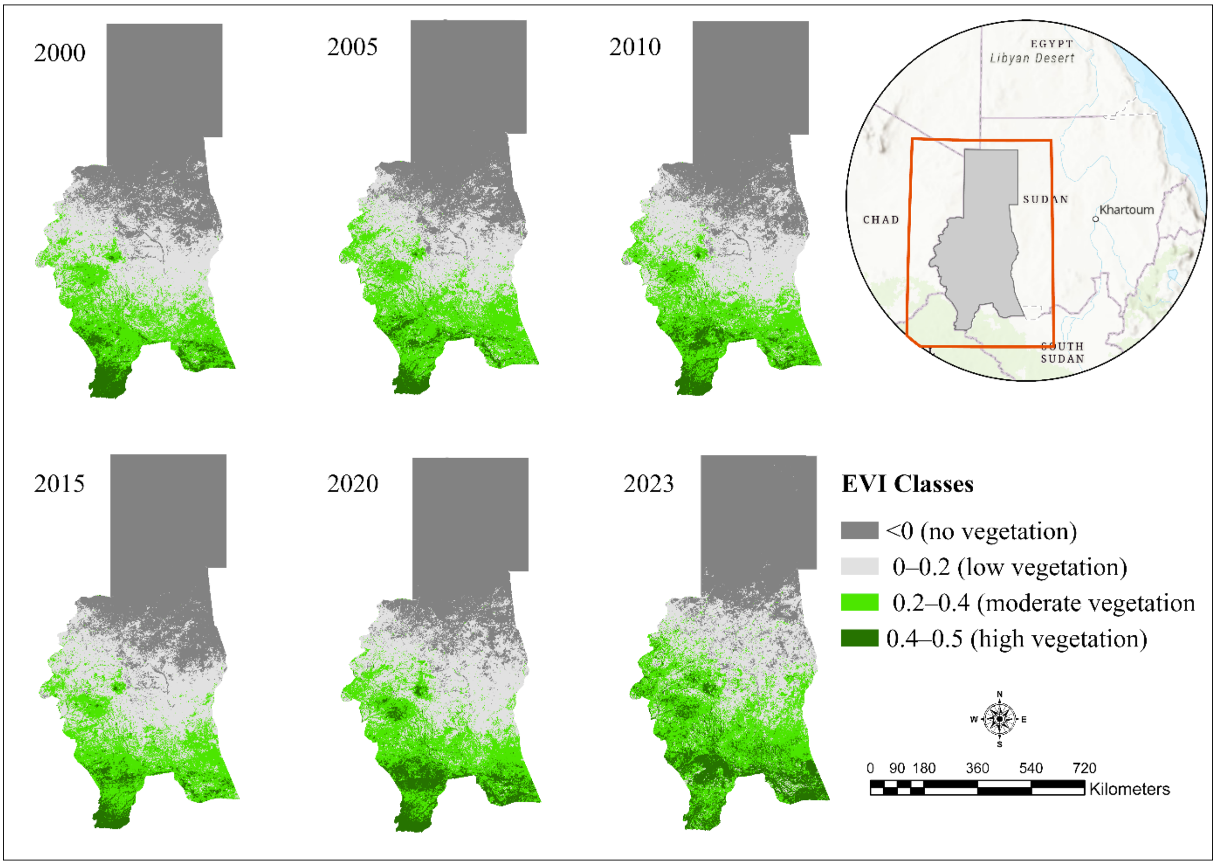

Figure 19. Spatial Distribution of EVI Vegetation Classes in Darfur for the years 2000, 2005, 2010, 2015, 2020, and 2023. Maps show significant decrease in no-vegetation zones and expansion of moderate to high vegetation, particularly in the southern and eastern parts.

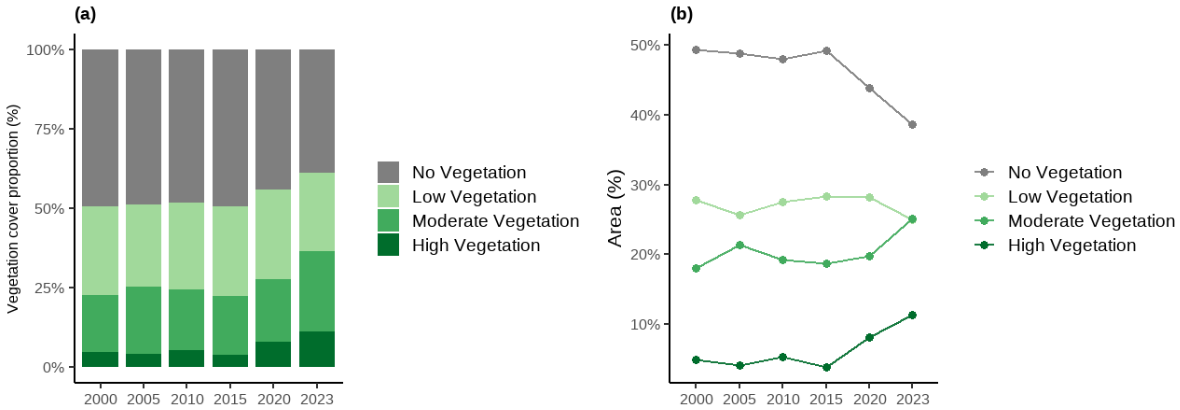

Figure 20. (a) EVI-based vegetation cover composition, and (b) temporal dynamics of vegetation cover over Darfur.

4.2.1.5.2 Patterns, Drivers, and Ecological Implications

The MODIS-EVI trends across the entire Darfur region underscored a significant and measurable greening trend, particularly between 2010 and 2023. Several interlinked drivers explained this trajectory.

4.2.1.5.3 Climatic Moderation and Rainfall Recovery

The post-2010 period was marked by increased rainfall, reduced drought severity, and improved moisture conditions as indicated by SPEI analysis (see Section 4.2.3). These conditions create a more favorable environment for vegetation regrowth, especially in the semi-arid and savannah zones. This aligns with the broader Sahelian climatic cycles reported by (Fensholt et al., 2012), confirming that rainfall recovery was a major contributor to the vegetation resurgence in Darfur.

4.2.1.5.4 Conflict-Induced Land Abandonment and Passive Reforestation

Many agricultural and pastoral zones have been abandoned because of conflicts, reducing anthropogenic pressure on degraded lands. These abandoned zones experienced passive regeneration, as vegetation reclaimed the previously exploited terrain particularly in buffer zones around IDP settlements. This phenomenon echoes similar findings in conflict-affected landscapes in Northern Uganda (Baral et al., 2023) and Sierra Leone (de Jong et al., 2021), where reduced land use intensity facilitated natural ecosystem restoration.

4.2.1.5.5 Community-Based Reforestation and Agroecological Interventions

Reports from Central and West Darfur have highlighted successful community-driven reforestation and agroforestry projects, contributing to localized greening. These initiatives often involve planting drought-tolerant native species, enhancing soil stability, biodiversity, and carbon sequestration. Such projects have also been documented in neighboring Sahelian countries (e.g., Niger and Burkina Faso) as key contributors to the so-called "Sahel Regreening" phenomenon (Reij et al., 2020).

4.2.1.5.6 Policy and Conservation Zones

Although not uniformly enforced, the presence of protected forest zones and traditional community conservation practices may have limited deforestation in key areas, contributing to the observed gains in moderate to high vegetation.

The transition from no/low vegetation to moderate/high vegetation across the large swaths of Darfur signals an ecological rebound with substantial implications: ecosystem services, including erosion control, microclimate regulation, and carbon storage, are likely to improve (see Section 4.2.6). Restoration opportunities exist in degraded areas that show signs of natural recovery as a foundation for climate-smart land management and sustainable development in post-conflict zones. However, this greening trend is spatially heterogeneous and remains vulnerable to renewed conflicts, unsustainable land use, and climatic shocks. Continuous remote sensing monitoring, integrated with ground-truthing and policy interventions, is essential to safeguard these ecological gains.

4.2.2 LULC Future Scenario - Central Darfur (Projection to 2034)

4.2.2.1 Simulation Inputs, Spatial Drivers, and Model Validation

To project future LULC patterns in Central Darfur, this study employed a Cellular Automata-Markov Chain model integrated with an ANN under a BAU scenario. The modeling framework incorporates a range of spatial driving factors that are recognized as key determinants of land dynamics in semi-arid ecosystems. These include Elevation, Slope, Aspect, Proximity to roads, rivers, and towns. illustrates the spatial distribution of these conditioning variables are visualized in Figure 21, which highlights the development corridors and ecological hotspots. Although social indicators such as the number and distribution of IDPs were not explicitly included in the simulation due to the unavailability of spatially and temporally consistent datasets, their influence was indirectly captured through proxy variables including proximity to roads, towns, and existing built-up areas. These variables serve as spatial surrogates for population pressure and settlement expansion, which are closely linked to IDP dynamics in Darfur. Furthermore, the baseline LULC maps (2017-2024) already reflect the cumulative spatial impacts of displacement-driven land transformation. Future research should incorporate gridded population data (e.g., WorldPop, IOM-DTM) or night-time light intensity (VIIRS/DMSP-OLS) as explicit social drives to strengthen socio-environmental coupling in predictive modeling frameworks.

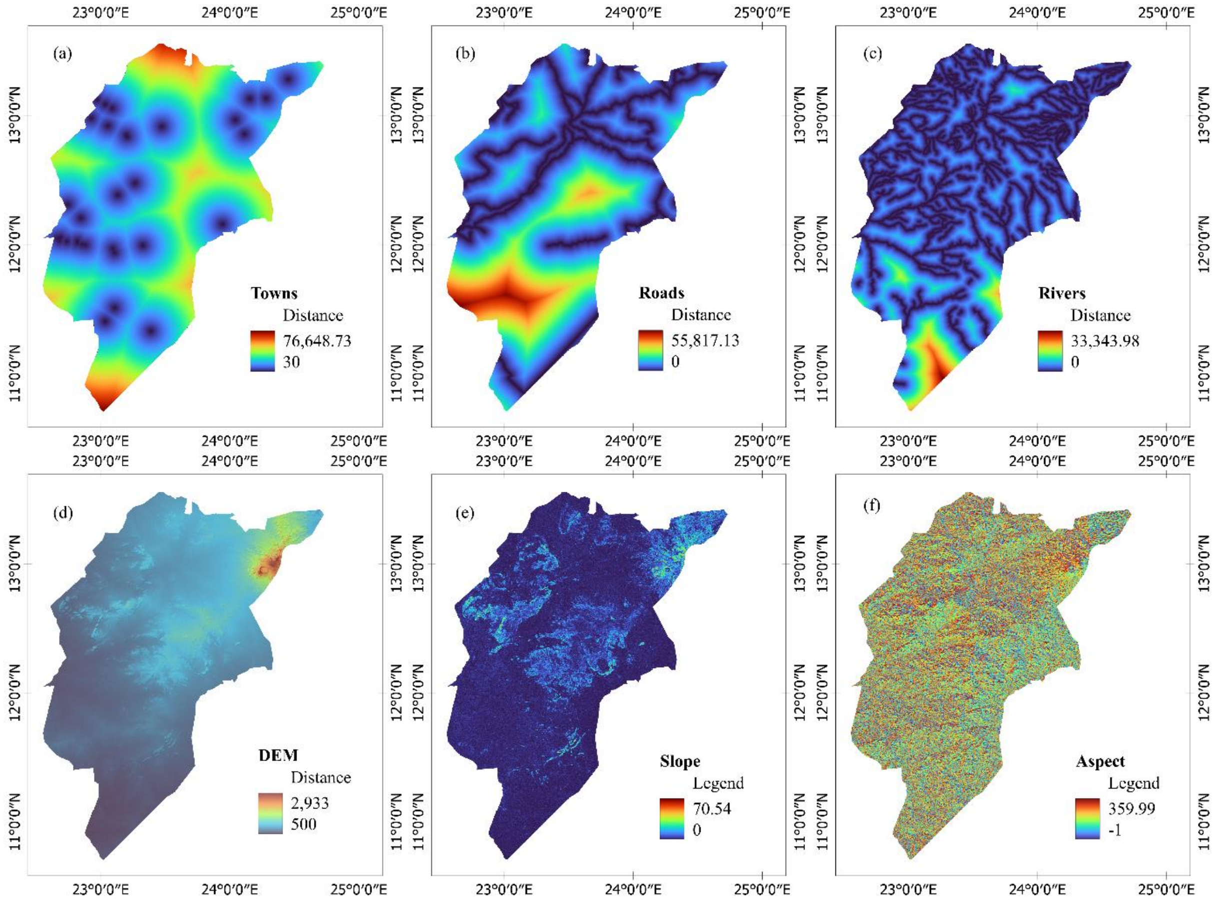

Figure 21. LULC conditioning factors (a) Proximity to towns, (b) Proximity to roads, (c) Proximity rivers, (d) elevation, (e) slope, and (f) aspect.

4.2.2.2 Model Validation and Performance

Before the full simulation, the predictive strength of the model was validated by comparing the 2024 predicted LULC map with the actual classified map for the same year. These results were highly encouraging. The Overall Kappa Index was 0.85, Location Kappa was 0.89, Histogram Kappa was 0.85, and the Correctness Rate was 89.87%. These values, illustrated in Figure 22, confirm the model's high spatial accuracy and temporal consistency, justifying its application in forecasting LULC trajectories up to 2034.

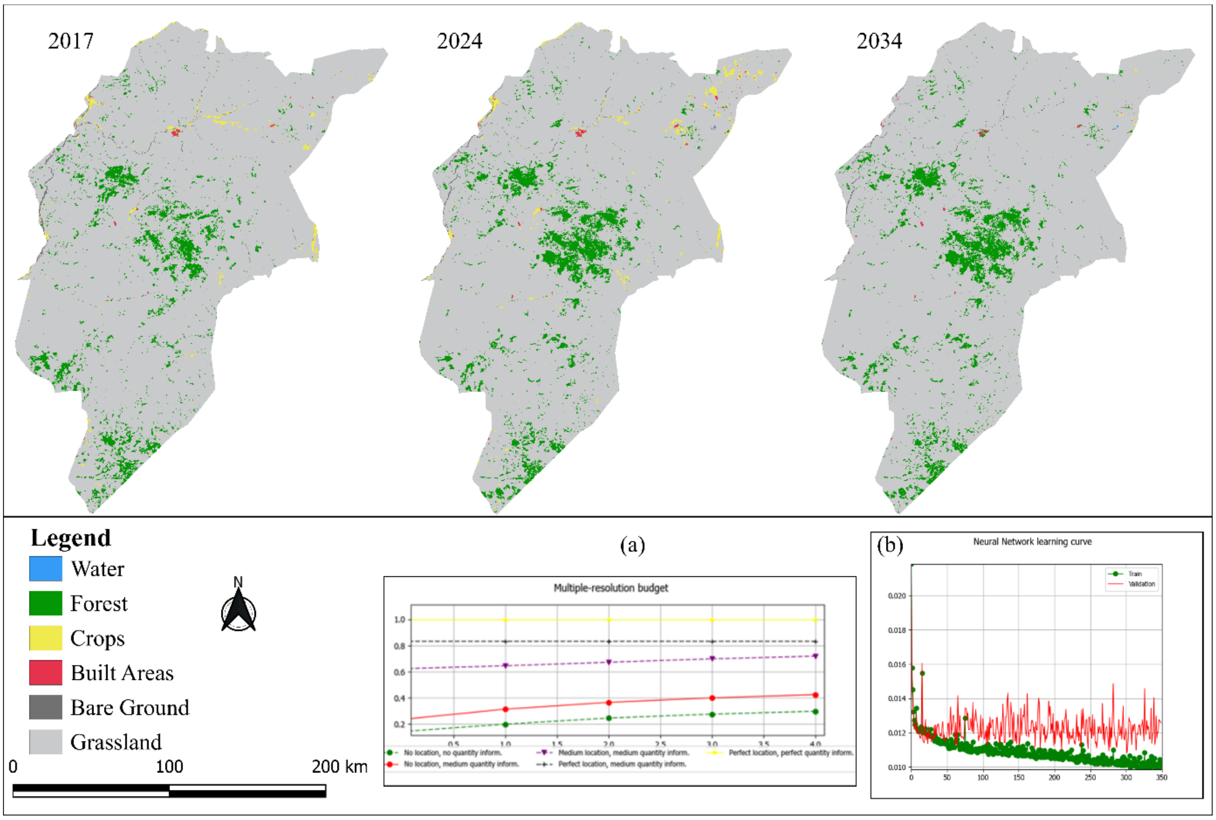

Figure 22. Displays LULC of 2017, 2024 and projected 2034 map, (a) The validation graph comparing observed (2024) and predicted maps, and (b) The ANN training curve.

4.2.2.3 Predicted LULC Changes (2024-2034)

The CA-Markov simulation results (Table 17; Figure 23) revealed a mixed pattern of expansion and contraction across different LULC classes in Central Darfur over the coming decade.

Grassland, projected change +364.00 km^2 (+0.98%). Grasslands are expected to remain the dominant land cover class, continuing their expansive trajectory in recent years. This may reflect natural regeneration of previously abandoned agricultural land or a climatic trend toward increased precipitation.

Forest, Projected change of +7.69 km^2 (+0.02%). The slight increase in forest cover, while modest, may indicate ongoing passive reforestation, supported by reduced anthropogenic pressure or localized community-led afforestation.

Cropland, Projected change –368.46 km^2 (–0.99%). This significant projected contraction of cropland likely reflects the continued displacement of rural populations, land degradation in overused agricultural zones, possible policy shifts favoring conservation or urban expansion, and reduced agricultural viability due to climatic variability. This decline in cropland could undermine local food security, unless mitigated by land restoration, adaptive agriculture, or diversified livelihoods.

Bare Ground, projected change –5.13 km^2 (–0.01%). The steady reduction in bare ground reflects a broader greening trend, consistent with NDVI/EVI and forest cover findings from other regions of Darfur (see Sections 4.2.1.3 and 4.2.1.5).

Built-Up Areas, Projected change of +1.90 km^2 (+0.005%). Urban or peri-urban growth is projected to continue, albeit only modestly. This suggests low-intensity urbanization, possibly linked to resettlement zones or IDP camp consolidation.
Water Bodies, Projected change +0.005 km^2 (+0.001%). While the increase is negligible in spatial terms, it reflects enhanced hydrological conditions tied to higher rainfall and watershed recovery post-2010.

Table 17. Predicted LULC Statistics for 2034 and Changes from 2024 to 2034

LULC Class	2024 Area (km^2)	2024 (%)	2034 Area (km^2)	2034 (%)	Change (km^2)	Change (%)
Water	2.60	0.01	2.61	0.01	+0.005	+0.001
Forest	2611.78	7.03	2619.47	7.05	+7.69	+0.02
Crops	382.81	1.03	14.35	0.04	-368.46	-0.99
Built Areas	53.37	0.14	55.27	0.15	+1.90	+0.005
Bare Ground	95.80	0.26	90.66	0.24	-5.13	-0.01
Grassland	34006.87	91.53	34370.87	92.51	+364.00	+0.98
Total	37153.24	100.00	37153.24	100.00	-	-

This projection highlights both promising ecological trends (e.g., forest and grassland expansion) and concerns regarding agricultural contraction, with significant implications for food security and land management in conflict-affected landscapes such as Central Darfur.

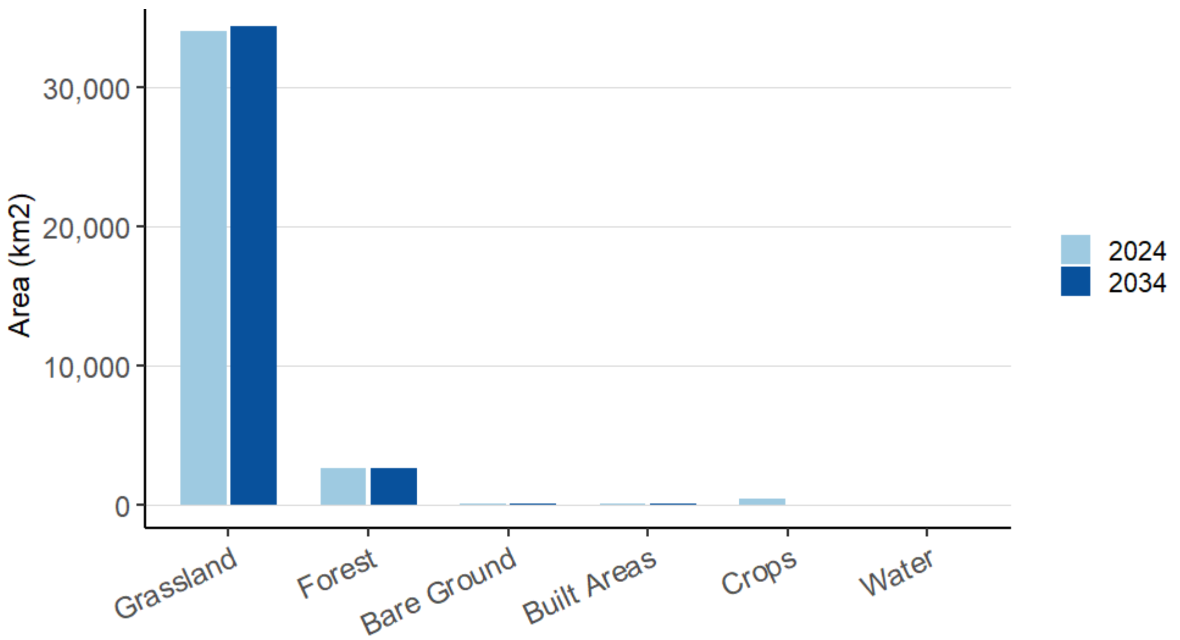

Figure 23. LULC area by classes 2024-2034.

These projections underscore several critical dynamics for Central Darfur's ecological and socio-economic trajectory:
Ecological Resilience: The projected gains in grassland and forest suggest ongoing ecosystem recovery, particularly in areas no longer under intensive cultivation.

Land Use Trade-offs: The decline in cropland contrasts sharply with vegetation and forest gains, revealing a potential land-use trade-off between ecological restoration and food production.

Policy Significance: These outcomes reinforce the importance of integrated land use planning, particularly in post-conflict zones where displaced communities return or resettle.

Future Risk: Without targeted interventions, continued cropland decline may exacerbate food insecurity, especially given the already fragile nature of the agricultural systems in the region.

The CA-Markov simulation illustrates that under current trends; Central Darfur may see modest ecological gains in forest and grassland areas but face serious challenges in maintaining agricultural productivity. This duality highlights the urgent need for climate-smart agricultural practices, conflict-sensitive reforestation policies, and community-based land stewardship programs to balance environmental sustainability with socio-economic recovery.

4.2.3 Vegetation Fragmentation Analysis (2018-2034)

4.2.3.1 Fragmentation Metrics and Temporal Trends

To assess the structural integrity and spatial dynamics of vegetation cover in Central Darfur, a set of landscape fragmentation metrics was computed across three critical timepoints: 2018 (baseline), 2024 (current), and 2034 (projected). These metrics include the Largest Patch Index (LPI), Landscape Proportion (PLAND), Edge Density (ED), and Number of Patches (NP). The results are presented in Table 18 and visualized in Figure 24, highlighting the changes in patch size, configuration, and connectivity.

The LPI increased sharply from 0.5871 to 1.5598 between 2018 and 2024, indicating the significant coalescence of vegetated areas into fewer but larger patches. This phenomenon is typically associated with habitat recovery, improved ecological connectivity, and reduced landscape fragmentation. However, between 2024 and 2034, the LPI remained nearly constant, suggesting a stabilization in patch size expansion, possibly signaling an equilibrium point in landscape restoration under current land-use trends.

The proportion of landscape covered by vegetated land increased gradually over time. This steady gain supports the vegetation recovery narrative observed in the EVI and NDVI trends across Darfur (see Section 4.2.1.5). Although the rate of increase slowed post-2024, this trend reflects ongoing ecosystem regeneration likely driven by improved rainfall, community agroforestry, and post-conflict land abandonment.

Edge density declined between 2018 and 2024, reflecting a simplification of patch boundaries, possibly because of restoration processes or less intensive land use. However, by 2034, a slight uptick in the ED suggests renewed landscape complexity, possibly from new land parceling due to returning populations, agricultural encroachment, and the expansion of fragmented secondary vegetation. This could indicate emerging pressures on restored landscapes, emphasizing the need for long-term zoning and land stewardship policies.

The decline in patch number between 2018 and 2024 reinforces the LPI and ED observations, suggesting a phase of spatial consolidation and vegetation connectivity enhancement. However, the rebound by 2034 indicates renewed fragmentation. This could result from increased land demand, settlement expansion, or climate-induced vegetation shifts, signaling a fragile balance between recovery and disturbance.

Table 18. Fragmentation Metrics for Central Darfur (2018-2034)

Year	Largest Patch Index	Landscape Proportion	Edge Density (m/m²)	Number of Patches
2018	0.5871	0.029164	0.00073275	29,631
2024	1.5598	0.035260	0.00072140	26,073
2034	1.5594	0.035368	0.00074965	28,598

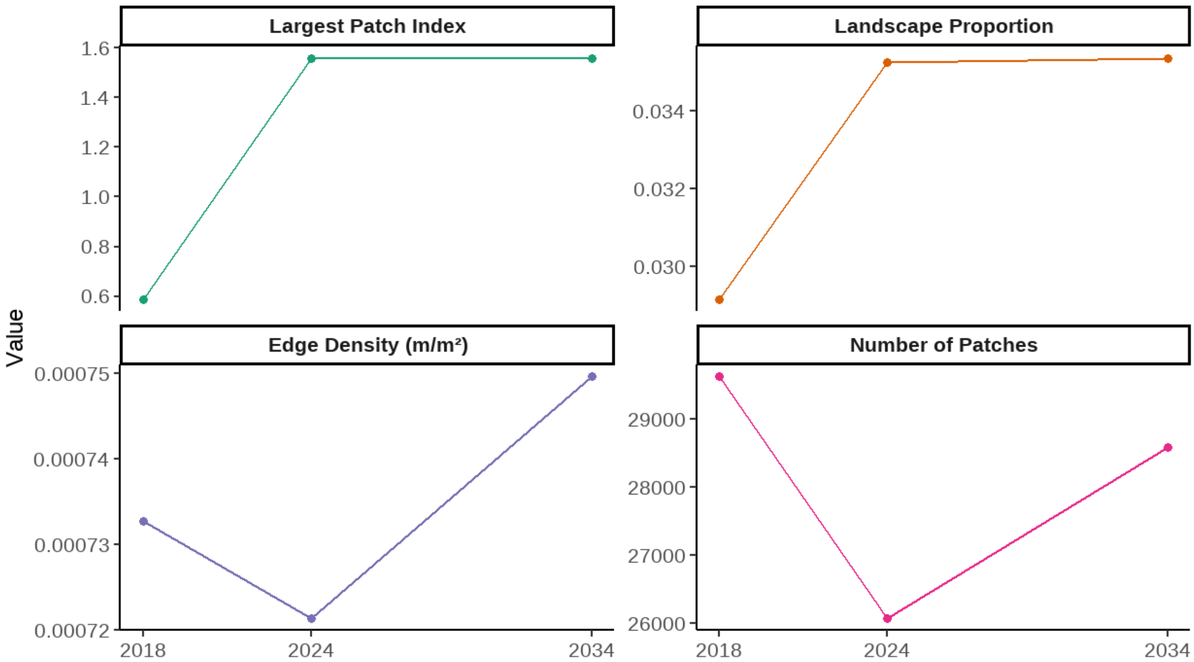

Figure 24. Illustrate the fragmentation metrics by indicator.

The vegetation fragmentation trends from 2018 to 2034 reflect a non-linear ecological trajectory: The period 2018-2024 was characterized by patch consolidation, indicating successful ecosystem recovery and reduced disturbance, likely benefiting from favorable climate conditions, reduced land-use pressure, and community-led interventions. The projected post-2024 phase revealed incipient re-fragmentation, necessitating proactive landscape planning to avoid the reversal of ecological gains.

These dynamics underscore the need for integrated land governance and long-term ecological monitoring in post-conflict settings. Continued recovery is not guaranteed and remains highly sensitive to resettlement patterns, resource use intensity, and climate variability.

4.2.4 Ecosystem Services Valuation (ESV) Analysis

To estimate the economic value of ESVs provided by different LULC types in Darfur, this study applied the benefit transfer method, which is suitable in data-scarce regions (Champ et al., 2003; Costanza et al., 1998; Rotich & Ojwang, 2021), we used adjusted biome-level coefficients from (Kindu et al., 2016), who developed modified estimates appropriate for East African ecological contexts.

Each LULC class in our dataset was matched with a representative biome and assigned a corresponding monetary value (US$ per hectare per year), as shown in (Table 19).

Table 19. LULC Types, Equivalent Biomes, and Valuation Coefficients

LULC type	Equivalent biome	Ecosystem service Coefficient (US$ ha^{-1} $year^{-1}$)
Forest	Tropical Forest	986.69
Crops	Cropland	225.56
Grassland	Grassland	293.25
Water	Water	8103.5
Bare ground	Bareland	0
Built-up area	Urban	0

As shown in Table 20, grasslands emerged as the dominant ESV contributor across all time points, consistently exceeding US$ 997 million annually. This dominance reflects both the spatial extent of grasslands in Central Darfur and their multifunctional ecological roles including erosion control, carbon storage, and water regulation.

Forests ranked second, with values increasing from US$ 213.12 million in 2017 to US$ 258.46 million in 2034. This upward trend aligns with observed forest regeneration patterns (Section 4.2.1.3), particularly in West and Central Darfur, where reforestation and agroforestry initiatives contributed to vegetation densification.

In contrast, Cropland exhibited a sharp decline in ecosystem value, dropping from US$ 8.63 million in 2024 to just US$ 0.32 million in 2034, corresponding with LULC projections (Section 4.2.2.2) that indicate a decrease in agricultural land. This underscores a key trade-off: while ecosystem health is improving overall, provisioning services (like food production) may be at risk, with potential implications for food security.

Though spatially minor, water bodies contributed disproportionately high value due to their elevated per-hectare coefficients. Values rose modestly from US$ 1.91 million in 2017 to US$ 2.12 million in 2034, reflecting both improved water availability and the critical importance of aquatic ecosystems in arid regions.

Table 20. Total ESVs (Million USD) by LULC Type (2017-2034)

LULC type	2017 ESV (US$)	2024 ESV (US$)	2034 ESV (US$)
Water	1.91	2.11	2.12
Forest	213.12	257.70	258.46
Crops	6.44	8.63	0.32
Grassland	1,012.00	997.25	1,007.93
Built-up area	0	0	0
Bare ground	0	0	0
TOTAL	**1,233.47**	**1,265.70**	**1,268.83**

As visualized in Figure 25, the total ESV across Darfur rose from US$ 1,233.47 million in 2017 to US$ 1,268.83 million by 2034, marking a net gain of US$ 35.36 million (2.87%). The peak value occurred in 2024, followed by a plateau, indicating ecological stabilization after forest recovery and reforestation (Section 4.2.1.4).

While this increase is modest, it reflects positive ecological recovery, especially in grassland and forest ecosystems, despite ongoing conflict pressures and population displacement. The steep post-2024 drop in cropland value was effectively offset by gains in regulating and supporting services, revealing a functional shift in Darfur's ecosystems toward sustainability and resilience.

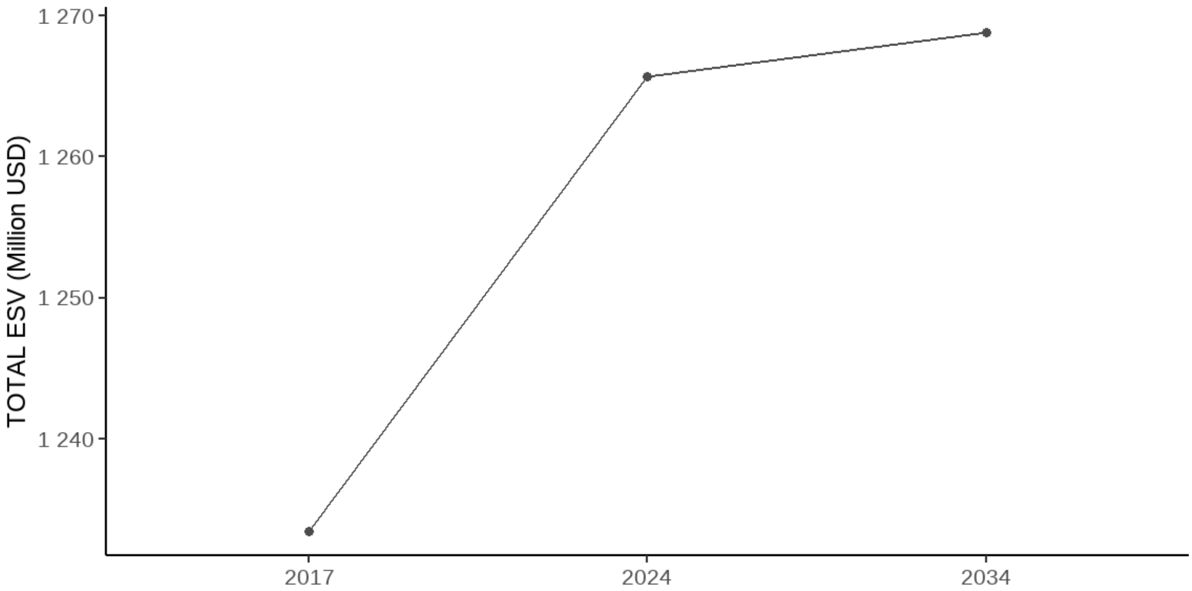

Figure 25. The total ESV values from 2017-2034.

4.2.4.1 Ecosystem Service Category Trends

Grouped into broader service types (Table 21; Figure 26), the trends showed distinct trajectories, provisioning services (e.g., food, and water) declined slightly due to cropland contraction. Regulating Services (e.g., water purification, carbon sequestration) rose steadily from US$ 652.06 million in 2017 to US$ 678.38 million in 2034, reflecting increased vegetation cover and land restoration. Supporting Services (e.g., nutrient cycling, and soil formation) showed moderate improvement, suggesting recovery of basic ecosystem processes. Cultural Services (e.g., aesthetic, spiritual, and recreational) remained the smallest in absolute value but improved incrementally. These results indicate a resilient ecological transition: while direct human benefits (such as food) may have declined, indirect ecosystem services that support long-term sustainability have expanded.

Table 21. Grouped Ecosystem Service Values (Million USD)

Category	ESV		
	2017	**2024**	**2034**
Cultural	4.24	4.51	4.54
Provisioning	439.74	441.69	439.15
Regulating	652.05	673.35	678.37
Supporting	137.42	146.14	146.74
TOTAL	**1,233.47**	**1,265.70**	**1,268.83**

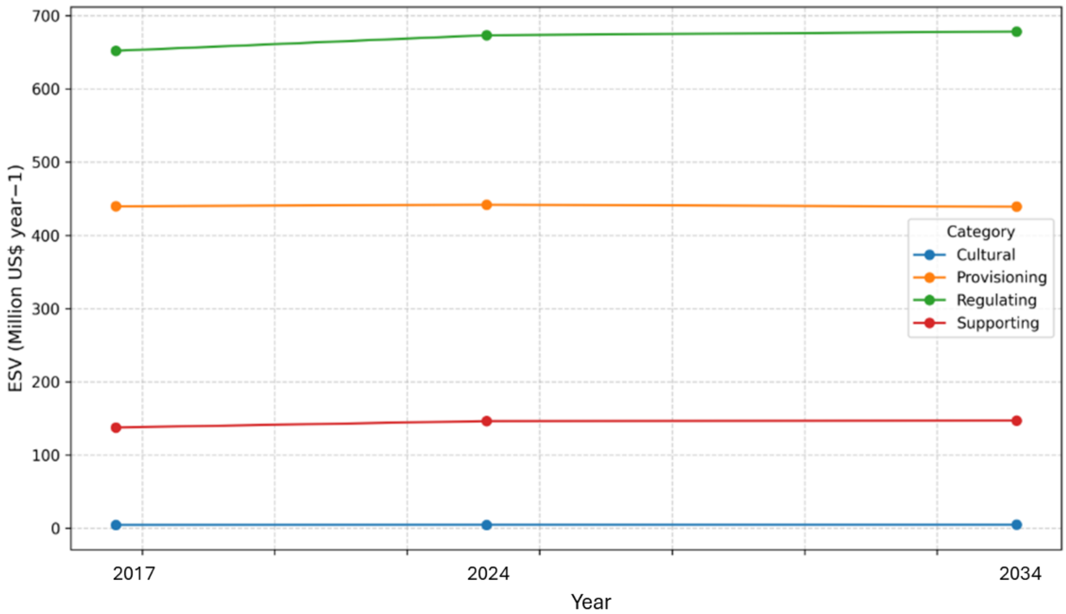

Figure 26. Grouped ecosystem services trends in Darfur (2017, 2024, and 2034).

4.2.4.2 Breakdown of Individual Ecosystem Services

At the service level (Table 22; Figure 27), the most economically significant contributors in 2034 were:

Water treatment: US$ 334.76 million

Erosion control: US$ 163.85 million

Food production: Declining to US$ 412.35 million

Pollination & biological control: Contributing consistently, reflecting vegetation recovery

This breakdown highlights the multifunctionality of Darfur's ecosystems. Grasslands and forests not only provide direct resources but also regulate environmental stability, which is a critical buffer in climate-vulnerable regions.

Table 22. Individual Ecosystem Services (ESV in million USD per year).

	ESV_f (US$)		
ECOSYSTEM SERVICES	**2017**	**2024**	**2034**
Biological control	80.05	79.13	79.08
Climate regulation	48.16	58.24	58.41
Cultural	0.43	0.52	0.52
Disturbance regulation	1.08	1.30	1.31
Erosion control	152.99	162.60	163.85
Food production	417.59	414.95	412.34
Gas regulation	27.11	27.37	27.64
Genetic resources	8.85	10.70	10.74
Habitat / refugia	3.73	4.51	4.53
Nutrient cycling	39.83	48.16	48.30
Pollination	88.24	87.45	87.85
Raw material	11.06	13.38	13.42
Recreation	3.81	3.99	4.02
Soil formation	5.61	6.01	6.05
Water regulation	12.931	13.19	13.307
Water supply	2.226	2.642	2.649
Water treatment	329.713	331.493	334.764
TOTAL	**1,233.47**	**1,265.70**	**1,268.83**

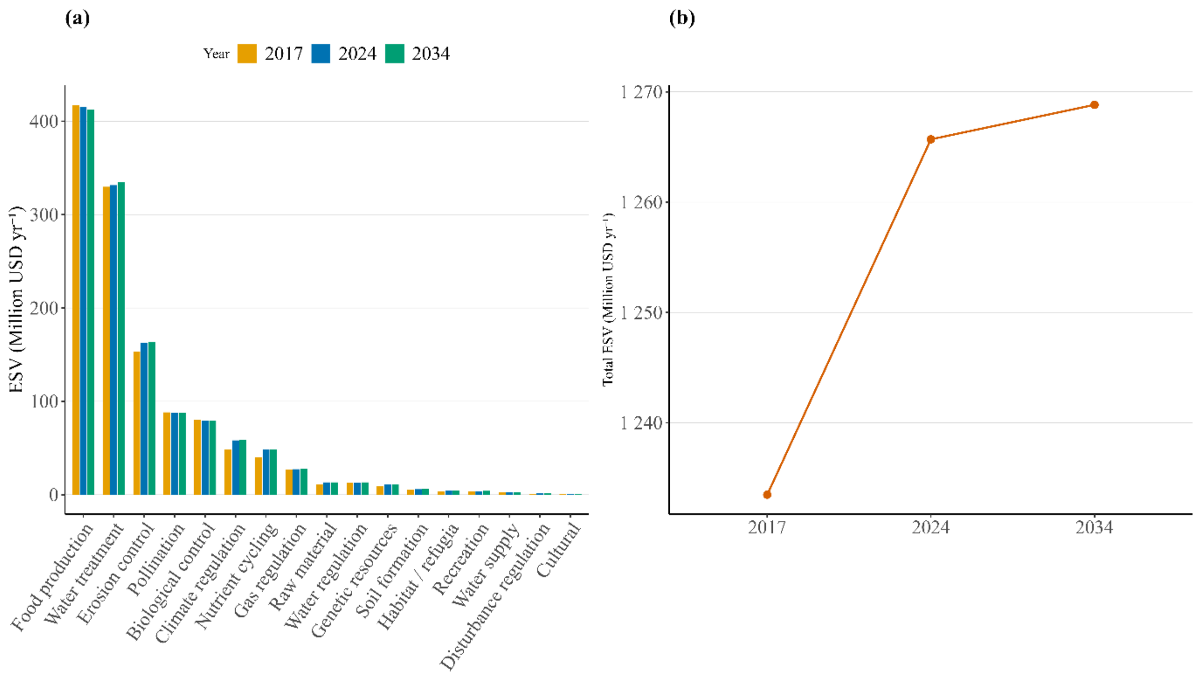

Figure 27. Illustrate (a) ESV and (b) total ESV of 2017, 2024, and 2034.

The ESV analysis demonstrated that ecosystem value is shifting from short-term provisioning functions to long-term regulatory and supporting functions. This evolution supports ecosystem resilience and climate buffering capacity but poses challenges for agricultural productivity and food systems in conflict-affected areas.

In conflict-displaced landscapes, such as Darfur, land use planning must strike a balance between ecological regeneration and socioeconomic recovery. The integration of forest conservation, sustainable agriculture, and climate-adaptive practices is essential for maintaining and enhancing ecosystem service flow.

4.2.4.3 Sensitivity Analysis of Ecosystem Service Value

CS analysis provides insight into how responsive total ESVs are proportional to changes in the unit value coefficients of each LULC type. It captures the elasticity of ESVs with respect to individual LULC contributions.

Key results and interpretation as shown in Table 23, the analysis from 2017 to 2034 reveals that grassland and forest are the two dominant contributors to ESV, with the highest CS values across all time points.

Table 23. ESV Sensitivity Analysis

LULC type	2017 CS (%)	2024 CS (%)	2034 CS (%)
Water features	0.15	0.17	0.17
Forest	17.28	20.36	20.37
Cropland	0.52	0.68	0.03
Grassland	82.04	78.79	79.44
Built-up area	0.00	0.00	0.00
Bareland	0.00	0.00	0.00

Grassland maintained the highest influence on total ESV, with CS values ranging from 82.04% in 2017 to 78.79% in 2024 and slightly declining to 76.94% in 2034. This consistent dominance is attributed to both its expansive spatial coverage in Central Darfur (see Section 4.2.1.4) and its high ecological functionality in regulating services, such as carbon sequestration, erosion control, and water regulation. Even small fluctuations in the grassland coefficient would significantly alter the total ESV, reinforcing the need for the careful calibration of grassland-related assumptions in ecosystem service models.

Forests show a steadily increasing CS contribution, rising from 17.28% in 2017 to 20.37% in 2034. This trajectory mirrors the observed patterns of forest regeneration (Sections 4.2.1.3 and 4.2.1.4), supported by improved climatic conditions, community-led afforestation, and reduced disturbance in certain regions. The upward trend in forest sensitivity indicates that forest restoration is not only ecologically beneficial but also economically significant from an ecosystem services perspective.

In contrast, cropland exhibited very low and declining CS values, dropping sharply from 0.53% in 2017 to just 0.03% in 2034. This marginal influence reflects both the reduced spatial extent of cropland (Section 4.2.2.2) and its relatively low ecosystem service coefficient compared to more ecologically intensive land cover. This decline could also indicate land abandonment or displacement-driven conversion to non-agricultural use, especially in conflict-affected zones.

Water bodies showed a slight increase in CS from 0.15% to 0.17%, which is consistent with minor increases in water coverage and improved surface water management. Despite their small area, water bodies have high per-unit ecosystem service values, especially for provisioning and regulating services such as irrigation, recharge, and biodiversity.

As expected, built-up areas and barelands consistently returned a CS of 0.00% throughout the study period. This indicates their negligible role in generating ecosystem services and highlights them as net ecological sinks, often associated with environmental degradation, urban encroachment, and displacement-induced settlement expansion.

The sensitivity analysis provides compelling evidence that ecosystem service valuations in Darfur are heavily skewed towards natural and semi-natural ecosystems, particularly grasslands and forests. Their large area, high ecological productivity, and multifunctional roles make them pivotal for sustaining ecological resilience and climate regulation in fragile, conflict-prone regions. This also implies that conservation and restoration strategies targeting these two land types offer the highest return on investment, both in ecological and economic terms. In contrast, the diminishing influence of croplands suggests an urgent need to reconcile agricultural productivity with ecological sustainability, particularly when considering the food security concerns discussed earlier (Section 4.2.4.1). In planning for future land use, sensitivity analysis should inform land-use trade-offs, prioritize ecosystem-supporting land cover, and integrate resilience-building policies for both human and natural systems.

4.2.5 Climate-Vegetation Interaction Analysis

Understanding the complex interactions between climatic variability and vegetation dynamics is essential in ecologically fragile and conflict-affected regions such as Darfur. Ecosystem productivity in such areas is tightly coupled with seasonal precipitation, drought intensity, and land use pressure (Funk et al., 2015; Nicholson et al., 2013). This section synthesizes vegetation index trends derived from NDVI and EVI with climatic indicators including precipitation (CHIRPS), temperature (MERRA-2), and drought stress (SPEI) to analyze spatial and temporal vegetation responses across Darfur from 2000 to 2023.

4.2.5.1 Temporal Trends and Correlation Patterns

Time-series decomposition using the BFAST model revealed distinct seasonal and long-term patterns of vegetation greenness across Darfur. The model detected sharp structural breaks in greenness trends corresponding to prolonged drought episodes, conflict-induced displacement, and major climate anomalies. For example, the 2006-2010 period a time of intensified displacement and rainfall scarcity, was characterized by pronounced NDVI declines, whereas post-2010 years exhibited a gradual upward trend in vegetation indices, aligning with increased precipitation and partial land abandonment in conflict zones (see also Section 4.2.1.3).

This temporal segmentation confirms that Darfur vegetation is highly responsive to both short-term climatic fluctuations and long-term socio-ecological disruptions. The identification of non-linear vegetation trajectories supports findings from other semi-arid regions of Africa, where ecosystem transitions often follow threshold dynamics rather than gradual trends (de Jong et al., 2021).

4.2.5.2 Pearson Correlation Analysis

Pearson's correlation analysis was used to statistically quantify the influence of climatic variables on vegetation performance (Figure 28). The results showed that:

Precipitation and NDVI/EVI had a strong positive correlation ($r = 0.72$, $p < 0.001$), underscoring that rainfall was the dominant driver of vegetation health. This was particularly evident in rain-fed agro-ecological systems such as Kas and Central Darfur, where smallholder farming depends heavily on seasonal rainfall.

Temperature and NDVI were negatively correlated ($r = -0.21$, $p < 0.001$), although its week correlation it might suggest that elevated temperatures may suppress photosynthetic activity by increasing evapotranspiration and inducing heat stress, particularly during the dry season. This aligns with the findings of (Fensholt et al., 2012), who highlighted the thermal sensitivity of Sahelian vegetation.

Elevation and NDVI showed no significant correlation ($r = 0.0032$, $p = 0.074$), reinforcing that topographic influence is minimal across Darfur's relatively flat semi-arid landscape, apart from the localized anomalies around the Jebel Marra region.

These relationships collectively reinforce the idea that precipitation is the principal climatic determinant of vegetative productivity in Darfur, with temperature becoming increasingly relevant under climate change scenarios.

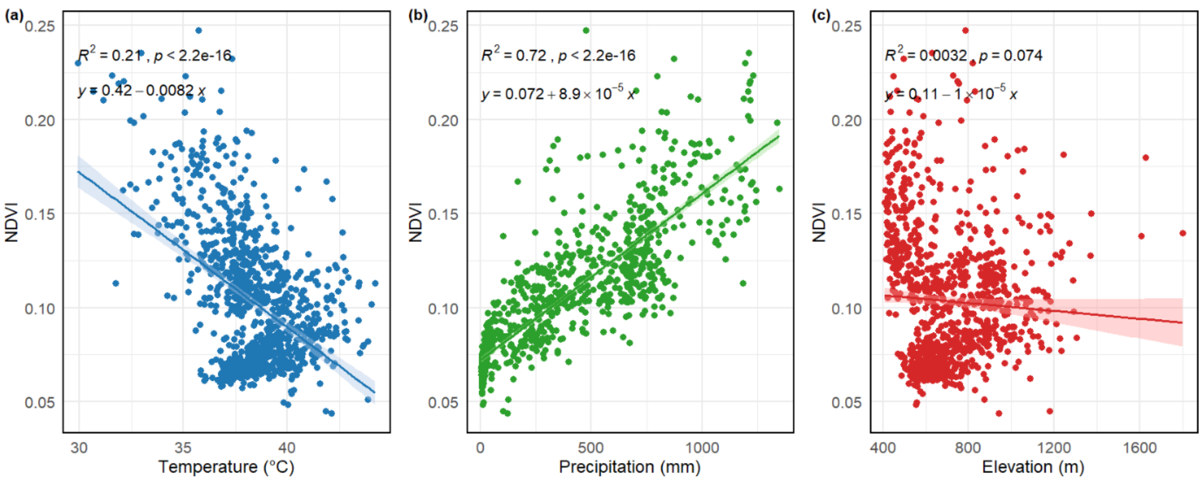

Figure 28. Pearson correlation of NDVI with (a) temperature, (b) precipitation, and (c) elevation (2000-2023).

4.2.5.3 Station vs Satellite Climate Consistency

Assessing the consistency between remotely sensed climate data and ground-based observations is critical for validating satellite-derived products for environmental monitoring in regions with scarce data. In this study, the CHIRPS and MERRA-2 temperature data were validated against available meteorological station records across Darfur.

The results indicated a moderate to strong positive correlation between CHIRPS and ground-measured precipitation ($r = 0.53$), demonstrating that CHIRPS reliably captures rainfall variability in this semi-arid region (Figure 29 a). In parallel, the MERRA-2 temperature data exhibited a moderate correlation with the observed station-based temperature records ($r = 0.47$), indicating acceptable agreement despite some variance (Figure 29 b).

These findings confirm the utility of CHIRPS and MERRA-2 as robust proxies for hydroclimatic assessment in conflict-affected and meteorologically under-instrumented zones such as Darfur. The ability to utilize these satellite datasets compensates for the frequent absence or incompleteness of conventional ground monitoring networks due to prolonged insecurity, infrastructural damage, and institutional fragility.

These results are consistent with those of prior validation studies. (Dinku et al., 2018) demonstrated CHIRPS' strong performance in rainfall representation across East Africa, particularly in agro-ecological transitional zones. Similarly, (Zambrano-Bigiarini et al., 2017) affirmed its suitability for climate assessments in low-data environments, especially for drought monitoring and agricultural planning.

The significance of this validation extends beyond Darfur. This affirms the broader applicability of satellite-derived climate datasets for longitudinal, regional-scale environmental analyses in crisis-prone areas where field data collection is constrained. This approach not only enhances replicability and scientific rigor but also supports the design of early warning systems and climate adaptation strategies in vulnerable landscapes.

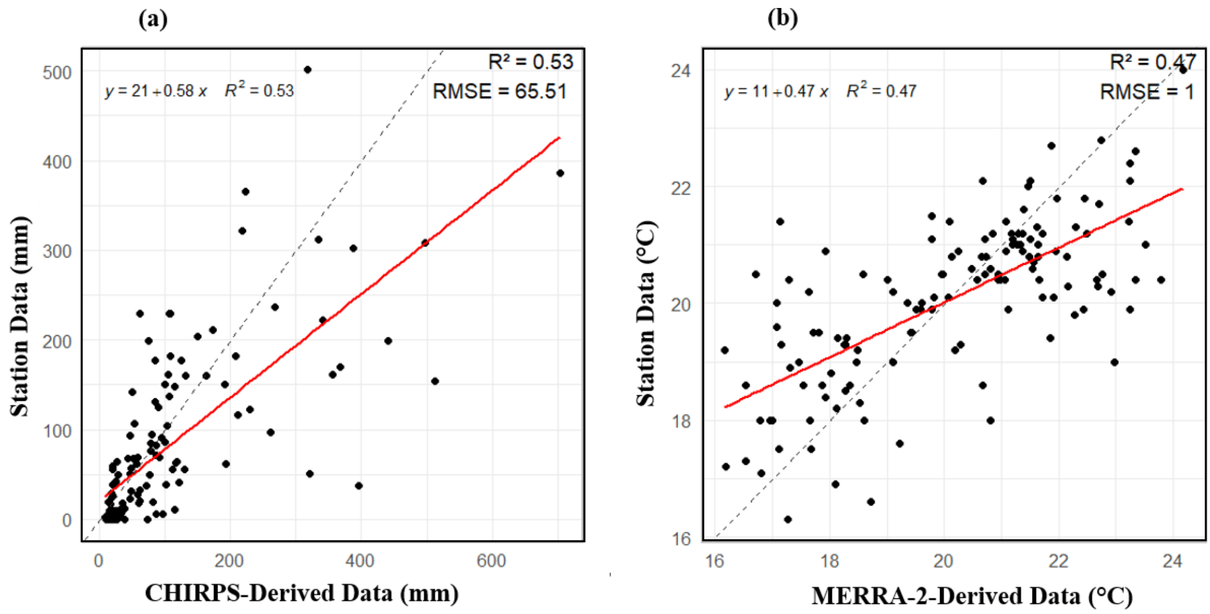

Figure 29. Correlation between satellite-derived and observed station data: (a) observed precipitation compared with CHIRPS data, (b) Station-measured temperature compared with MERRA-2 temperature data.

4.2.5.4 BFAST Breakpoint Detection

Further insight into long-term climate-vegetation dynamics was obtained using BFAST trend analysis of SPEI-12 (12-month drought index). The analysis revealed distinct breakpoints in 1990, 2000, and 2010, which corresponded to documented episodes of severe drought, conflict escalation, and displacement surges in Darfur (Adaawen et al., 2019) (Figure 30).

These breakpoints reflect periods of ecosystem stress and regime shifts, during which vegetation systems exhibit non-stationary behavior and reduced recovery potential. Notably, areas near IDP settlements and zones with intense land use pressure showed persistent NDVI suppression post-breakpoints, indicating compounded vulnerability due to both climatic and anthropogenic stressors.

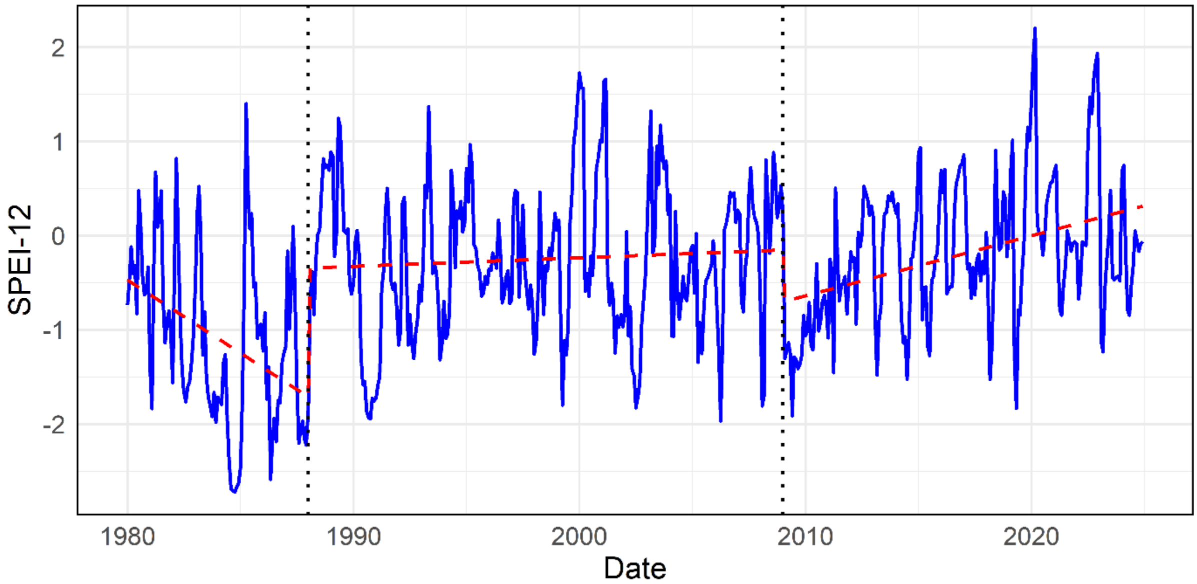

Figure 30. BFAST trend analysis for the 12-month SPEI index (1980-2023) showing breakpoints in climatic regime associated with ecosystem stress and degradation.

The findings of this section provide a multifactorial understanding of vegetation responses to climate variability in Darfur.
Rainfall is the dominant control, but its effect is modulated by temperature extremes, land use practices, and socio-political factors such as displacement and resettlement.
Remotely sensed climate proxies like CHIRPS and MERRA-2 are sufficiently reliable for environmental modeling in inaccessible conflict zones.
The non-linear behavior of vegetation systems, captured through BFAST and breakpoint analysis, underscores the importance of resilience-based management and early warning systems for ecosystem monitoring.
Longitudinal vegetation trends show signs of recovery post-2010, which aligns with the observed improvements in forest cover, grassland extent, and ecosystem service value (Sections 4.2.1.3, 4.2.2.2, and 4.2.4).

4.2.6 Rainfall and Temperature Trends

Understanding long-term rainfall and temperature variability is essential for evaluating the ecological sensitivity of semi-arid landscapes such as Darfur, where environmental and socio-political fragility intersect. This section synthesizes historical climate records (1981-2024) with spatial and statistical analyses to uncover decadal changes, inter-zonal differences, and climate variability impacts across North, West, and South Darfur. Emphasis is placed on rainfall patterns as the principal determinant of vegetation recovery, drought resilience, and agricultural viability.

4.2.6.1 Rainfall Trends

Historical Rainfall Patterns (1981-2024)

Longitudinal rainfall analysis based on CHIRPS datasets revealed an overall positive trend in annual precipitation across all three Darfur zones, although with distinct zonal characteristics (Figure 31).

North Darfur displayed a gradual upward trend, with notable peaks in 1997, 2001, 2007, and 2021, interrupted by a sharp decline in 2020. Post-2013 data showed a higher frequency of above-average rainfall years, indicating intensification of seasonal rainfall variability (Figure 31a).

West Darfur exhibited the most consistent increasing trend, with significant jumps in rainfall observed during 1997 and after 2015. The stable precipitation trajectory of this zone may support ongoing forest regeneration, as noted in Section 4.2.1.3 (Figure 31b).

South Darfur recorded the steepest rainfall increase across the time series. Significant spikes occurred in 1983, 1991, 2002, 2006, and 2011, supporting the episodic vegetation rebound documented in the previous sections (Figure 31c).

These spatially divergent rainfall patterns are closely tied to vegetation health and ecosystem services, particularly in IDP-influenced and reforestation-prone areas.

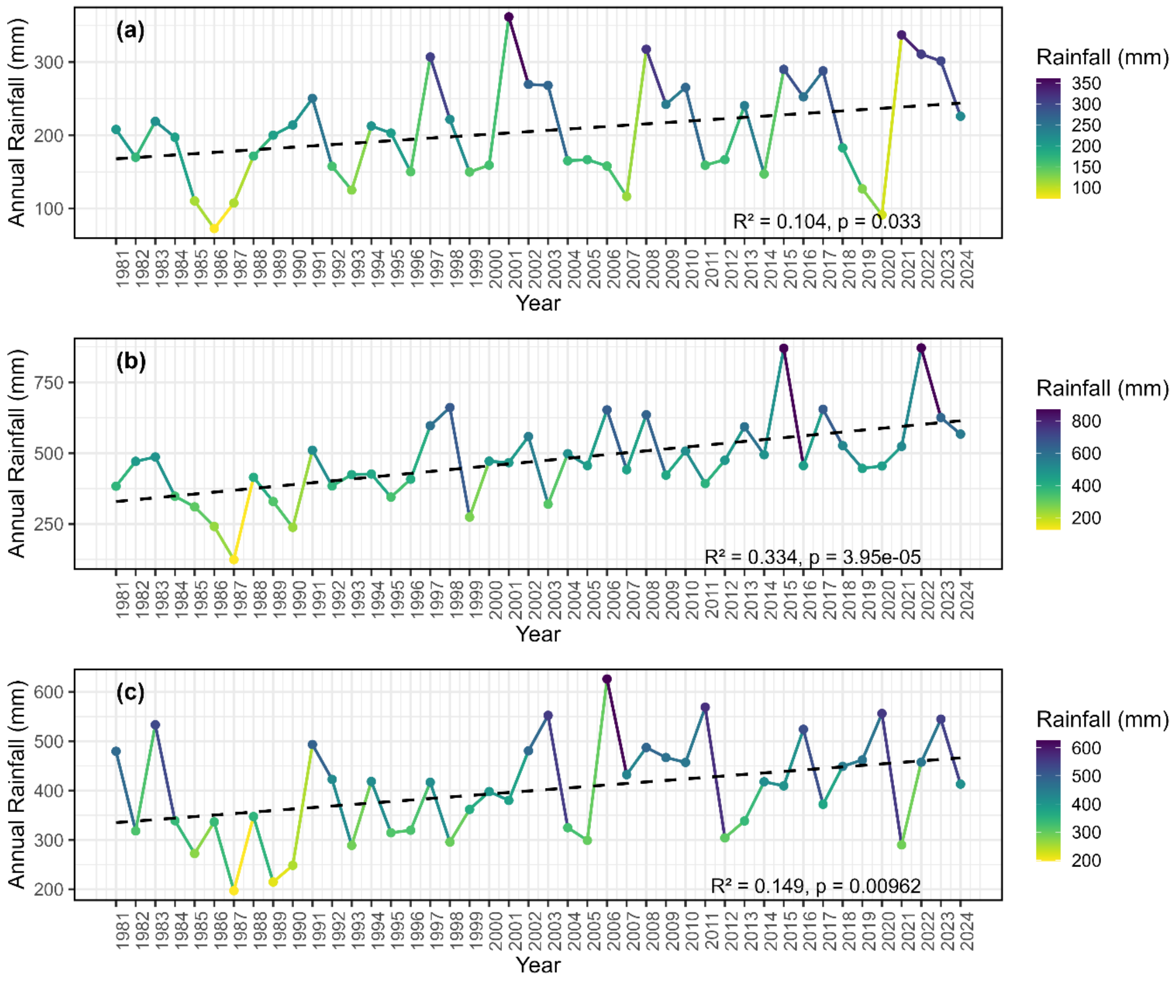

Figure 31. Rainfall trends across Darfur (1981-2024): (a) North Darfur, (b) West Darfur, (c) South Darfur.

4.2.6.2 Inter-Zonal Rainfall Differences

To statistically evaluate the rainfall disparities between zones, a Mann-Whitney-Wilcoxon test was conducted (Figure 32). North vs. West Darfur, highly significant difference ($p < 0.0001$), with West Darfur receiving markedly higher precipitation. West vs. South Darfur, moderate significance ($p < 0.01$), highlighting notable spatial heterogeneity. North vs. South Darfur, also, significant ($p < 0.001$), although the variability in South Darfur was more erratic. These findings underscore the non-uniform climatic drivers across Darfur, which have major implications for land productivity, food security, and ecosystem resilience under displacement pressures (Osman et al., 2023).

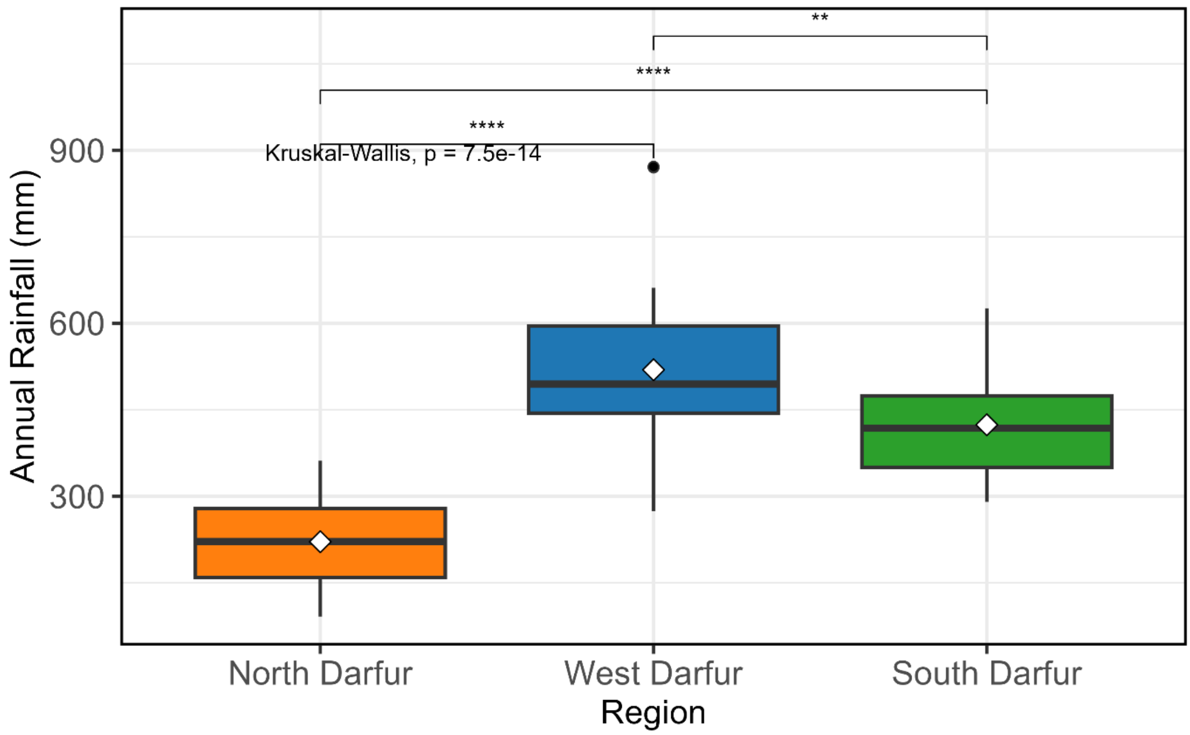

Figure 32. Mann-Whitney-Wilcoxon statistical comparison of rainfall across Darfur regions.

4.2.6.3 Temporal Rainfall Shifts: Innovative Trend Analysis (ITA) Analysis

To better understand the temporal changes in rainfall intensity and distribution, ITA was applied to split the rainfall series into two periods 1981-2003 and 2003-2024 (Figure 33).

South and West Darfur showed strong positive shifts in rainfall during the later period, particularly in the post-2010 period. This aligns with the trends of vegetation recovery and forest regrowth discussed in Section 4.2.1.3 and 4.2.4.

North Darfur, while still exhibiting a positive shift, modestly did so. Its relatively lower interannual variability suggests greater stability under lower rainfall conditions, which may limit large-scale vegetation transformations.

The ITA results validate the broader climatic moderation narrative noted throughout this study, indicating that post-conflict ecosystem recovery in Darfur is climatically reinforced, particularly in areas with higher baseline precipitation.

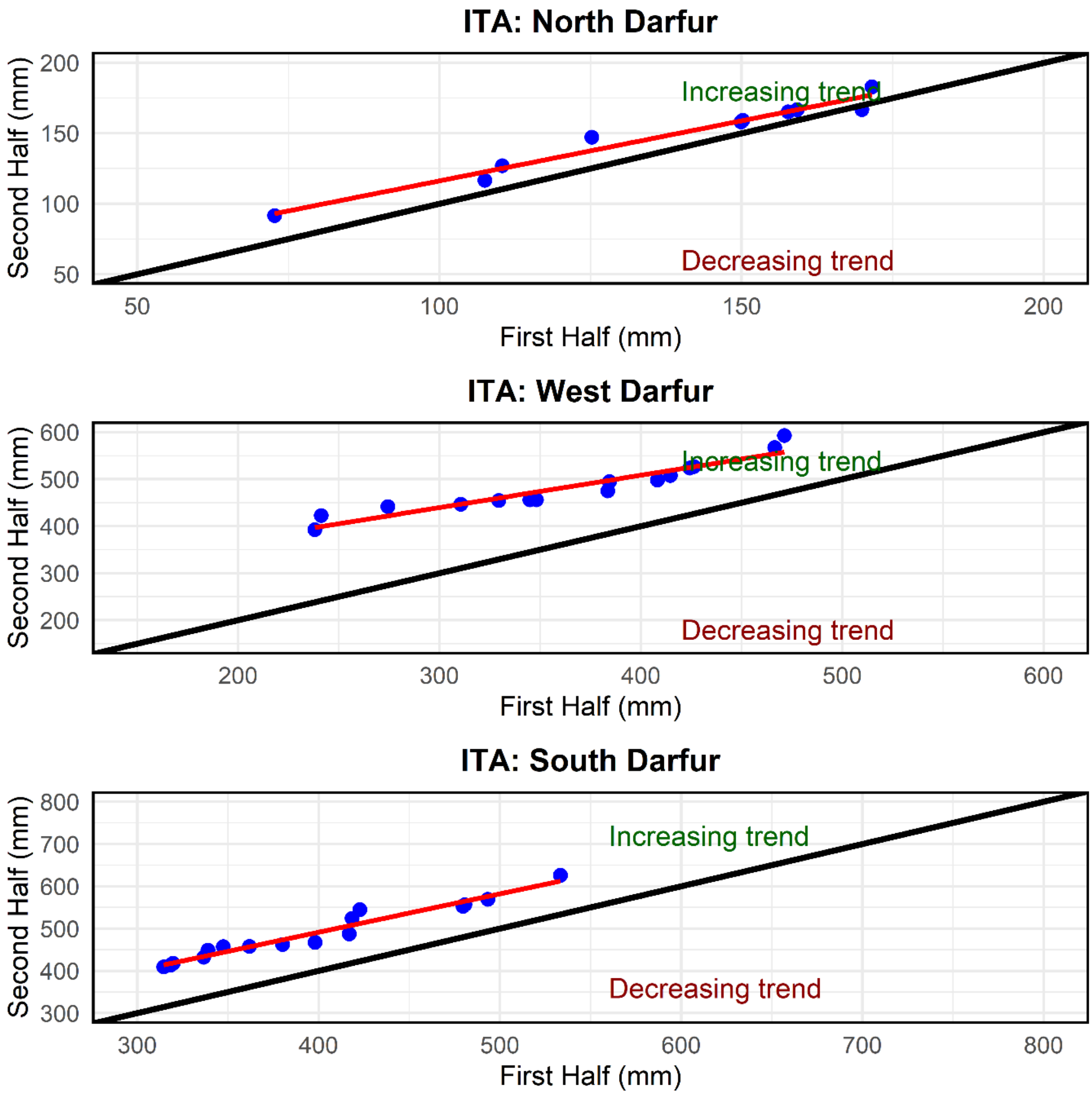

Figure 33. ITA rainfall trend analysis (1981-2003 vs. 2003-2024) for (a) South, (b) West, and (c) North Darfur.

4.2.6.4 Decadal Precipitation Variability

To assess long-term fluctuations and climatological baselines, rainfall data were aggregated by decade for North, West, and South Darfur between the 1980s and 2024 (Figure 34).

In North Darfur, the average rainfall increased from 120-210 mm in the 1980s to 290-300 mm by 2021-2024, marking a 140-170 mm rise over four decades.

West Darfur experienced the most pronounced change, with rainfall levels increasing from 250-400 mm in the 1980s to 600-700 mm in recent years, with an increase exceeding 250 mm.

In South Darfur, rainfall increased from 250-350 mm during the 1980s to 390-490 mm by 2024.

This inter-decadal analysis confirms a long-term greening trend across Darfur, reinforcing the findings of the MODIS-EVI vegetation analyses in Sections 4.2.1.5 and 4.2.5. However, high temporal uncertainty was observed during 2001-2010 and 2011-2020, reflecting the impact of severe droughts, erratic rainfall distributions, and localized humanitarian crises (Osman et al., 2023). These fluctuations exemplify the climate instability faced by agro-pastoral communities and the challenges in building resilient ecosystems in conflict-displaced landscapes.

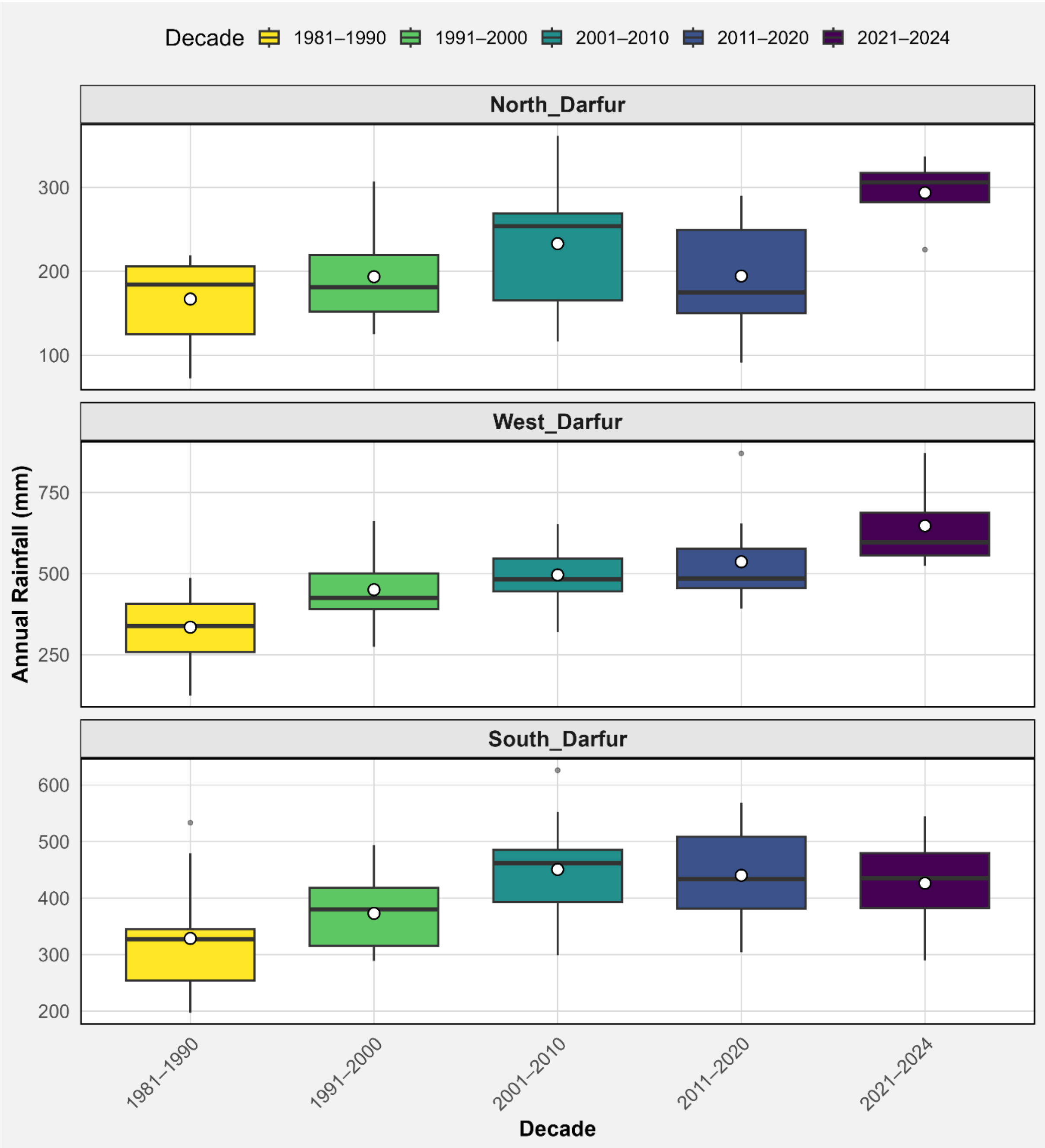

Figure 34. Decadal rainfall trend analysis (1981-2024) across Darfur.

4.2.6.5 Temperature Trends

Temperature trends from 1981 to 2024 show a clear regional warming signal, consistent with global and Sahelian climate change projections (Gebrechorkos et al., 2020; IPCC, 2023).

The maximum temperatures in North and South Darfur peaked at approximately 45°C by 2024, whereas West Darfur reached a slightly lower maximum of 43°C (Figure 35).
The mean annual temperatures across all zones stabilized between 34°C and 35°C, with South Darfur exhibiting marginally higher values than its northern and western counterparts.
Minimum temperatures, particularly in North Darfur, showed a significant shift from occasional dips below 15°C in the early 1990s to persistent warming post-2000, reflecting a decline in cold events and nighttime cooling.
These temperature increases are projected to exacerbate evapotranspiration rates, soil moisture loss, and vegetation stress, particularly in regions with shallow or sandy soils (see Section 4.2.6). Combined with rainfall shifts, these warming trends can facilitate vegetation recovery during wet years and undermine ecosystem resilience during dry periods.
The integration of precipitation and temperature data supports the climate-vegetation interaction findings in Section 4.2.5, confirming that precipitation is the dominant climatic driver, whereas rising temperatures increasingly modulate ecosystem responses and pose stressors to rain-fed agricultural systems, particularly in IDP-affected landscapes (Hamad et al., 2022; Ahmed et al., 2020).

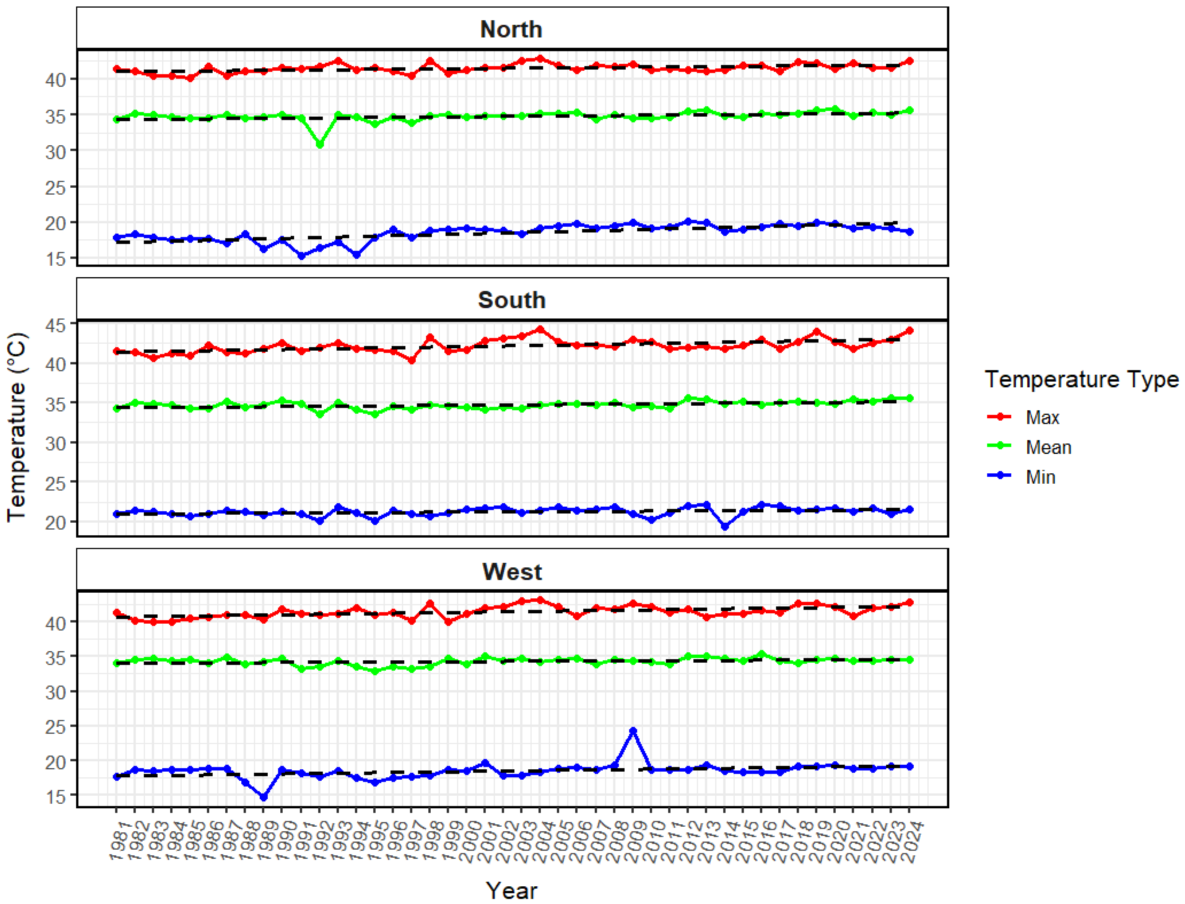

Figure 35. Historical trends in maximum, mean, and minimum temperatures across North, West, and South Darfur (1981-2024).

4.2.6.6 Rainfall and Temperature Forecast (2024-2034)

This subsection complements the historical climate analysis by presenting projected climatic trends for Darfur using time-series forecasting methods. Specifically, the ARIMA and ETS models were employed to forecast precipitation and temperature for North, West, and South Darfur for the period 2024-2034. These models were selected for their robustness in handling nonstationary environmental data and their ability to account for both trend and seasonal components (Athanasopoulos et al., 2020).

4.2.6.6.1 Rainfall Forecasting: ARIMA and ETS Models

Forecasts generated from both the ARIMA and ETS models (Figure 36) show continued north-to-south gradients in rainfall patterns, which is consistent with Darfur's semi-arid to sub-humid ecology.

In North Darfur, rainfall is projected to stabilize at approximately 210-250 mm, with substantial uncertainty bounds ranging between 120-390 mm. This underscores the region's vulnerability to inter-annual rainfall volatility, particularly under warming scenarios and conflict-driven land degradation.

West Darfur is projected to maintain higher rainfall levels, stabilizing at approximately 600 mm, with a forecast range of 420-750 mm. The wider band suggests variability due to convective rainfall systems, which have been increasingly intense in this zone.

South Darfur's rainfall is projected to converge near 440 mm, but with a significant spread ranging from 300-570 mm, indicating greater inter-seasonal unpredictability.

These forecasts affirm the persistence of the latitudinal climatic gradient (north drier, south wetter) but also highlight increasing intra-regional variability, which is a critical challenge for planning agricultural activities, water management, and IDP settlement resilience (Dinku et al., 2018; Osman et al., 2023).

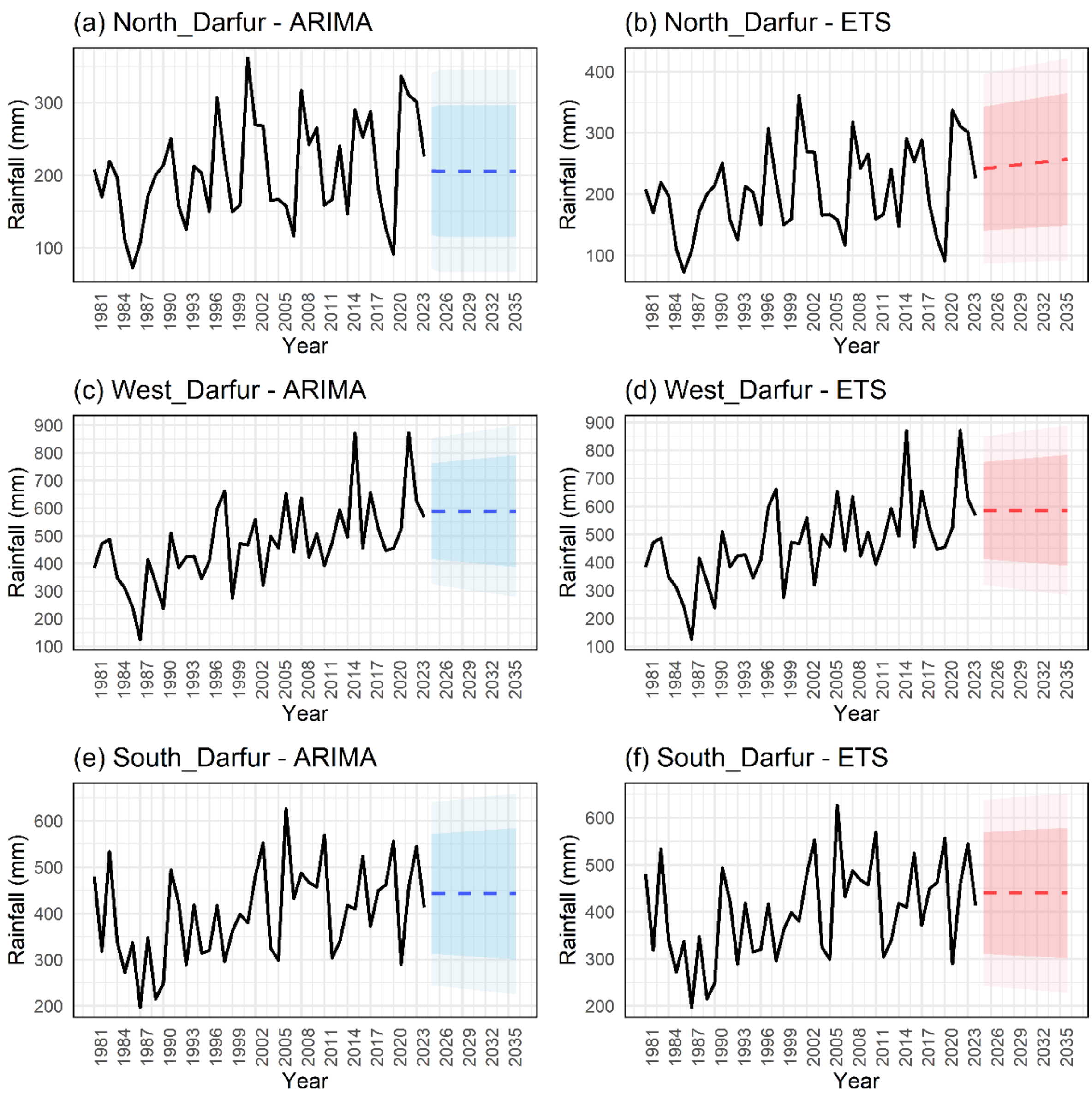

Figure 36. ARIMA and ETS rainfall forecasts for North, West, and South Darfur.

4.2.6.6.2 Temperature Forecasting

Temperature projections (Figure 37) suggest a continued warming trajectory across all three Darfur zones, aligned with regional climate projections from the IPCC, (2023) and the African climate adaptation literature (Gebrechorkos et al., 2020).

North Darfur: Mean annual temperatures are projected to stabilize around 35.4°C, with variation between 34.5°C and 35.9°C.

West Darfur: Expected to stabilize at 35.5°C, with a forecast range from 33.8°C to 35.9°C.

South Darfur: Forecasted to average 35.2°C, within a narrower uncertainty band (34.2°C-36.2°C), suggesting less temperature fluctuation and potential for persistent heat conditions.

These temperature trends have serious implications for evapotranspiration rates, crop suitability zones, and vegetation stress thresholds, particularly in areas of depleted soil moisture or increased IDP settlement pressures (Nicholson et al., 2013) Combined with rainfall forecasts. The outlook calls for proactive adaptation strategies including drought-resistant crop systems, climate-smart land use planning, and ecosystem service restoration.

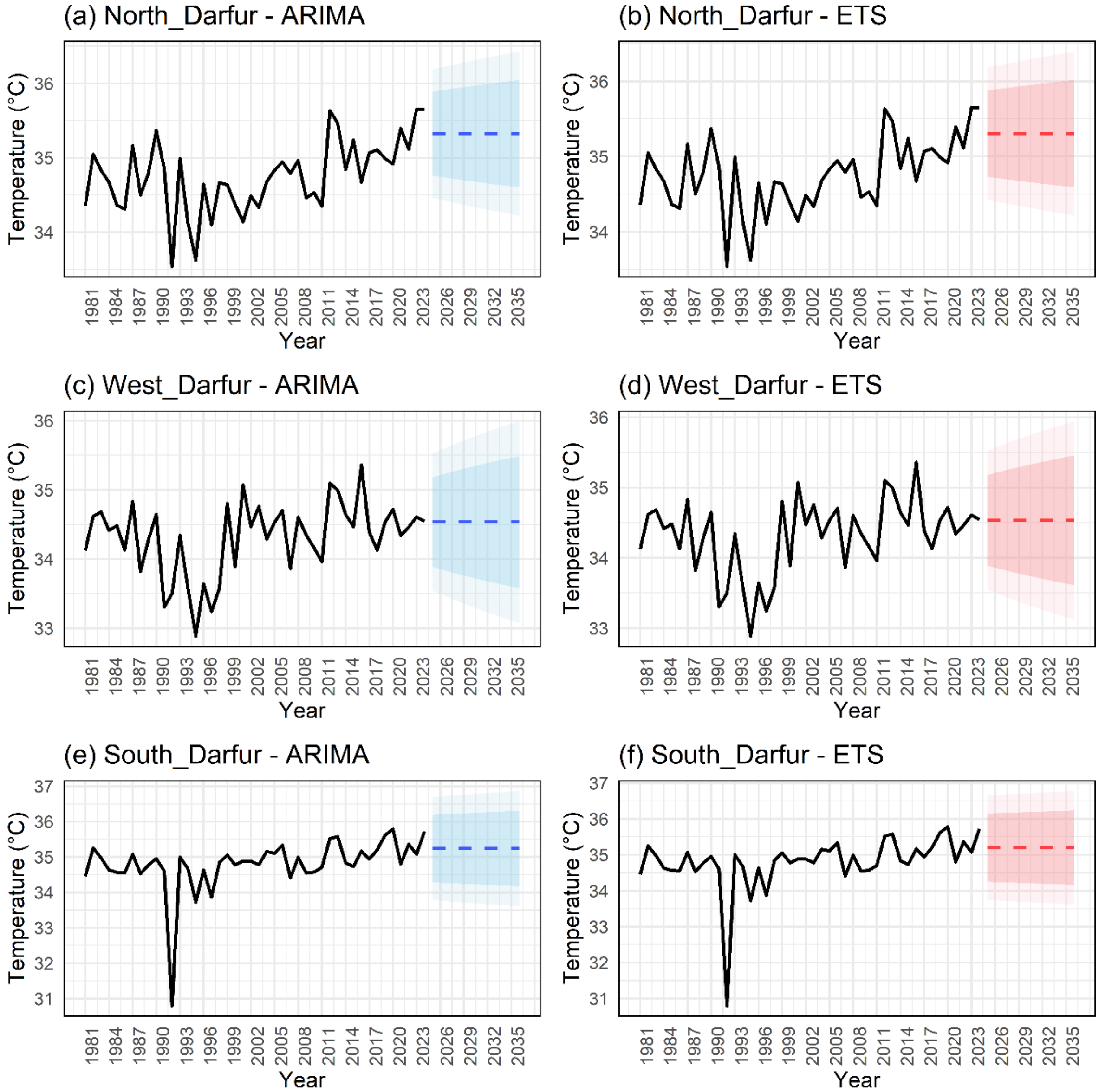

Figure 37. Forecast of annual temperature trends across Darfur zones (2024-2034) using ARIMA and ETS models.

4.2.7 Drought Analysis

Drought is a recurring climatic hazard with profound ecological and socio-economic implications for arid and semi-arid regions such as Darfur, where it exacerbates land degradation, vegetation loss, and human displacement. This section examines the spatiotemporal dynamics of drought using the SPEI across three states North, West, and South Darfur for the period 1981-2024. Two temporal scales were used SPEI-12 captures long term (hydrological) drought patterns, and SPEI-6 identifies short-term (agricultural) drought episodes.

4.2.7.1 Long-Term and Short-Term Drought Patterns

Figure 38 displays the SPEI-6 and SPEI-12 time-series across the study period:

1981-2000: This era was characterized by frequent and intense droughts in all zones, notably in the 1983-1985 Sahel drought crisis, leading to widespread ecological stress and socio-political consequences, including food insecurity and mass displacement. These conditions coincide with the well-documented Sahelian desiccation events (Nicholson et al., 2013).
2001-2024: A transition toward wetter conditions was observed. While episodic droughts persisted, particularly in North Darfur (notable years: 2010, 2017) and South Darfur, the overall drought frequency and severity declined significantly. This aligns with evidence from satellite vegetation indices indicating ecosystem recovery and climate moderation during the post-2010 period.

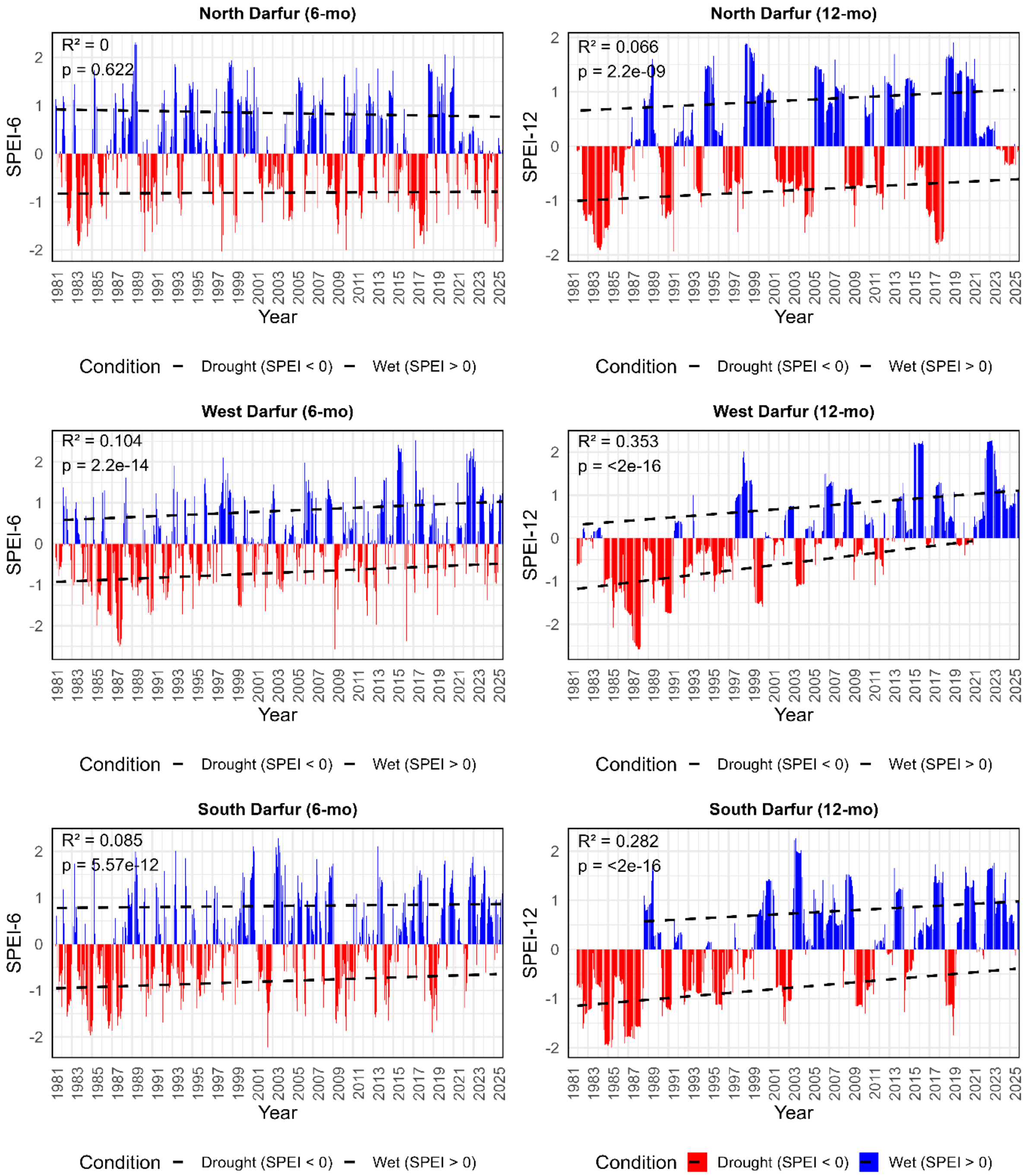

Figure 38. SPEI trends over 6-month and 12-month timescales in Darfur, highlighting dry (red) and wet (blue) phases.

4.2.7.2 SPEI Trend Analysis

Linear regression analysis was applied to both the long and short-term SPEI time series to detect significant trends.

4.2.7.2.1 SPEI-12 (Long-Term Drought Trends)

North Darfur: $R^2 = 0.075$, $p = 2.23$ Weak positive trend, suggesting a slight reduction in drought severity, although not statistically significant.
West Darfur: $R^2 = 0.341$, $p < 0.001$ moderate at maximum significant trend toward improved hydrological conditions and reduced long-term drought risk.
South Darfur: $R^2 = 0.279$, $p < 0.001$ moderate and significant trend toward lower drought severity.
These trends corroborate patterns of increasing vegetation cover and rainfall improvements noted in earlier sections (see Sections 4.2.1.5 and 4.2.7).

4.2.7.2.2 SPEI-6 (Short-Term Drought Trends)

North Darfur: $R^2 = 0.002$, $p = 0.359$ no statistically reliable trend; short-term droughts remain persistent.
West Darfur: $R^2 = 0.106$, $p = 2.31$ moderate reduction in short-term droughts, although with low statistical significance.
South Darfur: $R^2 = 0.081$, $p = 3.15$ slight decrease in short-term drought frequency, with limited confidence.
These results suggest that, while hydrological drought conditions are improving, agricultural drought stress remains a challenge, particularly in North Darfur.

4.2.7.3 Spatial Drought Variability

The spatial heatmaps of SPEI-6 (Figure 39) and SPEI-12 (Figure 40) highlight regional disparities in drought exposure:
West Darfur exhibits the strongest drought recovery, consistent with rising vegetation cover and ecosystem restoration efforts.
South Darfur shows a modest improvement, although some areas remain vulnerable.
North Darfur remains the most drought-prone region, especially in the short-term SPEI-6, underscoring persistent water stress and environmental fragility.
These spatial patterns align with the rainfall projections and vegetation trends described earlier and emphasize the need for targeted climate resilience interventions, especially in chronically stressed zones like North Darfur (Mohmed, 2013; M. Osman et al., 2023).

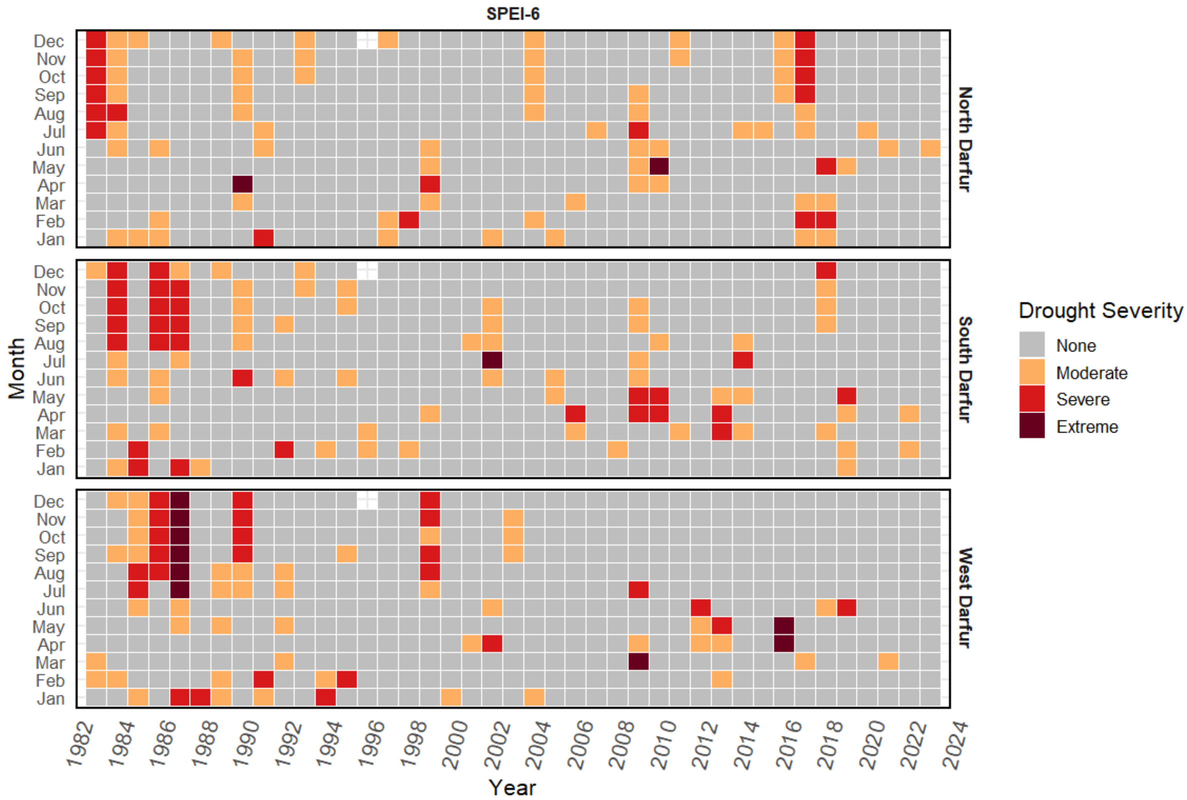

Figure 39. Heatmap visualization of SPEI (6-month) drought intensities across Darfur.

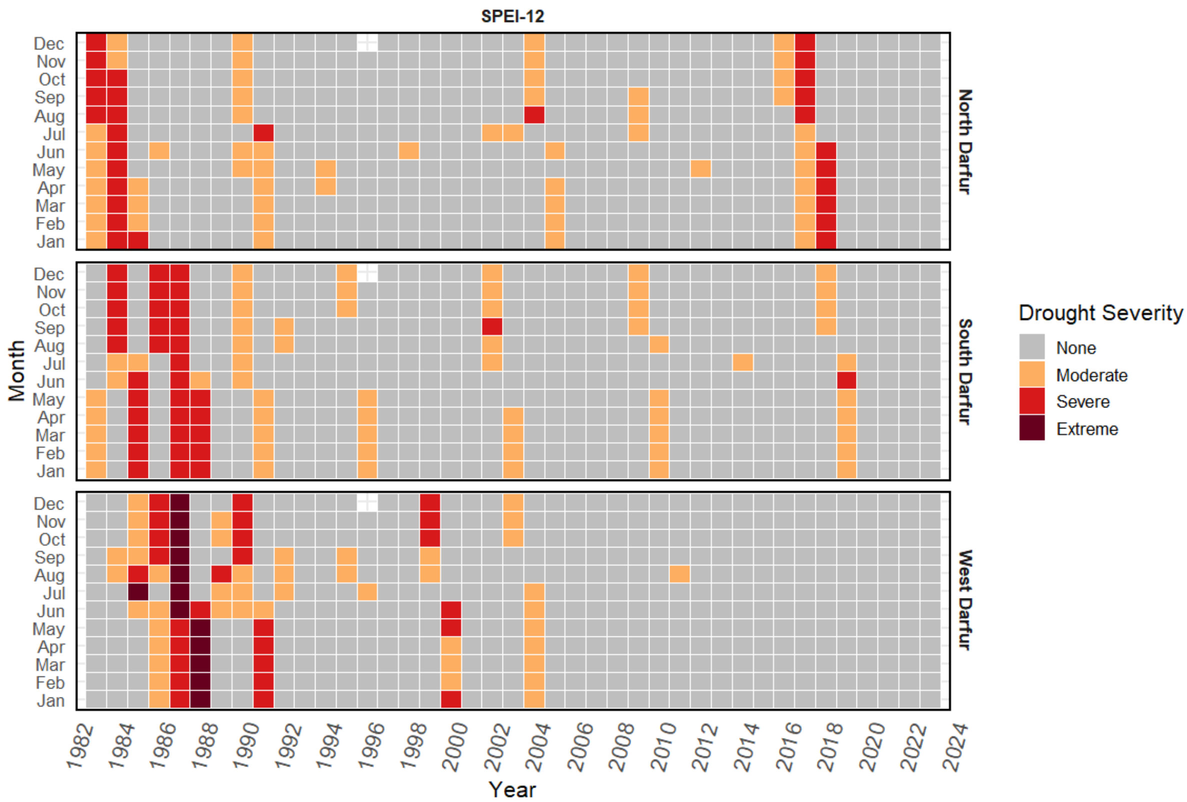

Figure 40. Heatmap visualization of SPEI (12-month) drought intensities across Darfur.

4.2.7.4 Interpretation and Implications

The post-2000 period in Darfur demonstrated an encouraging shift toward climatic moderation, particularly regarding reduced drought frequency and intensity, as evidenced by both SPEI-6 and SPEI-12 indicators. These improvements are largely driven by increased annual and seasonal rainfall (see Section 4.2.7.1) and appear to be further reinforced by positive land-use transitions, including the expansion of agroforestry, natural vegetation regeneration, and declining bareland cover (see Sections 4.2.1.4 and 4.2.4).

Despite this regional greening trend, North Darfur continued to exhibit pronounced drought vulnerability, particularly in the short-term agricultural cycle, as shown by the persistence of negative SPEI-6 values and weak trend statistics ($R^2 = 0.002$). This underscores the region's limited ecological resilience, likely due to its inherently arid climate, sparse vegetation, intensified human pressure from IDP camps, unsustainable land use, and resource scarcity (Hassan et al., 2021).

Moreover, the statistical insignificance of some regression trends, especially in the North and parts of South Darfur, highlights the complexity of drought dynamics in semi-arid ecosystems. These systems are not solely driven by climatic variables, but are also shaped by anthropogenic stressors, including:

- Deforestation and biomass harvesting,
- Displacement-induced land conversion,
- Lack of adaptive farming strategies, and
- Minimal investment in drought-resilient infrastructure.

The implications are two-fold:

1- Climate recovery is evident in terms of rainfall and vegetation trends, offering a potential window for ecological restoration and sustainable development.
2- However, the uneven spatial distribution of recovery signals and ongoing drought sensitivity in specific zones necessitate localized drought risk reduction strategies, early warning systems, and community-based adaptation measures tailored to regional vulnerabilities.

As such, integrated land management that accounts for biophysical constraints, climate projections, and sociopolitical dynamics is essential for sustaining these emerging ecological gains and ensuring long-term resilience in Darfur's fragile landscapes (Lambin & Meyfroidt, 2011; Malakar et al., 2023).

CHAPTER 5

Conclusion and Recommendation

5.1 Conclusion

This study provides a comprehensive and data-driven assessment of the interrelated dynamics of LULC change, vegetation transformation, climate variability, and human displacement, with a primary focus on the Central Darfur and broader contextualization across the Darfur region. Employing a multi-source remote sensing approach including MODIS, Sentinel-2, PlanetScope, and ESRI Land Cover data alongside spatial modeling CA-Markov, drought indices (SPEI-6 and SPEI-12), and benefit-transfer-based ecosystem service valuation, this study offers novel and actionable insights into environmental transformations between 1981 and 2024. Key Findings:

LULC Transitions: The study identified significant expansion in agricultural and built-up areas, particularly post-2000, largely driven by conflict-induced displacement, resettlement efforts, and urban development. This expansion was accompanied by a temporary decline in forest and grassland areas, which led to widespread degradation.

Ecological Recovery: From 2014 onwards, a reversal of degradation trends was observed. Vegetation regeneration, particularly in Central and West Darfur, is supported by improved rainfall, land abandonment, community-based reforestation, and agroforestry initiatives. MODIS NDVI/EVI analysis captured this regreening trend, with increased vegetation cover and reduced non-vegetated areas.

Climate Variability: The region has experienced a warming trend and increasing precipitation, particularly after 2000. SPEI analysis revealed clear drought-recovery cycles severe droughts dominated the 1980s-1990s, while post-2010 witnessed fewer and less intense droughts. These climatic shifts directly contributed to vegetation recovery and land cover stabilization.

Ecosystem Services Dynamics: The valuation of ecosystem services revealed that regulating (e.g., erosion control, climate regulation) and supporting (e.g., nutrient cycling, soil formation) services improved with forest and grassland expansion. However, the decline in croplands has reduced provisioning services (e.g., food supply), emphasizing the trade-off between ecological restoration and food security. The sensitivity analysis further confirmed that grasslands and forests are the most critical LULC classes for ESV sustainability.

Conflict and Displacement Effects: IDP settlements initially intensify environmental stress through deforestation and resource exploitation. However, in some areas, displacement also leads to passive reforestation due to land abandonment, demonstrating complex socio-ecological interactions. Community-led conservation and peacebuilding have emerged as pivotal factors in driving recovery.

Overall Synthesis: This study challenges the deterministic narrative of the inevitable environmental decline in conflict zones. Instead, it presents evidence that post-conflict landscapes such as Darfur can transition towards ecological recovery when favorable climatic conditions, local stewardship, and policy interventions align. Although the region remains ecologically fragile, it is not beyond restoration. Vegetation recovery, drought reduction, and

rising ecosystem service values collectively indicate that resilience is attainable even in conflict-affected, data-scarce, and semi-arid regions.
The findings not only offer new scientific knowledge but also provide strategic directions for land management, environmental governance, and climate adaptation in fragile socio-political contexts.

5.2 Recommendations

5.2.1 Policy Recommendations

1. Mainstream Conflict-Sensitive Environmental Governance
Environmental restoration must be integrated into broader peacebuilding and post-conflict recovery strategies, particularly in areas hosting IDPs. Strengthening land tenure systems is essential for preventing land encroachment, supporting equitable land distribution, and reducing land related conflicts. This requires multi-level institutional coordination, legal reforms, and stakeholder engagement across governance tiers.
2. Expand Community-Based Reforestation and Agroforestry Programs
Scaling up locally led reforestation and agroforestry initiatives particularly those that promote drought-resilient native species should be prioritized. Technical and financial support must be mobilized from government agencies (e.g., Forest National Corporation), international development partners, and environmental NGOs to support seedling distribution, training, and monitoring. These interventions must be embedded in national forest policies and climate adaptation plans.
3. Promote Alternative Energy and Sustainable Livelihoods in IDP Areas
The heavy dependence on biomass for energy in IDP camps has driven deforestation. Introducing clean energy solutions, such as solar cookstoves, liquefied petroleum gas (LPG), and biogas systems, can significantly reduce the pressure on forest resources. In parallel, supporting alternative income-generating activities (e.g., agro-processing, and small-scale irrigation farming) will diversify livelihoods and enhance socio-ecological resilience.
4. Integrate Climate Adaptation into Spatial and Land Use Planning
Policymakers should embed climate resilience strategies in land use and spatial planning frameworks. Key priorities include promoting climate-smart agriculture, investing in water harvesting technologies, reinforcing early warning systems, and prioritizing drought-tolerant crops. Local Development Plans should incorporate these measures into the climate-vulnerable zones.
5. Implement Ecological Zoning and Buffer Zones Around IDP Settlements
Clear land-use zoning should delineate ecological buffer zones to mitigate environmental degradation near IDP camps. These buffers must be supported by community awareness, legal enforcement, and sustainable resource-access mechanisms. Such zoning can also act as a mechanism for restoring degraded land adjacent to settlements.

5.2.2 Research Recommendations

1. Establish Regional Environmental Monitoring Units
Universities and environmental research centers in the region should establish permanent units dedicated to remote sensing-based monitoring, GIS-based modelling, and field

validation of land cover and vegetation changes. These centers should also serve as data repositories and hubs for capacity building in environmental informatics.

2. Conduct Field-Based ESV

Future research should prioritize the empirical, ground-controlled valuation of ecosystem services at local scales to complement benefit-transfer methods. This is particularly critical for provisioning and regulating services in agro-pastoral and forest ecosystems where data gaps are most acute.

3. Advance LULC Classification Using Machine Learning

Emerging machine-learning techniques, such as RF, SVM, and CNNs, offer improved accuracy in complex and heterogeneous landscapes. Incorporating these into land cover classification workflows can yield more robust and spatially consistent results, especially in data-poor, and post-conflict regions.

4. Investigate Soil Carbon and Hydrological Feedback

The ecological effects of vegetation recovery on soil carbon sequestration, surface runoff, infiltration rates, and evapotranspiration remain underexplored. Multidisciplinary studies linking land cover change with hydrological and soil health indicators will inform restoration effectiveness and carbon credit assessment.

5.2.3 Community-Level Actions

1. Strengthen Environmental Stewardship Among IDP Communities

Environmental education, awareness campaigns, and community forestry initiatives should be scaled up to engage IDP communities as restoration partners. Support should include tools, training, seedlings, and access to secure land tenure to incentivize sustained ecological stewardship.

2. Facilitate South-South Knowledge Exchange and Peer Learning

Platforms should be established for peer-to-peer knowledge sharing across Sahelian and East African regions facing the similar challenges of conflict, displacement, and land degradation. Regional cooperation and the exchange of restoration models, climate-smart practices, and institutional innovations can accelerate the learning and uptake of successful interventions.

6. Future Research Directions

This research provides a foundation for understanding vegetation recovery, climate variability, and ecosystem services in conflict-affected landscapes. Building on these findings, future studies should advance toward higher-resolution, data-driven, and socio-ecologically integrated frameworks.

1. Multi-Temporal and Uncertainty Validation

Future work should employ multi-year validation and uncertainty quantification using probabilistic ensemble models (e.g., CA-ANN, FLUS) to improve predictive confidence under dynamic socio-ecological conditions.

2. Integration of High-Resolution Multi-Sensor Data

The incorporation of very high-resolution imagery (e.g., PlanetScope, WorldView-3, PRISMA hyperspectral) and radar–optical fusion (Sentinel-1 + Sentinel-2) will enhance classification accuracy, detect fine-scale vegetation regeneration, and capture micro-level land-use transitions around IDP settlements.

3. Temporal Densification of LULC Time Series

Expanding LULC analysis to annual or seasonal intervals will improve the detection of short-term landscape variability, refine trend accuracy, and strengthen simulation reliability for CA-Markov and hybrid dynamic models.

4. Dynamic Climate-Vegetation Modelling

Coupled biophysical models such as IBIS and DGVMs should be adopted to evaluate climate vegetation feedback, particularly how regreening influences evapotranspiration, soil moisture, and local microclimates under future climate scenarios.

5. Socio-Ecological Modelling of IDP Dynamics

Integrating agent-based models, social surveys, and spatial simulations will enable a deeper understanding of how displacement, livelihoods, and governance shape land cover transitions informing conflict-sensitive land management and settlement planning.

6. Empirical Valuation of Ecosystem Services

Future studies should conduct field-based ecosystem service valuation through household surveys, contingent valuation, and biophysical sampling. This will refine local value coefficients, reduce transfer errors, and better represent the economic dimensions of ecosystem recovery.

7. Linking Vegetation Recovery to Soil Carbon and Hydrology

The ecological implications of regreening soil carbon sequestration, infiltration rates, and hydrological resilience remain underexplored. Integrating LiDAR data, soil sampling, and hydrological models will quantify these linkages and assess restoration co-benefits.

8. Advancing Machine and Deep Learning Applications

Emerging deep learning architectures (CNNs, U-Net, Transformer-based models) can enhance LULC classification and vegetation anomaly detection, capturing spatial-temporal complexity across multi-sensor datasets.

9. Drought Early Warning and Monitoring Systems

Developing real-time, geospatial drought early warning systems using SPEI, NDVI/EVI anomalies, and satellite precipitation will strengthen resilience planning and humanitarian response mechanisms.

10. Regional and Transboundary Comparative Research

Given Darfur's ecological alignment with the wider Sahel, future research should pursue cross-border comparative analyses linking Sudan, Chad, Niger, and South Sudan to identify shared regreening drivers and adaptive governance mechanisms.

In summary Figure 41, future research must adopt an integrated, multi-scale, and participatory framework that couples advanced remote sensing, field-based validation, and socio-ecological modelling. By doing so, it will transform empirical findings from Darfur into scalable models for restoration, resilience, and climate adaptation across the Sahel and other fragile dryland ecosystems.

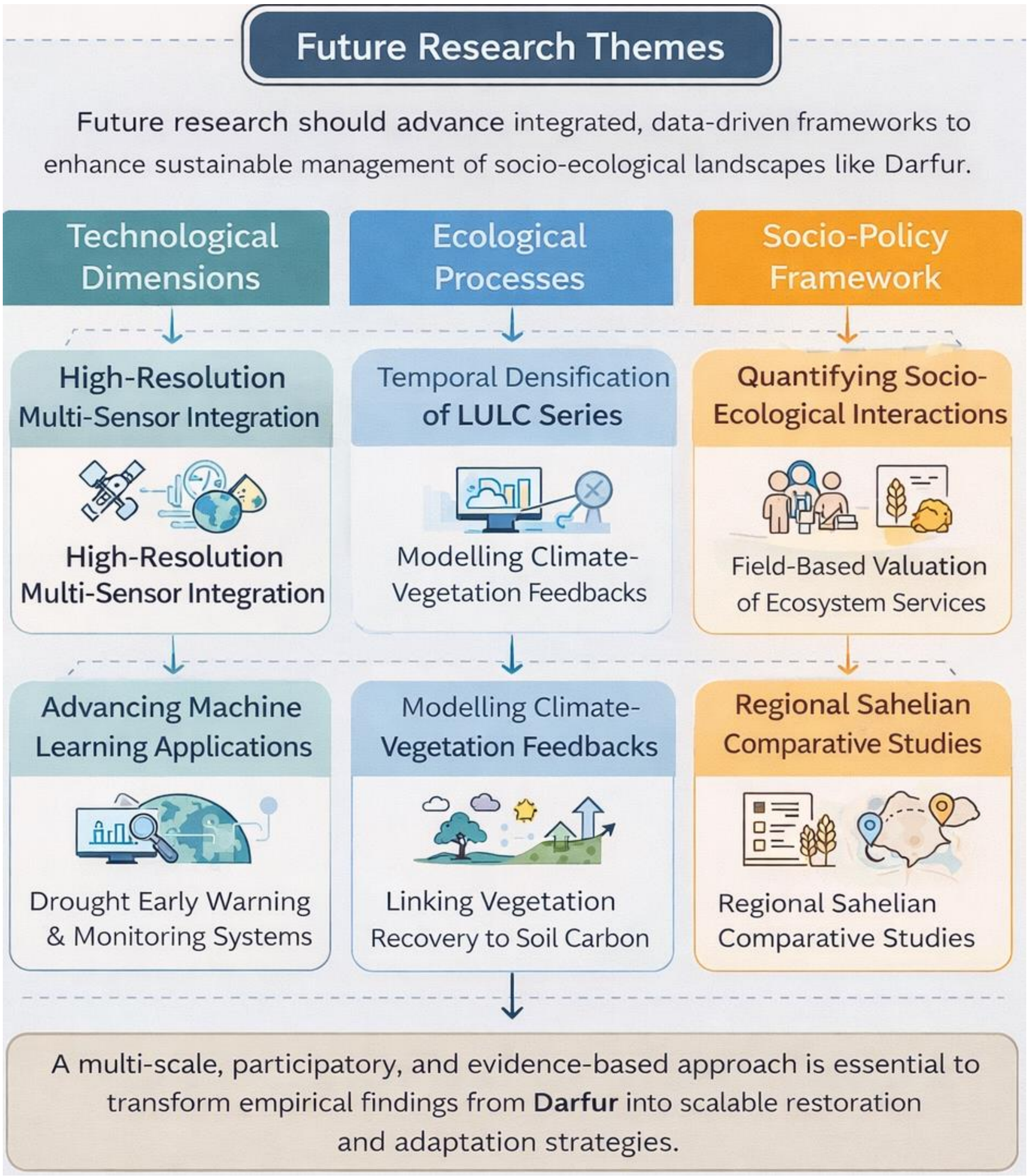

Figure 41. flow diagram illustrates future research directions.

7. New Scientific Results

This research introduces five novel scientific contributions that contribute to the fields of environmental monitoring, land use dynamics, and post-conflict ecological assessment in arid and semi-arid landscapes. By integrating the spatial, temporal, and socio-ecological dimensions, this study offers innovative methods and context-specific findings that advance current knowledge and inform policy and practice in fragile environments (Figure 42).

Scientific Result 1: Methodological Advancement in Multi-Scale Environmental Assessment (Supporting Contribution)

This is the first study in the region to employ a synergistic integration of MODIS (250 m), Sentinel-2 (10 m), PlanetScope (3 m), and ESRI global land cover datasets to analyze vegetation dynamics and LULC transitions. This multi resolution fusion enabled the detection of both large-scale trends and fine-grained local changes, overcoming the limitations of single-sensor studies. It enhances classification accuracy, facilitates temporal continuity, and provides robust spatial context for ecosystem monitoring in complex socio-ecological settings. While primarily methodological, the integration of multi-resolution satellite platforms (MODIS, Sentinel-2, PlanetScope, ESRI LULC) represents a supporting scientific advancement enabling:

- Cross-scale validation,
- Improved temporal continuity,
- Context-specific classification in IDP-affected micro-landscapes.

Although not claimed as a standalone scientific discovery, this methodological synthesis underpins and strengthens all other scientific results presented in the dissertation.

Scientific Result 2: First CA-Markov LULC Projection for Central Darfur

This study presents the first spatially explicit LULC simulation for Central Darfur, using the CA-Markov modeling. Forecasts to 2034 indicate the continued expansion of grasslands and forest cover under a business-as-usual scenario, alongside a projected decline in cropland. Unlike previous descriptive studies, this work:

- Integrates multi-driver spatial variables (topography, proximity to roads, rivers, and settlements).
- Validates predictive performance through cross-comparison with observed LULC for 2024.
- Demonstrates strong predictive reliability (overall Kappa = 0.85; correctness rate ≈ 90%).

This predictive modeling offers a valuable planning tool for land managers, conservationists, and policymakers to anticipate ecological outcomes in data-scarce conflict-affected regions.

Scientific Result 3: Quantitative Drought-Vegetation Coupling via SPEI and BFAST

The dissertation introduces a quantitative, multi-scale assessment of climate–vegetation interactions by integrating:

- SPEI (6- and 12-month) drought indices,
- MODIS NDVI/EVI time series,
- Breakpoint detection using the BFAST algorithm.

This approach reveals clear structural breaks in vegetation dynamics around 1990, 2000, and 2010, corresponding to major drought episodes and socio-political crises, a statistically strong precipitation–vegetation coupling ($r = 0.72$, $p < 0.001$), and regional contrasts in drought recovery, with West Darfur showing the strongest post-2010 recovery.

This contribution advances drought-ecosystem analysis by explicitly linking climatic shocks, vegetation response, and temporal non-stationarity in fragile landscapes.

Scientific Result 4: New Evidence Linking IDP Dynamics and Vegetation Recovery

This study challenges the prevailing narrative that displacement leads to environmental degradation. Instead, it provides empirical evidence that in post-conflict settings, IDP communities, when supported by improved rainfall, reforestation, and agroecological initiatives, can contribute to vegetation recovery and ecosystem restoration, through high-resolution Sentinel-2 and PlanetScope classification in Kas Locality and El-Salam Camp, dense NDVI time series analysis, and spatial comparison of IDP-proximal and distal zones, the study demonstrates that:

- Initial vegetation loss is often followed by natural regeneration, agroforestry expansion, and land abandonment-driven recovery, particularly under improved rainfall conditions.
- Vegetation recovery is spatially heterogeneous, with regrowth dominated by shrubland and open woodland rather than closed-canopy forest.

This finding underscores the potential of conflict-sensitive land use planning and community-based adaptation.

Scientific Result 5: First ESV in Conflict-Affected Darfur

This study conducted the first ESV assessment in Darfur using benefit-transfer methods linked to LULC classifications. The results revealed a dual pattern: an increase in regulating services due to forest and grassland gains, and a concurrent decline in provisioning services resulting from cropland reduction. This nuanced insight enhances our understanding of ecological trade-offs and informs integrated land restoration strategies in post-disaster settings. Key findings include:

- A net increase in total ESV between 2017 and 2034,
- Dominance of regulation and supporting services, driven by forest and grassland recovery,
- Declining provisioning services due to Cropland contraction.

Sensitivity analysis further confirms that grasslands and forests account for over 95% of ESV elasticity, emphasizing their strategic importance for sustainable land management and climate adaptation. This contribution fills a critical gap in ecosystem economics for conflict-affected drylands.

Summary Statement

Together, these scientific results demonstrate that vegetation recovery, climate variability, and ecosystem service dynamics in conflict-displaced landscapes are neither linear nor uniformly negative. Instead, they reflect a complex interaction between climate recovery, land-use change, and human adaptation, which can be quantified, modeled, and forecast using advanced geospatial methods. They also established a methodological foundation for future research in similarly fragile contexts across Africa and beyond.

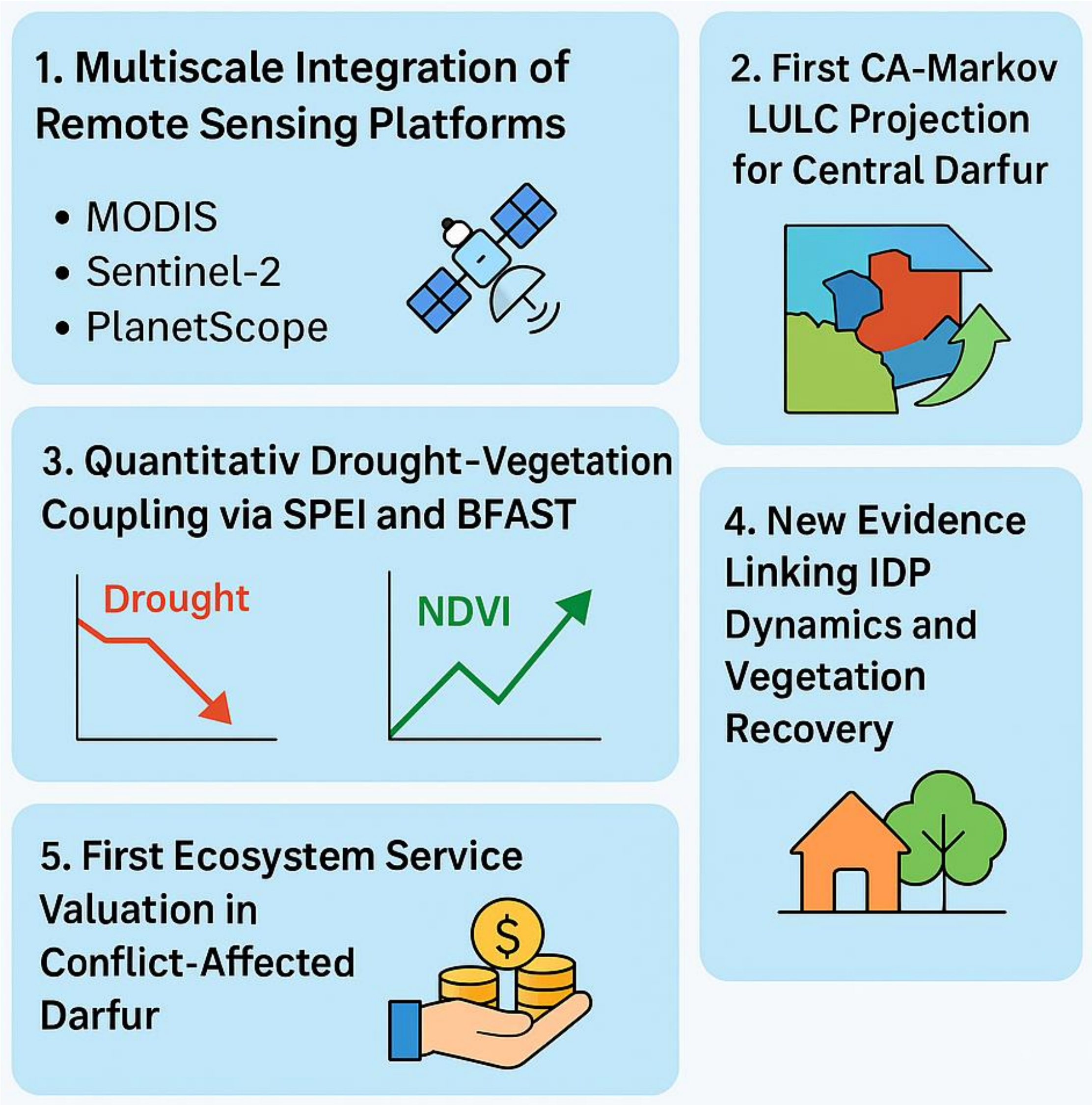

Figure 42. The New Scientific Findings Graphical Map.

7. Published Research Articles

1. Ahmed, A., & Czimber, K. (2025). Spatiotemporal dynamics of vegetation cover and drought conditions in West Darfur, Sudan: Implications of climate variability and future projections. Geo: Geography and Environment, 12(2). https://doi.org/10.1002/GEO2.70016
2. Ahmed, A., Rotich, B., & Czimber, K. (2024). Assessment of the environmental impacts of conflict-driven Internally Displaced Persons: A sentinel-2 satellite based analysis of land use/ cover changes in the Kas locality, Darfur, Sudan. PLoS ONE, 19(5 May). https://doi.org/10.1371/journal.pone.0304034
3. Ahmed, A., Rotich, B., & Czimber, K. (2025). Climate Change as a Double-Edged Sword: Exploring the Potential of Environmental Recovery to Foster Stability in Darfur, Sudan. Climate 2025, Vol. 13, Page 63, 13(3), 63. https://doi.org/10.3390/CLI13030063

4. Ahmed, A., Rotich, B., Kipkulei, H. K., Lameck, A. S., Gallai, B., & Czimber, K. (2025). Vegetation Dynamics and Climate Variability in Conflict Zones: A Case Study of Sortony Internally Displaced Camp, Darfur, Sudan. Land 2025, Vol. 14, Page 1680, 14(8), 1680. https://doi.org/10.3390/LAND14081680
5. Ahmed, A., Kornel, C., Ahmed, A., & Kornel, C. (2024). Analysing the climate variability and reforestation activities in the areas adjacent to internally displaced camps in Darfur.

8. References

1. Abad-Segura, E., González-Zamar, M. D., Vázquez-Cano, E., & López-Meneses, E. (2020). Remote Sensing Applied in Forest Management to Optimize Ecosystem Services: Advances in Research. Forests 2020, Vol. 11, Page 969, 11(9), 969. https://doi.org/10.3390/F11090969
2. Abdalla, Eldoma. Ibrahim, Elaagip, E., & Hou. Fujiang. (2020). Effects of indigenous cultivation practices on soil conservation in the Hilly Semiarid areas of Western Sudan. Water (Switzerland), 12(6). https://doi.org/10.3390/W12061554
3. Abrahams, D. (2021). Land is now the biggest gun: climate change and conflict in Karamoja, Uganda. Climate and Development, 13(8), 748–760. https://doi.org/10.1080/17565529.2020.1862740
4. ACAP. (2023). ACAP, 2023. Thematic report: Sudan's impact of the current conflict on WASH needs. In ACAPS analysis hub. 〈https://www.acaps.org/fileadmin/Data_Product/Main_medi a/20230911 ACAPS thematic report Sudan impact of current conflict on WAS H needs.pdf - Google Search.
5. Acharki, S. (2022). PlanetScope contributions compared to Sentinel-2, and Landsat-8 for LULC mapping. Remote Sensing Applications: Society and Environment, 27, 100774. https://doi.org/10.1016/J.RSASE.2022.100774
6. Adaawen, S., Rademacher-Schulz, C., Schraven, B., & Segadlo, N. (2019). Drought, migration, and conflict in sub-Saharan Africa: what are the links and policy options? 2, 15–31. https://doi.org/10.1016/B978-0-12-814820-4.00002-X
7. Adhikari, K., Minasny, B., Greve, M. B., & Greve, M. H. (2014). Constructing a soil class map of Denmark based on the FAO legend using digital techniques. Geoderma, 214–215, 101–113. https://doi.org/10.1016/J.GEODERMA.2013.09.023
8. Agariga, F., Abugre, S., & Appiah, M. (2021). Spatio-temporal changes in land use and forest cover in the Asutifi North District of Ahafo Region of Ghana, (1986–2020). Environmental Challenges, 5, 100209. https://doi.org/10.1016/J.ENVC.2021.100209
9. Ahmadalipour, A., Moradkhani, H., & Demirel, M. C. (2017). A comparative assessment of projected meteorological and hydrological droughts: Elucidating the role of temperature. Journal of Hydrology, 553, 785–797. https://doi.org/10.1016/J.JHYDROL.2017.08.047
10. Ahmed, A., & Czimber, K. (2025). Spatiotemporal dynamics of vegetation cover and drought conditions in West Darfur, Sudan: Implications of climate variability and

future projections. Geo: Geography and Environment, 12(2). https://doi.org/10.1002/GEO2.70016

11. Ahmed, A., Rotich, B., & Czimber, K. (2024). Assessment of the environmental impacts of conflict-driven Internally Displaced Persons: A sentinel-2 satellite based analysis of land use/ cover changes in the Kas locality, Darfur, Sudan. PLoS ONE, 19(5 May). https://doi.org/10.1371/journal.pone.0304034
12. Ahmed, A., Rotich, B., & Czimber, K. (2025). Climate Change as a Double-Edged Sword: Exploring the Potential of Environmental Recovery to Foster Stability in Darfur, Sudan. Climate 2025, Vol. 13, Page 63, 13(3), 63. https://doi.org/10.3390/CLI13030063
13. Ahmed, A., Rotich, B., Kipkulei, H. K., Lameck, A. S., Gallai, B., & Czimber, K. (2025). Vegetation Dynamics and Climate Variability in Conflict Zones: A Case Study of Sortony Internally Displaced Camp, Darfur, Sudan. Land 2025, Vol. 14, Page 1680, 14(8), 1680. https://doi.org/10.3390/LAND14081680
14. Akasha, M. (2013). Darfur: A tragedy of climate change. Anchor Academic Publishing. https://books.google.com/books?hl=en&lr=&id=0P2mAgAAQBAJ&oi=fnd&pg=PA7&dq=Darfur+a+tragedy+of+climate+change&ots=uUQR4LGHhj&sig=YZhvzkbRsi6iCPTMde3HjqPaaTo. (Accessed 29 December 2024)
15. Almulhim, A. I., Alverio, G. N., Sharifi, A., Shaw, R., Huq, S., Mahmud, J., Ahmad, S., & Rimi Abubakar, I. (2024). Climate-induced migration in the Global South: an in depth analysis. Nature.ComAI Almulhim, GN Alverio, A Sharifi, R Shaw, S Huq, MJ Mahmud, S Ahmad, IR Abubakarnpj Climate Action, 2024•nature.Com, 3(1). https://doi.org/10.1038/s44168-024-00133-1
16. Annette, B. S. (2024). Environmental Changes in the Lake Chad Basin: A Case Study Analyzing Its Influence on Boko Haram's Violent Activities in Northern Nigeria. https://www.duo.uio.no/handle/10852/112879
17. Armenteras, D., Murcia, U., González, T. M., Barón, O. J., & Arias, J. E. (2019). Scenarios of land use and land cover change for NW Amazonia: Impact on forest intactness. Global Ecology and Conservation, 17, e00567. https://doi.org/10.1016/J.GECCO.2019.E00567
18. Arowolo, A. O., Deng, X., Olatunji, O. A., & Obayelu, A. E. (2018). Assessing changes in the value of ecosystem services in response to land-use/land-cover dynamics in Nigeria. Science of The Total Environment, 636, 597–609. https://doi.org/10.1016/J.SCITOTENV.2018.04.277
19. Aschonitis, V. G., Gaglio, M., Castaldelli, G., & Fano, E. A. (2016). Criticism on elasticity-sensitivity coefficient for assessing the robustness and sensitivity of ecosystem services values. Ecosystem Services, 20, 66–68. https://doi.org/10.1016/J.ECOSER.2016.07.004
20. Athanasopoulos, G., Gamakumara, P., Panagiotelis, A., Hyndman, R. J., & Affan, M. (2020). Hierarchical forecasting. Springer, 52, 689–719. https://doi.org/10.1007/978-3-030-31150-6_21
21. Attaalmannan. (2019). Traditional Tribal Conflicts in Darfur Reasons and Seasons. Journal of Education and Practice. https://doi.org/10.7176/JEP/10-32-11

22. Avtar, R., Kouser, A., Kumar, A., Singh, D., Misra, P., Gupta, A., Yunus, A. P., Kumar, P., Johnson, B. A., Dasgupta, R., Sahu, N., & Rimba, A. B. (2021). Remote Sensing for International Peace and Security: Its Role and Implications. Remote Sensing 2021, Vol. 13, Page 439, 13(3), 439. https://doi.org/10.3390/RS13030439
23. Bai, Z. G., Dent, D. L., Olsson, L., & Schaepman, M. E. (2008). Proxy global assessment of land degradation. Wiley Online Library, 24(3), 223–234. https://doi.org/10.1111/J.1475-2743.2008.00169.X
24. Baral, R., Jagadish, S. V. K., Hein, N., Lollato, R. P., Shanoyan, A., Giri, A. K., Kim, J., Kim, M., & Min, D. (2023). Exploring the impact of soil water variability and varietal diversity on alfalfa yield, nutritional quality, and farm profitability. Grassland Research, 2(4), 266–278. https://doi.org/10.1002/GLR2.12067
25. Barltrop, R. (2010). Darfur and the international community. https://www.torrossa.com/it/resources/an/5203590
26. Becker, W. R., Ló, T. B., Johann, J. A., & Mercante, E. (2021). Statistical features for land use and land cover classification in Google Earth Engine. Remote Sensing Applications: Society and Environment, 21(December 2020), 100459. https://doi.org/10.1016/j.rsase.2020.100459
27. Behrends, A. (2024). Lifeworlds in Crisis: Making Refugees in the Chad-Sudan Borderlands. https://doi.org/10.1093/OSO/9780197781333.001.0001
28. Benjaminsen, T. A. (2016). Does Climate Change Lead to Conflicts in the Sahel? 99–116. https://doi.org/10.1007/978-3-642-16014-1_4
29. Bingkun, L. U. O., Minnett, P. J., Szczodrak, M., Nalli, N. R., & Morris, V. R. (2020). Accuracy Assessment of MERRA-2 and ERA-Interim Sea Surface Temperature, Air Temperature, and Humidity Profiles over the Atlantic Ocean Using AEROSE Measurements. Journal of Climate, 33(16), 6889–6909. https://doi.org/10.1175/JCLI-D-19-0955.1
30. Birech, R. (2009). Giving reconciliation a chance in Sudan seeking an alternative response to the Darfur conflict. https://calhoun.nps.edu/bitstream/handle/10945/4387/09Dec_Birech.pdf?sequence=1
31. Brander, L. M., de Groot, R., Schägner, J. P., Guisado-Goñi, V., van 't Hoff, V., Solomonides, S., McVittie, A., Eppink, F., Sposato, M., Do, L., Ghermandi, A., Sinclair, M., & Thomas, R. (2024). Economic values for ecosystem services: A global synthesis and way forward. Ecosystem Services, 66, 101606. https://doi.org/10.1016/J.ECOSER.2024.101606
32. Brendan, B. (2008). Environmental degradation and conflict in Darfur: implications for peace and recovery | Humanitarian Practice Network. https://odihpn.org/publication/environmental-degradation-and-conflict-in-darfur-implications-for-peace-and-recovery/
33. Bríd, G. (2022). Internally displaced persons and international refugee law. 212. https://books.google.com/books/about/Internally_Displaced_Persons_and_Interna.html?id=st5eEAAAQBAJ
34. Bullock, E. L., Healey, S. P., Yang, Z., Oduor, P., Gorelick, N., Omondi, S., Ouko, E., & Cohen, W. B. (2021). Three Decades of Land Cover Change in East Africa. Land 2021, Vol. 10, Page 150, 10(2), 150. https://doi.org/10.3390/LAND10020150

35. Cabral, P., Feger, C., Levrel, H., Chambolle, M., & Basque, D. (2016). Assessing the impact of land-cover changes on ecosystem services: A first step toward integrative planning in Bordeaux, France. Ecosystem Services, 22, 318–327. https://doi.org/10.1016/J.ECOSER.2016.08.005
36. Cai, S., Zuo, D., Wang, H., Han, Y., Xu, Z., Wang, G., & Yang, H. (2024). Improvement of drought assessment capability based on optimal weighting methods and a new threshold classification scheme. Journal of Hydrology, 631, 130758. https://doi.org/10.1016/J.JHYDROL.2024.130758
37. Champ, P., Boyle, K., Brown, T., & Peterson, L. (2003). A primer on nonmarket valuation. https://doi.org/10.1007/978-94-007-7104-8.PDF
38. Congalton, R. G. (1991). A review of assessing the accuracy of classifications of remotely sensed data. Remote Sensing of Environment, 37(1), 35–46. https://doi.org/10.1016/0034-4257(91)90048-B
39. Congalton, R. G., & Green, K. (2019). Assessing the accuracy of remotely sensed data: principles and practices. In Assessing the Accuracy of Remotely Sensed Data. CRC Press. https://doi.org/10.1201/9780429052729/ASSESSING-ACCURACY-REMOTELY-SENSED-DATA-RUSSELL-CONGALTON-KASS-GREEN
40. Corbera, E., Roth, D., & Work, C. (2019). Climate change policies, natural resources and conflict: implications for development. Climate Policy, 19(sup1), S1–S7. https://doi.org/10.1080/14693062.2019.1639299
41. Costanza, R., D'Arge, R., De Groot, R., Farber, S., Grasso, M., Hannon, B., Limburg, K., Naeem, S., O'Neill, R. V., Paruelo, J., Raskin, R. G., Sutton, P., & Van Den Belt, M. (1997). The value of the world's ecosystem services and natural capital. Nature, 387(6630), 253–260. https://doi.org/10.1038/387253A0;KWRD=SCIENCE
42. Costanza, R., d'Arge, R., de Groot, R., Farber, S., Grasso, M., Hannon, B., Limburg, K., Naeem, S., O'Neill, R. V., Paruelo, J., Raskin, R. G., Sutton, P., & van den Belt, M. (1998). The value of the world# s ecosystem services and natural capital. Elibrary.RuR Costanza, R de Groot, S Farber, M Grasso, B Hannon, K Limburg, S Naeem, J ParueloEcological Economics, 1998•elibrary.Ru, 25(1), 3–15. https://doi.org/10.1016/S0921-8009(98)00020-2
43. Costanza, R., de Groot, R., Sutton, P., van der Ploeg, S., Anderson, S. J., Kubiszewski, I., Farber, S., & Turner, R. K. (2014). Changes in the global value of ecosystem services. Global Environmental Change, 26(1), 152–158. https://doi.org/10.1016/J.GLOENVCHA.2014.04.002
44. Dai, A. (2011). Characteristics and trends in various forms of the Palmer Drought Severity Index during 1900-2008. Journal of Geophysical Research Atmospheres, 116(12), 12115. https://doi.org/10.1029/2010JD015541;REQUESTEDJOURNAL:JOURNAL:21562202D;PAGE:STRING:ARTICLE/CHAPTER
45. Daoudy, M. (2021). Rethinking the Climate–Conflict Nexus: A Human–Environmental–Climate Security Approach. Global Environmental Politics, 21(3), 4–25. https://doi.org/10.1162/GLEP_A_00609
46. Darfur. (2024). Darfur. (2024). https://en.wikipedia.org/wiki/Darfur - Google Search. Accessend on 5-September-2025.

47. De Groot, R., Brander, L., & Solomonides, S. (2020). Update of global ecosystem service valuation database (ESVD). FSD report No 2020-06 Wageningen, The Netherlands (58 pp).
48. de Groot, R., Brander, L., van der Ploeg, S., Costanza, R., Bernard, F., Braat, L., Christie, M., Crossman, N., Ghermandi, A., Hein, L., Hussain, S., Kumar, P., McVittie, A., Portela, R., Rodriguez, L. C., ten Brink, P., & van Beukering, P. (2012). Global estimates of the value of ecosystems and their services in monetary units. Ecosystem Services, 1(1), 50–61. https://doi.org/10.1016/J.ECOSER.2012.07.005
49. de Jong, L., De Bruin, S., Knoop, J., & van Vliet, J. (2021). Understanding land-use change conflict: a systematic review of case studies. Journal of Land Use Science, 16(3), 223–239. https://doi.org/10.1080/1747423X.2021.1933226
50. Deng, Y., Wang, J., & Rubiao, M. (2013). Dynamic monitoring of vegetation coverage in Shangri-La County of Northwest Yunnan based on MODIS-NDVI. Ieeexplore.Ieee.OrgY Deng, J Wang, M Rubiao2013 21st International Conference on Geoinformatics, 2013•ieeexplore.Ieee.Org. https://ieeexplore.ieee.org/abstract/document/6626120/
51. Dewan, A. M., Yamaguchi, Y., & Rahman, M. Z. (2012). Dynamics of land use/cover changes and the analysis of landscape fragmentation in Dhaka Metropolitan, Bangladesh. GeoJournal, 77(3), 315–330. https://doi.org/10.1007/S10708-010-9399-X/FIGURES/5
52. Didan, K., Munoz, A., … R. S.-U. of A., & 2015, undefined. (2015). MODIS vegetation index user's guide (MOD13 series). Modis-Land.Gsfc.Nasa.GovK Didan, AB Munoz, R Solano, A HueteUniversity of Arizona: Vegetation Index and Phenology Lab, 2015•modis-Land.Gsfc.Nasa.Gov, 1–2. https://modis-land.gsfc.nasa.gov/pdf/MOD13_User_Guide_V61.pdf
53. Diffenbaugh, N., Swain, D., National, D. T.-P. of the, & 2015, undefined. (2015). Anthropogenic warming has increased drought risk in California. Pnas.OrgNS Diffenbaugh, DL Swain, D ToumaProceedings of the National Academy of Sciences, 2015•pnas.Org, 112(13), 3931–3936. https://doi.org/10.1073/pnas.1422385112
54. Dinku, T., Funk, C., Peterson, P., Maidment, R., Tadesse, T., Gadain, H., & Ceccato, P. (2018). Validation of the CHIRPS satellite rainfall estimates over eastern Africa. Quarterly Journal of the Royal Meteorological Society, 144, 292–312. https://doi.org/10.1002/QJ.3244
55. Dirie, K., Maamor, S., & Alam, M. M. (2024). Impacts of climate change in post-conflict Somalia: Is the 2030 Agenda for SDGs endangered? World Development Perspectives, 35, 100598. https://doi.org/10.1016/J.WDP.2024.100598
56. Drusch, M., Del Bello, U., Carlier, S., Colin, O., Fernandez, V., Gascon, F., Hoersch, B., Isola, C., Laberinti, P., Martimort, P., Meygret, A., Spoto, F., Sy, O., Marchese, F., & Bargellini, P. (2012). Sentinel-2: ESA's Optical High-Resolution Mission for GMES Operational Services. Remote Sensing of Environment, 120, 25–36. https://doi.org/10.1016/J.RSE.2011.11.026
57. Duan, H., Xue, X., Wang, T., Kang, W., Liao, J., & Liu, S. (2021). Spatial and Temporal Differences in Alpine Meadow, Alpine Steppe and All Vegetation of the

Qinghai-Tibetan Plateau and Their Responses to Climate Change. Remote Sensing 2021, Vol. 13, Page 669, 13(4), 669. https://doi.org/10.3390/RS13040669

58. Ejaz, N., Bahrawi, J., Alghamdi, K. M., Rahman, K. U., & Shang, S. (2023). Drought Monitoring Using Landsat Derived Indices and Google Earth Engine Platform: A Case Study from Al-Lith Watershed, Kingdom of Saudi Arabia. Remote Sensing 2023, Vol. 15, Page 984, 15(4), 984. https://doi.org/10.3390/RS15040984

59. Elamin, E. M. (2018). Assessment of Sustainable Production of Stable Food Crops in Southern Darfur State, Sudan. Current Investigations in Agriculture and Current Research, 5(3). https://doi.org/10.32474/CIACR.2018.05.000211

60. Elhag, M., & Walker, S. (2009). Impact of climate variability on vegetative cover in the Butana area of Sudan. African Journal of Ecology, 47(SUPPL. 1), 11–16. https://doi.org/10.1111/J.1365-2028.2008.01044.X

61. Eltahir, M. E. S., Fadl, K. E. M., Hamad, M. A. A., Safi, A. I. A., Elamin, H. M. A., Abutaba, Y. I. M., Musa, F. I., Mahmoud, T. E., Alemeu, A., Abdelrhman, H. A., Adlan, O. E., Tutu, S. O., Mohammed, M. H., Gumaa, Y. O. A., Khalifa, A. S. O., Hamad, A. E., Faragallah, S. A. D. A., Hassan, M. O., Ismaeil, M., … Kheiry, M. A. (2023). Tapping tools for gum Arabic and resins production: A review paper. American Journal of Engineering and Technology Management, 8(3), 33–40. https://doi.org/10.11648/j.ajetm.20230803.12

62. FAO. (2015). FAO, 2015. Global Forest Resources Assessment 2015, Rome, Italy. - Google Search. https://www.google.com/search?q=FAO%2C+2015.+Global+Forest+Resources+Assessment+2015%2C+Rome%2C+Italy.&sca_esv=b65bf429607cdb9a&rlz=1C1GCEA_enHU1096HU1096&sxsrf=AE3TifPcche8VfS3YC1zkSwK9Fw_z7t9SA%3A1755891405502&ei=zcaoaJaxHvKKi-gP-K22uQs&ved=0ahUKEwjWy_SblZ-PAxVyxQIHHfiWLbcQ4dUDCBA&uact=5&oq=FAO%2C+2015.+Global+Forest+Resources+Assessment+2015%2C+Rome%2C+Italy.&gs_lp=Egxnd3Mtd2l6LXNlcnAiQEZBTywgMjAxNS4gR2xvYmFsIEZvcmVzdCBSZXNvdXJjZXMgQXNzZXNzbWVudCAyMDE1LCBSb21lLCBJdGFseS4yBBAjGCdI6wZQAFgAcAB4AJABAJgB5gGgAeYBqgEDMi0xuAEDyAEA-AEC-AEBmAIBoALvAZgDAJIHAzItMaAHuwmyBwMyLTG4B-8BwgcDMi0xyAcF&sclient=gws-wiz-serp

63. FAO. (2023). The impact of disasters on agriculture and food security 2023. The Impact of Disasters on Agriculture and Food Security 2023. https://doi.org/10.4060/CC7900EN

64. Fensholt, R., Langanke, T., Rasmussen, K., Reenberg, A., Prince, S. D., Tucker, C., Scholes, R. J., Le, Q. B., Bondeau, A., Eastman, R., Epstein, H., Gaughan, A. E., Hellden, U., Mbow, C., Olsson, L., Paruelo, J., Schweitzer, C., Seaquist, J., & Wessels, K. (2012). Greenness in semi-arid areas across the globe 1981–2007 — an Earth Observing Satellite based analysis of trends and drivers. Remote Sensing of Environment, 121, 144–158. https://doi.org/10.1016/J.RSE.2012.01.017

65. Fisher, B., & Kerry Turner, R. (2008). Ecosystem services: Classification for valuation. Biological Conservation, 141(5), 1167–1169. https://doi.org/10.1016/J.BIOCON.2008.02.019

66. Foerstel. (2010). Crisis in Darfur. Books.Google.Com. https://books.google.com/books?hl=en&lr=&id=iY_OAwAAQBAJ&oi=fnd&pg=PA143&dq=+Foerstel,+K.+(2008).+Crisis+in+Darfur.&ots=eCiFFjD6sR&sig=RsZWM5Lx_O-s69dm5JDZOXtlg88
67. Fu, R., Chen, R., Wang, C., Chen, X., Gu, H., Wang, C., Xu, B., Liu, G., & Yin, G. (2022). Generating High-Resolution and Long-Term SPEI Dataset over Southwest China through Downscaling EEAD Product by Machine Learning. Remote Sensing 2022, Vol. 14, Page 1662, 14(7), 1662. https://doi.org/10.3390/RS14071662
68. Funk, C., Peterson, P., Landsfeld, M., Pedreros, D., Verdin, J., Shukla, S., Husak, G., Rowland, J., Harrison, L., Hoell, A., & Michaelsen, J. (2015). The climate hazards infrared precipitation with stations - A new environmental record for monitoring extremes. Scientific Data, 2. https://doi.org/10.1038/SDATA.2015.66
69. Füssel, M. H. (2009). An updated assessment of the risks from climate change based on research published since the IPCC Fourth Assessment Report. Springer, 97(3), 469–482. https://doi.org/10.1007/s10584-009-9648-5
70. Gaglio, M., Aschonitis, V. G., Mancuso, M. M., Puig, J. P. R., Moscoso, F., Castaldelli, G., & Fano, E. A. (2017). Changes in land use and ecosystem services in tropical forest areas: a case study in Andes mountains of Ecuador. International Journal of Biodiversity Science, Ecosystem Services & Management, 13(1), 264–279. https://doi.org/10.1080/21513732.2017.1345980
71. Gashaw, T., Tulu, T., Argaw, M., Worqlul, A. W., Tolessa, T., & Kindu, M. (2018). Estimating the impacts of land use/land cover changes on Ecosystem Service Values: The case of the Andassa watershed in the Upper Blue Nile basin of Ethiopia. Ecosystem Services, 31, 219–228. https://doi.org/10.1016/J.ECOSER.2018.05.001
72. Gbanie, S. P., Griffin, A. L., & Thornton, A. (2018). Impacts on the Urban Environment: Land Cover Change Trajectories and Landscape Fragmentation in Post-War Western Area, Sierra Leone. Remote Sensing 2018, Vol. 10, Page 129, 10(1), 129. https://doi.org/10.3390/RS10010129
73. Gebrechorkos, S. H., Hülsmann, S., & Bernhofer, C. (2020). Analysis of climate variability and droughts in East Africa using high-resolution climate data products. Global and Planetary Change, 186, 103130. https://doi.org/10.1016/J.GLOPLACHA.2020.103130
74. Giriraj, A., Irfan-Ullah, M., Murthy, M. S. R., & Beierkuhnlein, C. (2008). Modelling Spatial and Temporal Forest Cover Change Patterns (1973-2020): A Case Study from South Western Ghats (India). Sensors 2008, Vol. 8, Pages 6132-6153, 8(10), 6132–6153. https://doi.org/10.3390/S8106132
75. Gorelick, D. E., Lin, L., Zeff, H. B., Kim, Y., Vose, J. M., Coulston, J. W., Wear, D. N., Band, L. E., Reed, P. M., & Characklis, G. W. (2020). Accounting for Adaptive Water Supply Management When Quantifying Climate and Land Cover Change Vulnerability. Water Resources Research, 56(1), e2019WR025614. https://doi.org/10.1029/2019WR025614
76. Gorsevski, V., Kasischke, E., Dempewolf, J., Loboda, T., & Grossmann, F. (2012). Analysis of the Impacts of armed conflict on the Eastern Afromontane forest region on

the South Sudan - Uganda border using multitemporal Landsat imagery. Remote Sensing of Environment, 118, 10–20. https://doi.org/10.1016/j.rse.2011.10.023
77. Gurrapu, S., Chipanshi, A., … D. S.-P. of the 28th, & 2014, undefined. (2014). Comparison of the SPI and SPEI on predicting drought conditions and streamflow in the Canadian prairies. Academia.EduS Gurrapu, A Chipanshi, D Sauchyn, A HowardProceedings of the 28th Conference on Hydrology, 2014•academia.Edu. https://www.academia.edu/download/80351004/Howard_AMS_2014_Conference_Extended_20Abstract.pdf
78. HAC. (2017). Household biogas digester for slums, IDPs and refugees camps: case study of Kass South Darfur, Sudan. 9th ICAT, 234.
79. Hagan, J., & Kaiser, J. (2011). The displaced and dispossessed of Darfur: Explaining the sources of a continuing state-led genocide. British Journal of Sociology, 62(1), 1–25. https://doi.org/10.1111/J.1468-4446.2011.01357.X
80. Hagenlocher, Lang, S., & Tiede, D. (2012). Integrated assessment of the environmental impact of an IDP camp in Sudan based on very high resolution multi-temporal satellite imagery. ElsevierM Hagenlocher, S Lang, D TiedeRemote Sensing of Environment, 2012•Elsevier. https://www.sciencedirect.com/science/article/pii/S0034425712003227?casa_token=dsf_nnuYcqEAAAAA:_JS5YkAWkc3vfDrvY04UGEww4EqhjAapIBWj3G46EE6LI8LDtQcaHNfEYc24rqo5WSBIR8Rms-s
81. Hamadalnel, M., Zhu, Z., Lu, R., Almazroui, M., & Shahid, S. (2022). Evaluating the aptitude of global climate models from CMIP5 and CMIP6 in capturing the historical observations of monsoon rainfall over Sudan from 1946 to 2005. International Journal of Climatology, 42(5), 2717–2738. https://doi.org/10.1002/JOC.7387
82. Hardt, J., & Brief, J. S. (2019). Environmental peacebuilding and climate change: peace and conflict studies at the edge of transformation. Toda.OrgJN Hardt, J ScheffranPolicy Brief, 2019•toda.Org. https://www.toda.org/assets/files/resources/policy-briefs/t-pb-68_hardt-and-scheffran_environmental-peacebuilding-and-climate-change.pdf
83. Hartemink, A. E., Krasilnikov, P., & Bockheim, J. G. (2013). Soil maps of the world. Geoderma, 207–208(1), 256–267. https://doi.org/10.1016/J.GEODERMA.2013.05.003
84. Hassan, M. O., Salih, A. A., Eltahir, M. E. S., & Musa, F. I. (2021). Gum Arabic value chain and the share of stakeholders under the applied free- trade policy , Sudan. Asian Journal of Research and Review in Agriculture, 3(May), 85–96.
85. Hassani, H., & Yeganegi, M. R. (2020). Selecting optimal lag order in Ljung–Box test. Physica A: Statistical Mechanics and Its Applications, 541, 123700. https://doi.org/10.1016/J.PHYSA.2019.123700
86. He, B., Chang, J., Wang, Y., Wang, Y., Zhou, S., & Chen, C. (2021). Spatio-temporal evolution and non-stationary characteristics of meteorological drought in inland arid areas. Ecological Indicators, 126. https://doi.org/10.1016/j.ecolind.2021.107644
87. Herrmann, S. M., Anyamba, A., & Tucker, C. J. (2005). Recent trends in vegetation dynamics in the African Sahel and their relationship to climate. Global Environmental Change, 15(4), 394–404. https://doi.org/10.1016/J.GLOENVCHA.2005.08.004

88. Huang, Q., Jin, G., Xiong, X., Ye, H., & Xie, Y. (2023). Monitoring Urban Change in Conflict from the Perspective of Optical and SAR Satellites: The Case of Mariupol, a City in the Conflict between RUS and UKR. Remote Sensing 2023, Vol. 15, Page 3096, 15(12), 3096. https://doi.org/10.3390/RS15123096
89. Ifeanyichukwu, N. E., Mshelbara Asabe, H., James, O. C., Ugonna, I. A., & Chima, O. A. (2022). Quality Assessment of the Water Sources in the IDP Camps a Case Study of IDP Camp in Borno Nigeria. Researchgate.Net, 11(4), 55–71. https://doi.org/10.9734/jenrr/2022/v11i430287
90. IPCC. (2023). Integration of climate change adaptation in land use planning. https://climate-adapt.eea.europa.eu/en/metadata/adaptation-options/adaptation-of-integrated-land-use-planning
91. Islam, M. R. (2006). The sudanese Darfur crisis and internally displaced persons in international law: The least protection for the most vulnerable. International Journal of Refugee Law, 18(2), 354–385. https://doi.org/10.1093/IJRL/EEL012
92. Jude, M. D. (2009). Environmental Degradation, a Threat to Environmental Security, Peace and Sustainable Development in Africa: A Case Study of Darfur. SSRN Electronic Journal. https://doi.org/10.2139/SSRN.1464052
93. Jung, M. (2016). LecoS — A python plugin for automated landscape ecology analysis. Ecological Informatics, 31, 18–21. https://doi.org/10.1016/J.ECOINF.2015.11.006
94. Kamta, F. N., Schilling, J., & Scheffran, J. (2020). Insecurity, Resource Scarcity, and Migration to Camps of Internally Displaced Persons in Northeast Nigeria. Sustainability 2020, Vol. 12, Page 6830, 12(17), 6830. https://doi.org/10.3390/SU12176830
95. Kamusoko, C., Wada, Y., Furuya, T., Tomimura, S., Nasu, M., & Homsysavath, K. (2013). Simulating Future Forest Cover Changes in Pakxeng District, Lao People's Democratic Republic (PDR): Implications for Sustainable Forest Management. Land 2013, Vol. 2, Pages 1-19, 2(1), 1–19. https://doi.org/10.3390/LAND2010001
96. Kaplan, G., Rashid, T., Gasparovic, M., Pietrelli, A., & Ferrara, V. (2022). Monitoring war-generated environmental security using remote sensing: A review. Wiley Online Library, 33(10), 1513–1526. https://doi.org/10.1002/LDR.4249
97. Karahalil, U., Kadiogullari, A., … E. B.-A. J. of, & 2009, undefined. (2009). The spatiotemporal forest cover changes in Köprülü Canyon National Park (1965-2008) in Turkey. Ajol.InfoU Karahalil, A Kadiogullari, E Bagkent, S KöseAfrican Journal of Biotechnology, 2009•ajol.Info, 8(18), 4495–4507. https://www.ajol.info/index.php/ajb/article/view/62406/50377
98. Karongo, J., Mwaniki, J., Ndiritu, J., Reports, V. M.-S., & 2025, undefined. (2024). Sorghum yield prediction based on remote sensing and machine learning in conflict affected South Sudan. Nature.Com. https://doi.org/10.1038/s41598-025-89030-z
99. Karra, K., Kontgis, C., Statman-Weil, Z., Mazzariello, J. C., Mathis, M., & Brumby, S. P. (2021). GLOBAL LAND USE/LAND COVER WITH SENTINEL 2 AND DEEP LEARNING. International Geoscience and Remote Sensing Symposium (IGARSS), 2021-July, 4704–4707. https://doi.org/10.1109/IGARSS47720.2021.9553499

100. Kashim, I., & Kashim, R. (2020). An assessment of environmental awareness of internally displaced people in the north east of Nigeria. European Journal of Public Health, 30(Supplement_5). https://doi.org/10.1093/EURPUB/CKAA166.113
101. Khan, M. (2015). The Hidden puppeteer: environmental degradation and the Darfur conflict. JSTORM KhanHarvard International Review, 2015•JSTOR. https://www.jstor.org/stable/43649307
102. Kikstra, J. S., Nicholls, Z. R. J., Smith, C. J., Lewis, J., Lamboll, R. D., Byers, E., Sandstad, M., Meinshausen, M., Gidden, M. J., Rogelj, J., Kriegler, E., Peters, G. P., Fuglestvedt, J. S., Skeie, R. B., Samset, B. H., Wienpahl, L., Van Vuuren, D. P., Van Der Wijst, K. I., Al Khourdajie, A., … Riahi, K. (2022). The IPCC Sixth Assessment Report WGIII climate assessment of mitigation pathways: from emissions to global temperatures. Geoscientific Model Development, 15(24), 9075–9109. https://doi.org/10.5194/GMD-15-9075-2022
103. Kindu, M., Schneider, T., Teketay, D., & Knoke, T. (2013). Land Use/Land Cover Change Analysis Using Object-Based Classification Approach in Munessa-Shashemene Landscape of the Ethiopian Highlands. Remote Sensing 2013, Vol. 5, Pages 2411-2435, 5(5), 2411–2435. https://doi.org/10.3390/RS5052411
104. Kindu, M., Schneider, T., Teketay, D., & Knoke, T. (2016). Changes of ecosystem service values in response to land use/land cover dynamics in Munessa-Shashemene landscape of the Ethiopian highlands. Science of the Total Environment, 547, 137–147. https://doi.org/10.1016/j.scitotenv.2015.12.127
105. Kipkulei, H., Rotich, B., Ahmed, A., Lameck, A., Burudi, J., Hounkpati, K., Makindi, S., Boitt, M. K., Sieber, S., & Kindu, M. (2025). Land use/land cover dynamics in an arid and semi-arid landscape: A 24-year analysis of Baringo County, Kenya (2000–2024). Global and Earth Surface Processes Change, 4, 100006. https://doi.org/10.1016/J.GESPCH.2025.100006
106. Knoth, C., Slimani, S., Appel, M., Geography, E. P.-A., & 2018, undefined. (2018). Combining automatic and manual image analysis in a web-mapping application for collaborative conflict damage assessment. Elsevier. https://www.sciencedirect.com/science/article/pii/S014362281730783X
107. Kocaaslan, S., Musaoglu, N., & Karamzadeh, S. (2021). Evaluating Drought Events by Time-Frequency Analysis: A Case Study in Aegean Region of Turkey. IEEE Access, 9, 125032–125041. https://doi.org/10.1109/ACCESS.2021.3110816
108. Kopytsia, Y. M. (2024). The Russian War Against Ukraine: a Case Study in Climate, Conflict, and Green Recovery. Проблеми Законності, 284(Special), 226–248.
109. Kranz, O., Sachs, A., & Lang, S. (2015). Assessment of environmental changes induced by internally displaced person (IDP) camps in the Darfur region, Sudan, based on multitemporal MODIS data. International Journal of Remote Sensing, 36(1), 190–210. https://doi.org/10.1080/01431161.2014.999386
110. Kreuter, U. P., Harris, H. G., Matlock, M. D., & Lacey, R. E. (2001). Change in ecosystem service values in the San Antonio area, Texas. Ecological Economics, 39(3), 333–346. https://doi.org/10.1016/S0921-8009(01)00250-6

111. Kumar, S., Radhakrishnan, N., & Mathew, S. (2014). Land use change modelling using a Markov model and remote sensing. Geomatics, Natural Hazards and Risk, 5(2), 145–156. https://doi.org/10.1080/19475705.2013.795502

112. Kyrpychova, I., Berezenko, K., Bordiuhova, O., Skakovskyi, S., Sopova, N., Chupryna, Y., Liubytskyi, S., Komarysta, B., Bendiuh, V., & Nosyriev, O. (2024). IDENTIFYING THE RISKS OF ARMED CONFLICT IMPACT ON THE ECOSYSTEM. Search.Ebscohost.ComI Kyrpychova, K Berezenko, O Bordiuhova, S Skakovskyi, N Sopova, Y ChuprynaEastern-European Journal of Enterprise Technologies, 2024•search.Ebscohost.Com, 1(10(127)), 6–14. https://doi.org/10.15587/1729-4061.2024.298430

113. Lambin, E. F., & Meyfroidt, P. (2011). Global land use change, economic globalization, and the looming land scarcity. Proceedings of the National Academy of Sciences, 108(9), 3465–3472. https://doi.org/10.1073/PNAS.1100480108

114. Lang, S., Tiede, D., Hölbling, D., Füreder, P., & Zeil, P. (2010). Earth observation (EO)-based ex post assessment of internally displaced person (IDP) camp evolution and population dynamics in Zam Zam, Darfur. International Journal of Remote Sensing, 31(21), 5709–5731. https://doi.org/10.1080/01431161.2010.496803

115. Lawler, J. J., Lewis, D. J., Nelson, E., Plantinga, A. J., Polasky, S., Withey, J. C., Helmers, D. P., Martinuzzi, S., Penningtonh, D., & Radeloff, V. C. (2014). Projected land-use change impacts on ecosystem services in the United States. Proceedings of the National Academy of Sciences of the United States of America, 111(20), 7492–7497. https://doi.org/10.1073/PNAS.1405557111/SUPPL_FILE/PNAS.1405557111.SD01.XLSX

116. Levin, N., Ali, S., & Crandall, D. (2018). Utilizing remote sensing and big data to quantify conflict intensity: The Arab Spring as a case study. Applied Geography, 94, 1–17. https://doi.org/10.1016/J.APGEOG.2018.03.001

117. Liu, Z., Chen, Y., & Chen, C. (2023). Analysis of the Spatiotemporal Characteristics and Influencing Factors of the NDVI Based on the GEE Cloud Platform and Landsat Images. Remote Sensing, 15(20). https://doi.org/10.3390/rs15204980

118. Macauley, T. (2016). Climate and Crisis: Environmental Degradation and Humanitarian Disaster in Darfur. Master's Thesis. https://research.library.fordham.edu/environ_2015/25/

119. MacDicken, K. G. (2015). Global Forest Resources Assessment 2015: What, why and how? Forest Ecology and Management, 352, 3–8. https://doi.org/10.1016/J.FORECO.2015.02.006

120. Macpherson, B., Broddle, M., Mcneil, C., Jason Barnett -Booz, A., Hamilton, A., Mikovitz, C., & Zhang, T. (2021). Introduction to the Prediction Of Worldwide Energy Resources (POWER) Project: NASA Applied Sciences Week 2021. Ntrs.Nasa.Gov. https://ntrs.nasa.gov/api/citations/20210019346/downloads/NASAPOWERProject-2021AppliedSceincesWeek.pdf

121. Malakar, K. Das, Kumar, M., Anand, S., & Kuzur, G. (2023). Climate Change and Socio-Ecological Transformation. https://doi.org/10.1007/978-981-99-4390-6

122. Mbaye, A. (2020). Climate change, livelihoods, and conflict in the Sahel. HeinOnlineAA MbayeGeo. J. Int'l Aff., 2020•HeinOnline, 21, 12–20. https://doi.org/10.1353/GIA.2020.0020
123. Mendoza-González, G., Martínez, M. L., Lithgow, D., Pérez-Maqueo, O., & Simonin, P. (2012). Land use change and its effects on the value of ecosystem services along the coast of the Gulf of Mexico. Ecological Economics, 82, 23–32. https://doi.org/10.1016/J.ECOLECON.2012.07.018
124. Mengist, W., Soromessa, T., & Feyisa, G. L. (2021). Monitoring Afromontane forest cover loss and the associated socio-ecological drivers in Kaffa biosphere reserve, Ethiopia. Trees, Forests and People, 6, 100161. https://doi.org/10.1016/J.TFP.2021.100161
125. Mengist, W., Soromessa, T., & Feyisa, G. L. (2022). Estimating the total ecosystem services value of Eastern Afromontane Biodiversity Hotspots in response to landscape dynamics. Environmental and Sustainability Indicators, 14, 100178. https://doi.org/10.1016/J.INDIC.2022.100178
126. Mengist, W., Soromessa, T., & Legese, G. (2020). Ecosystem services research in mountainous regions: A systematic literature review on current knowledge and research gaps. Science of The Total Environment, 702, 134581. https://doi.org/10.1016/J.SCITOTENV.2019.134581
127. Mermut, A. R., & Eswaran, H. (2001). Some major developments in soil science since the mid-1960s. Geoderma, 100(3–4), 403–426. https://doi.org/10.1016/S0016-7061(01)00030-1
128. Mohamed, M. A., Anders, J., & Schneider, C. (2020). Monitoring of Changes in Land Use / Land Cover in Imagery and GIS.
129. Mohmed. (2013). Darfur: A Tragedy of Climate Change - Mohamed Osman Akasha - Google Books. https://books.google.hu/books?hl=en&lr=&id=0P2mAgAAQBAJ&oi=fnd&pg=PA7&dq=Political+instability+and+climate+change+in+Darfur&ots=uUQR4FDFij&sig=fG9dTipfYDpFIysnrhVidUvoor0&redir_esc=y#v=onepage&q&f=false
130. Molikevych, R., Professor, A., & Roman S Molikevych, P. D. (2023). ANALYSIS OF THE CONSEQUENCES OF MILITARY OPERATIONS: INTEGRATION OF SPECTRAL INDICES AND REMOTE SENSING TO ASSESS. Researchgate.NetPDRS MolikevychInternational Multidisciplinary Scientific GeoConference: SGEM, 2023•researchgate.Net, 23(2.1), 277–282. https://doi.org/10.5593/SGEM2023/2.1/S10.35
131. Montgomery, D. (2017). Growing a revolution: bringing our soil back to life. https://books.google.com/books?hl=en&lr=&id=0R5DDQAAQBAJ&oi=fnd&pg=PT4&dq=(Montgomery,+2017).+soil&ots=hlLJNDHUVW&sig=hW2vnQ7sOUGlINQdu-9nJiyoSbk
132. Moyo, M. M., & Blake, R. (2024). PASTORALIST CONFLICT IN ETHIOPIA FROM 2015 TO 2022: CLIMATE CHANGE AND FOOD INSECURITY AS EXACERBATING FACTORS A mini-dissertation submitted in partial fulfilment of the requirement for the degree MASTER OF ARTS IN SECURITY STUDIES In the

Department of Political Sciences, Faculty of Humanities at the UNIVERSITY OF PRETORIA.

133. Munsi, M., Areendran, G., & Joshi, P. K. (2012). Modeling spatio-temporal change patterns of forest cover: A case study from the Himalayan foothills (India). Regional Environmental Change, 12(3), 619–632. https://doi.org/10.1007/S10113-011-0272-3/FIGURES/5

134. Mwabumba, M., Yadav, B. K., Rwiza, M. J., Larbi, I., & Twisa, S. (2022). Analysis of land use and land-cover pattern to monitor dynamics of Ngorongoro world heritage site (Tanzania) using hybrid cellular automata-Markov model. Current Research in Environmental Sustainability, 4, 100126. https://doi.org/10.1016/J.CRSUST.2022.100126

135. Naghizadeh, M. H. (2025). What we Don't see: Uncovering intercommunal violence through remote sensing. Political Geography, 116, 103259. https://doi.org/10.1016/J.POLGEO.2024.103259

136. Nicholson, S. E., Acs, F., Bordi, I., & Wang, D.-Y. (2013). The West African Sahel: A review of recent studies on the rainfall regime and its interannual variability. Wiley Online Library, 2013, 1–32. https://doi.org/10.1155/2013/453521

137. Nweke, A. C. (2021). Transition From Fragility to Sustainable Development : Case Study of Darfur in Sudan Walden University. 34.

138. Nzabarinda, V., Bao, A., Xu, W., Uwamahoro, S., Jiang, L., Duan, Y., Nahayo, L., Yu, T., Wang, T., & Long, G. (2021). Assessment and Evaluation of the Response of Vegetation Dynamics to Climate Variability in Africa. Sustainability 2021, Vol. 13, Page 1234, 13(3), 1234. https://doi.org/10.3390/SU13031234

139. OCHA. (2023). Sudan OCHA: The Sudan Humanitarian Fund. https://www.unocha.org/sudan

140. OCHA. (2024). Sudan Humanitarian Update (29 July 2024) [EN/AR] | OCHA. https://www.unocha.org/publications/report/sudan/sudan-humanitarian-update-29-july-2024

141. Ogbue, S., Omiunu, F., and, C. O.-A. J. of P., & 2024, undefined. (2024). Internally Displaced Persons and Human Security in North-East Nigeria. Ajol.Info. https://www.ajol.info/index.php/ajpas/article/view/284410

142. Okpara, U. T., Stringer, L. C., & Dougill, A. J. (2018). Integrating climate adaptation, water governance and conflict management policies in lake riparian zones: Insights from African drylands. Environmental Science & Policy, 79, 36–44. https://doi.org/10.1016/J.ENVSCI.2017.10.002

143. Olaf, K., Gunter, Z., Dirk, T., Stephen, C., Denis, B., Thomas, K., Stefan, L., & Mathidlde, C. (2016). Monitoring Refugee IDP Camps to Support International Relief Action.

144. Olumba, E. E., Nwosu, B. U., Okpaleke, F. N., & Okoli, R. C. (2022). Conceptualising eco-violence: moving beyond the multiple labelling of water and agricultural resource conflicts in the Sahel. Third World Quarterly, 43(9), 2075–2090. https://doi.org/10.1080/01436597.2022.2083601;WEBSITE:WEBSITE:TFOPB;PAGEGROUP:STRING:PUBLICATION

145. Omer, S., & Abdoun, M. (2020). Incentives for Reforestation and Forest's Plantations Option, under the National Strategy of REDD+Program in Sudan (Vol. 5).
146. Osman, M., Abdel-Rahman, E., Onono, J. O., Olaka, L. A., Elhag, M. M., Adan, M., & Tonnang, H. E. Z. (2023). Mapping, intensities and future prediction of land use/land cover dynamics using google earth engine and CA- artificial neural network model. PLoS ONE, 18(7 JULY). https://doi.org/10.1371/journal.pone.0288694
147. Osman, M. A. A., Onono, J. O., Olaka, L. A., Elhag, M. M., & Abdel-Rahman, E. M. (2021). Climate Variability and Change Affect Crops Yield under Rainfed Conditions: A Case Study in Gedaref State, Sudan. Agronomy 2021, Vol. 11, Page 1680, 11(9), 1680. https://doi.org/10.3390/AGRONOMY11091680
148. Pal, M., Maxwell, A. E., & Warner, T. A. (2013). Kernel-based extreme learning machine for remote-sensing image classification. Remote Sensing Letters, 4(9), 853–862. https://doi.org/10.1080/2150704X.2013.805279
149. Peters, L. E. R. (2021). Beyond disaster vulnerabilities: An empirical investigation of the causal pathways linking conflict to disaster risks. International Journal of Disaster Risk Reduction, 55, 102092. https://doi.org/10.1016/J.IJDRR.2021.102092
150. Pham-Duc, B., Nguyen, H., & Nguyen-Quoc, H. (2024). Unveiling the research landscape of planetscope data in addressing earth-environmental issues: a bibliometric analysis. Earth Science Informatics 2024 18:1, 18(1), 52-. https://doi.org/10.1007/S12145-024-01497-Y
151. Polasky, S., Nelson, E., Pennington, D., & Johnson, K. A. (2011). The impact of land-use change on ecosystem services, biodiversity and returns to landowners: A case study in the state of Minnesota. Environmental and Resource Economics, 48(2), 219–242. https://doi.org/10.1007/S10640-010-9407-0/METRICS
152. Pushkarenko, Y., & Zaslavskyi, V. (2024). Research on the state of areas in Ukraine affected by military actions based on remote sensing data and deep learning architectures. Radioelectronic and Computer Systems, 2024(2), 5–18. https://doi.org/10.32620/reks.2024.2.01
153. Qiao, Y., Ji, D., Shang, H., Xu, J., Xu, R., & Shi, C. (2023). The Fusion of ERA5 and MERRA-2 Atmospheric Temperature Profiles with Enhanced Spatial Resolution and Accuracy. Remote Sensing 2023, Vol. 15, Page 3592, 15(14), 3592. https://doi.org/10.3390/RS15143592
154. Quintas-Soriano, C., Castro, A. J., Castro, H., & García-Llorente, M. (2016). Impacts of land use change on ecosystem services and implications for human well-being in Spanish drylands. Land Use Policy, 54, 534–548. https://doi.org/10.1016/J.LANDUSEPOL.2016.03.011
155. Racek, D., Thurner, P. W., Davidson, B. I., Zhu, X. X., & Kauermann, G. (2024). Conflict forecasting using remote sensing data: An application to the Syrian civil war. International Journal of Forecasting, 40(1), 373–391. https://doi.org/10.1016/J.IJFORECAST.2023.04.001
156. Reddy, C. S., Jha, C. S., & Dadhwal, V. K. (2013). Assessment and monitoring of long-term forest cover changes in Odisha, India using remote sensing and GIS. Environmental Monitoring and Assessment, 185(5), 4399–4415. https://doi.org/10.1007/S10661-012-2877-5/TABLES/8

157. Reddy, C. S., Singh, S., Dadhwal, V. K., Jha, C. S., Rao, N. R., & Diwakar, P. G. (2017). Predictive modelling of the spatial pattern of past and future forest cover changes in India. Journal of Earth System Science, 126(1), 1–16. https://doi.org/10.1007/S12040-016-0786-7/TABLES/8
158. Reij, C., Pasiecznik, N., Mahamoudou, S., Kassa, H., Winterbottom, R., & Livingstone, J. (2020). Dryland restoration successes in the Sahel and Greater Horn of Africa show how to increase scale and impact. https://hdl.handle.net/10568/111706
159. Rome, G. T. (2007). Manual on deforestation, degradation, and fragmentation using remote sensing and GIS. Openknowledge.Fao.OrgG TejaswiMAR-SFM Working Paper. ROME, ITALY, 2007•openknowledge.Fao.Org. https://openknowledge.fao.org/bitstreams/946c965e-b340-4632-a440-42a697284a04/download
160. Rotich, B., & Ojwang, D. (2021). Trends and drivers of forest cover change in the Cherangany hills forest ecosystem, western Kenya. Global Ecology and Conservation, 30(August), e01755. https://doi.org/10.1016/j.gecco.2021.e01755
161. Rudolf de Groot. (2020). Ecosystem Services Valuation Database (ESVD) Update of global ecosystem service valuation data Final report (June 2020) - Google Search. https://www.google.com/search?q=Ecosystem+Services+Valuation+Database+(ESVD)+Update+of+global+ecosystem+service+valuation+data+Final+report+(June+2020)&rlz=1C1GCEA_enHU1096HU1096&oq=Ecosystem+Services+Valuation+Database+(ESVD)++Update+of+global+ecosystem+service+valuation+data+Final+report+(June+2020)&gs_lcrp=EgZjaHJvbWUyBggAEEUYOTIHCAEQIRiPAtIBCDEzNDNqMGo3qAIAsAIA&sourceid=chrome&ie=UTF-8
162. Sachs, J. D. (2007). Poverty and environmental stress fuel Darfur crisis [1]. Nature, 449(7158), 24. https://doi.org/10.1038/449024A;KWRD=SCIENCE
163. Sakieh, Y., & Salmanmahiny, A. (2016). Performance assessment of geospatial simulation models of land-use change—a landscape metric-based approach. Environmental Monitoring and Assessment, 188(3), 1–16. https://doi.org/10.1007/S10661-016-5179-5/FIGURES/5
164. Sakr, S. (2023). Climate Change and Darfur: A Holistic Security Approach. Capstone and Graduation Projects. https://fount.aucegypt.edu/capstone/174
165. Salih, A. A., Hussein, M. B., & Bashir, O. (2017). Assessment the Food Security Situation of IDP ' s at Nyala Adjacent Camps. 2(1), 1–10. https://doi.org/10.13140/RG.2.2.21867.69926
166. Samah, W. T. (2022). THE JUBA PEACE AGREEMENT AND THE PROTECTION OF DISPLACED PERSONS: Between Regional Migratory Routes and IDP Camps. African Conflict and Peacebuilding Review, 12(2), 106–132. https://doi.org/10.2979/AFRICONFPEACREVI.12.2.07
167. Schimmel, N. (2022). TRAPPED BY SOVEREIGNTY: The Fate of Internally Displaced Persons and Their Lack of Equal Human Rights Protection under International Law. World Affairs, 185(3), 500–529. https://doi.org/10.1177/00438200221104498;WEBSITE:WEBSITE:SAGE;WGROUP:STRING:PUBLICATION

168. Schwarz, M., Landmann, T., Jusselme, D., Zambrano, E., Danzeglocke, J., Siegert, F., & Franke, J. (2022). Assessing the Environmental Suitability for Transhumance in Support of Conflict Prevention in the Sahel. Remote Sensing 2022, Vol. 14, Page 1109, 14(5), 1109. https://doi.org/10.3390/RS14051109
169. Sharma, R., Rimal, B., Baral, H., Nehren, U., Paudyal, K., Sharma, S., Rijal, S., Ranpal, S., Acharya, R. P., Alenazy, A. A., & Kandel, P. (2019). Impact of Land Cover Change on Ecosystem Services in a Tropical Forested Landscape. Resources 2019, Vol. 8, Page 18, 8(1), 18. https://doi.org/10.3390/RESOURCES8010018
170. Siam, M. S., Demory, M. E., & Eltahir, E. A. B. (2013). Hydrological Cycles over the Congo and Upper Blue Nile Basins: Evaluation of General Circulation Model Simulations and Reanalysis Products. Journal of Climate, 26(22), 8881–8894. https://doi.org/10.1175/JCLI-D-12-00404.1
171. Simangan, D. (2024). Post-growth peacebuilding. Review of International Studies, 50(5), 877–887. https://doi.org/10.1017/S026021052400007X
172. Solomon, N., Birhane, E., Gordon, C., Haile, M., Taheri, F., Azadi, H., & Scheffran, J. (2018). Environmental impacts and causes of conflict in the Horn of Africa: A review. Earth-Science Reviews, 177, 284–290. https://doi.org/10.1016/J.EARSCIREV.2017.11.016
173. Solomon, S., Qin, D., Manning, M., Chen, Z., Marquis, M., Averyt, K. B., Tignor, M., & Miller, H. L. (2007). IPCC fourth assessment report (AR4). Lrl.Mn.Gov. https://www.lrl.mn.gov/docs/2015/other/150681/PFEISref_2/Solomon%20et%20al.%202007.pdf
174. Stackhouse, P., Macpherson, B., … B. H.-2023 A. A., & 2023, undefined. (2023). Using Time Series Data Products to Support ASHRAE's Historic and Future Climate Data Needs through NASA's POWER Web Services. Ntrs.Nasa.Gov. https://ntrs.nasa.gov/citations/20230008796
175. Styers, D. M., Chappelka, A. H., Marzen, L. J., & Somers, G. L. (2010). Developing a land-cover classification to select indicators of forest ecosystem health in a rapidly urbanizing landscape. Landscape and Urban Planning, 94(3–4), 158–165. https://doi.org/10.1016/J.LANDURBPLAN.2009.09.006
176. Suarez, A., Árias-Arévalo, P. A., & Martínez-Mera, E. (2018). Environmental sustainability in post-conflict countries: insights for rural Colombia. Environment, Development and Sustainability, 20(3), 997–1015. https://doi.org/10.1007/S10668-017-9925-9/TABLES/6
177. Tadese, S., Soromessa, T., & Bekele, T. (2021). Analysis of the Current and Future Prediction of Land Use/Land Cover Change Using Remote Sensing and the CA-Markov Model in Majang Forest Biosphere Reserves of Gambella, Southwestern Ethiopia. The Scientific World Journal, 2021(1), 6685045. https://doi.org/10.1155/2021/6685045
178. Thornton, P. K., Jones, P. G., Owiyo, T., Kruska, R. L., Herrero, M., Kristjanson, P. M., Notenbaert, A. M. O., Bekele, N., & Omolo, A. (2006). Mapping climate vulnerability and poverty in Africa. International Livestock Research Institute. https://hdl.handle.net/10568/2307

179. Tolessa, T., Gessese, H., Tolera, M., & Kidane, M. (2018). Changes in Ecosystem Service Values in Response to Changes in Landscape Composition in the Central Highlands of Ethiopia. Environmental Processes, 5(3), 483–501. https://doi.org/10.1007/S40710-018-0326-3/TABLES/10
180. UNEP. (2008). Environmental degradation and conflict in Darfur implications for.
181. UNEP. (2017). New report - Environmental Governance in Sudan – an Expert Review. https://www.unep.org/news-and-stories/story/new-report-environmental-governance-sudan-expert-review
182. USCRI. (2025). SUDAN-SITUATION-UPDATE-APRIL-2025 - United State Committees for Refugees and Immigrants. https://www.google.com/search?q=SUDAN-SITUATION-UPDATE-APRIL-2025&rlz=1C1GCEA_enHU1096HU1096&oq=SUDAN-SITUATION-UPDATE-APRIL-2025&gs_lcrp=EgZjaHJvbWUyBggAEEUYOTIKCAEQABiABBiiBDIHCAIQABjvBTIKCAMQABiABBiiBDIHCAQQABjvBTIKCAUQABiABBiiBDIGCAYQRRg80gEIMjg1OWowajeoAgCwAgA&sourceid=chrome&ie=UTF-8
183. Vehnämäki, M. (2006). Darfur Scorched: looming genocide in Western Sudan1. Journal of Genocide Research, 8(1), 51–82. https://doi.org/10.1080/14623520600552868
184. Venter, Z. S., Barton, D. N., Chakraborty, T., Simensen, T., & Singh, G. (2022). Global 10 m Land Use Land Cover Datasets: A Comparison of Dynamic World, World Cover and Esri Land Cover. Remote Sensing, 14(16), 4101. https://doi.org/10.3390/RS14164101/S1
185. Verbesselt, J., Hyndman, R., Zeileis, A., & Culvenor, D. (2010). Phenological change detection while accounting for abrupt and gradual trends in satellite image time series. Remote Sensing of Environment, 114(12), 2970–2980. https://doi.org/10.1016/J.RSE.2010.08.003
186. Vicente-Serrano, S. M., Beguería, S., & López-Moreno, J. I. (2010). A multiscalar drought index sensitive to global warming: The standardized precipitation evapotranspiration index. Journal of Climate, 23(7), 1696–1718. https://doi.org/10.1175/2009JCLI2909.1
187. Wadsworth, R. A., & Lebbie, A. R. (2019). What Happened to the Forests of Sierra Leone? Land 2019, Vol. 8, Page 80, 8(5), 80. https://doi.org/10.3390/LAND8050080
188. Wahelo, T. T., Mengistu, D. A., & Merawi, T. M. (2024). Spatiotemporal trends and drivers of forest cover change in Metekel Zone forest areas, Northwest Ethiopia. Environmental Monitoring and Assessment, 196(12), 1170. https://doi.org/10.1007/s10661-024-13294-7
189. Wang, J., Liu, X., Li, Y., Powell, T., Wang, X., Wang, G., & Zhang, P. (2019). Microplastics as contaminants in the soil environment: A mini-review. Science of The Total Environment, 691, 848–857. https://doi.org/10.1016/J.SCITOTENV.2019.07.209
190. Wang, Zhang, M. ;, Wang, C. ;, Wang, K. ;, Li, Y. ;, Bai, X. ;, Zhou, Y., Yu, K., Wang, H., Zhang, M., Wang, C., Wang, K., Wang, C., Li, Y., Bai, X., & Zhou, Y. (2022). Spatial and Temporal Changes of Landscape Patterns and Their Effects on Ecosystem

Services in the Huaihe River Basin, China. Land 2022, Vol. 11, Page 513, 11(4), 513. https://doi.org/10.3390/LAND11040513
191. Xie, G., Zhang, C., Zhen, L., & Zhang, L. (2017). Dynamic changes in the value of China's ecosystem services. Ecosystem Services, 26, 146–154. https://doi.org/10.1016/J.ECOSER.2017.06.010
192. Xie, X., Hao, M., Ding, F., Scheffran, J., … T. I.-E., & 2024, undefined. (2024). The impacts of climate change on violent conflict risk: a review of causal pathways. Iopscience.Iop.OrgX Xie, M Hao, F Ding, J Scheffran, T Ide, JF Maystadt, Y Qian, Q Wang, S Chen, J Wu, K SunEnvironmental Research Communications, 2024•iopscience.Iop.Org, 6(11). https://doi.org/10.1088/2515-7620/ad8a21
193. Xu, X., Chen, F., Wang, B., Harrison, M. T., Chen, Y., Liu, K., Zhang, C., Zhang, M., Zhang, X., Feng, P., & Hu, K. (2024). Unleashing the power of machine learning and remote sensing for robust seasonal drought monitoring: A stacking ensemble approach. Journal of Hydrology, 634, 131102. https://doi.org/10.1016/J.JHYDROL.2024.131102
194. Yagub. (2019). Divergent Views of Internal Displacement Person on Developmental Options in North Darfur State, Sudan. Researchgate.NetAIA YagubJ Soc Sci, 2019•researchgate.Net. https://www.researchgate.net/profile/Daniel-Kipo-Sunyehzi/publication/335205744_Street-level_Bureaucrats'_Coping_Strategies_and_How_They_Affect_Public_Service_Delivery_in_Ghana/links/609081a092851c490fb51b8f/Street-level-Bureaucrats-Coping-Strategies-and-How-They-Affect-Public-Service-Delivery-in-Ghana.pdf?_sg%5B0%5D=started_experiment_milestone&origin=journalDetail&_rtd=e30%3D
195. Yakubu, U., Res, M. S.-Int. J. Glob. Oper., & 2022, undefined. (2022). Time series model analysis using autocorrelation function (ACF) and partial autocorrelation function (PACF) for E-wallet transactions during a pandemic. Pdfs.Semanticscholar.Org, 3(3), 80–85. https://pdfs.semanticscholar.org/eabe/2448dd294388ace1717bd0ca45051c1acfe6.pdf
196. Yengoh, G. T., Dent, D., Olsson, L., Tengberg, A. E., & Tucker, C. J. (2015). Applications of NDVI for Land Degradation Assessment. 17–25. https://doi.org/10.1007/978-3-319-24112-8_3
197. Young, H., & Ismail, M. A. (2019). Complexity, continuity and change: livelihood resilience in the Darfur region of Sudan. Disasters, 43(Suppl 3), S318. https://doi.org/10.1111/DISA.12337
198. Younis, A. Y. I., Jonathan, B. N., Togun, A. O., Yasin, E. H. E., Omer, S. O., Hamad, G. E. A. I., & Aïssata, S. D. (2022). Assessment of land use and land cover change on Gum Talha (Acacia seyal var. seyal) forest in Bahar Alarab, Sudan. Biodiversitas, 23(9), 4549–4560. https://doi.org/10.13057/biodiv/d230922
199. Yousif, L. A., Khatir, A. A., El-Hag, F. M., Abdelkarim, A. M., Adam, H. S., Wahab, A. A., Kurosaki, Y., & Ali-Babiker, I. A. (2018). Rainfall variability and its implications for agricultural production in Gedarif State, Eastern Sudan. African Journal of Agricultural Research, 13(31), 1577–1590. https://doi.org/10.5897/AJAR2018.13365

200. Yuan, K., Li, F., Yang, H., & Wang, Y. (2019). The Influence of Land Use Change on Ecosystem Service Value in Shangzhou District. International Journal of Environmental Research and Public Health 2019, Vol. 16, Page 1321, 16(8), 1321. https://doi.org/10.3390/IJERPH16081321

201. Yue, W., Qin, C., Su, M., Teng, Y., & Xu, C. (2024). Simulation and prediction of land use change in Dongguan of China based on ANN cellular automata - Markov chain model. Environmental and Sustainability Indicators, 22, 100355. https://doi.org/10.1016/J.INDIC.2024.100355

202. Yvonne, M., Ouma, G., Olago, D., Geography, M. O.-, Environment, undefined, & 2020, undefined. (2020). Trends in climate variables (temperature and rainfall) and local perceptions of climate change in Lamu, Kenya. Ges.Rgo.RuM Yvonne, G Ouma, D Olago, M OpondoGeography, Environment, Sustainability, 2020•ges.Rgo.Ru, 13(3), 102–109. https://doi.org/10.24057/2071-9388-2020-24

203. Zambrano-Bigiarini, M., Nauditt, A., Birkel, C., Verbist, K., & Ribbe, L. (2017). Temporal and spatial evaluation of satellite-based rainfall estimates across the complex topographical and climatic gradients of Chile. Hydrology and Earth System Sciences, 21(2), 1295–1320. https://doi.org/10.5194/HESS-21-1295-2017

204. Zeng, Y., Hao, D., Huete, A., Dechant, B., Berry, J., Chen, J., Joiner, J., Frankenberg, C., Bond-Lamberty, B., Ryu, Y., Xiao, J., Asrar, G. R., & Chen, M. (2022). Optical vegetation indices for monitoring terrestrial ecosystems globally. Nature.ComY Zeng, D Hao, A Huete, B Dechant, J Berry, JM Chen, J Joiner, C FrankenbergNature Reviews Earth & Environment, 2022•nature.Com. https://www.nature.com/articles/s43017-022-00298-5

205. Zilio, M. I., Bohn, V. Y., Cintia Piccolo, M., & Perillo, G. M. E. (2022). Land cover changes and ecosystem services at the Negro River Basin, Argentina: what is missing for better assessing nature's contribution? International Journal of River Basin Management, 20(2), 265–278. https://doi.org/10.1080/15715124.2021.1901727

206. Zwijnenburg, W., & Ballinger, O. (2023). Leveraging emerging technologies to enable environmental monitoring and accountability in conflict zones. Cambridge.Org. https://www.cambridge.org/core/journals/international-review-of-the-red-cross/article/leveraging-emerging-technologies-to-enable-environmental-monitoring-and-accountability-in-conflict-zones/048F61CD42B7C21931B37C091FC2C95F.

9. Annexes

Annex 1. Multi-Sensor Remote Sensing Framework

This conceptual diagram illustrates the complementary use of MODIS, Sentinel-2, and PlanetScope datasets in monitoring land use and vegetation transitions in complex environments. The MODIS NDVI/EVI time-series enables the detection of broad regional patterns and long-term greening or browning trends. Sentinel-2 provides decadal changes in vegetation density and land cover composition owing to its medium-resolution multispectral data. PlanetScope imagery, with high spatial resolution, is critical for assessing micro-level changes in urban encroachment, IDP settlements, and fragmented ecosystems.

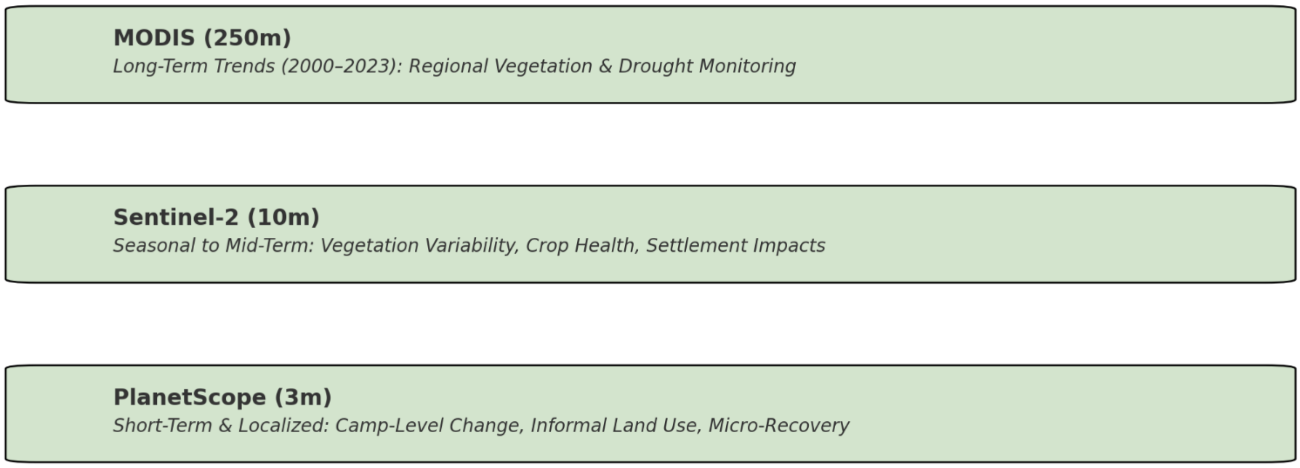

Multi-Sensor Remote Sensing Framework for Vegetation Monitoring. An integrated framework combining MODIS (250m), Sentinel-2 (10m), and PlanetScope (3m) for effective monitoring of vegetation dynamics across spatial and temporal scales. This fusion allows for long-term trend analysis, fine-scale LULC mapping, and ecological change detection in post-conflict and climate-sensitive landscapes.

Annex 2. Problem Tree

This figure presents a theory of change framework outlining the root causes and cascading effects of environmental degradation in the conflict-affected areas of Darfur. It identifies conflict, unregulated resource use, and climate variability as the primary drivers, leading to vegetation loss, declining livelihoods, and increased resource-based tensions. The diagram supports the justification for a system-based approach to environmental recovery and peacebuilding.

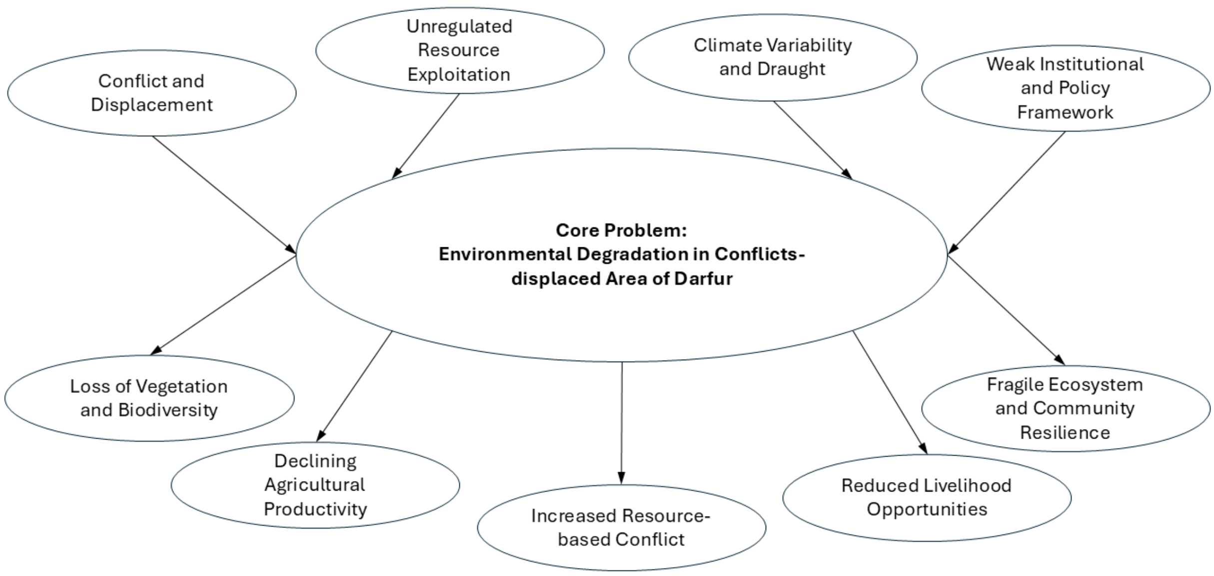

Problem Tree / Theory of Change Diagram

Annex 3. Pathways from Environmental Recovery to Sustainable Peacebuilding

This conceptual model outlines how targeted environmental interventions, such as sustainable land management and community-led adaptation strategies, can promote ecosystem recovery, enhance community resilience, and foster conditions conducive to sustainable peace in post-conflict Darfur.

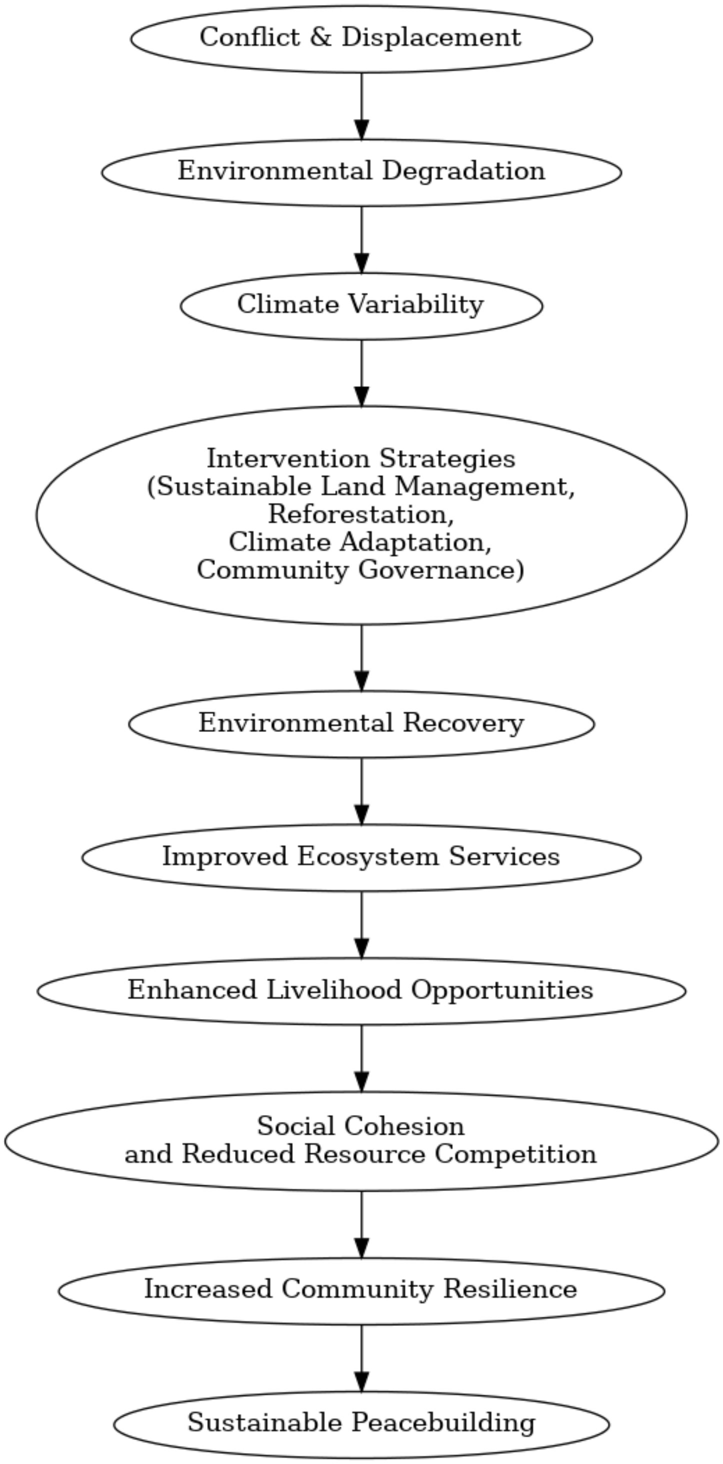

Annex 4. Conceptual framework

Conceptual framework mind map, visually representing the interaction between conflict, displacement, environmental pressure, and the dual role of climate in driving both degradation and recovery. Key components include:

- Conflict and IDPs as starting points of environmental stress
- Land abandonment and climate variability as potential drivers of regeneration
- Remote sensing tools facilitating monitoring and policy formulation
- Environmental stabilization feeding into peacebuilding opportunities
- sustainable peace in post-crisis settings.

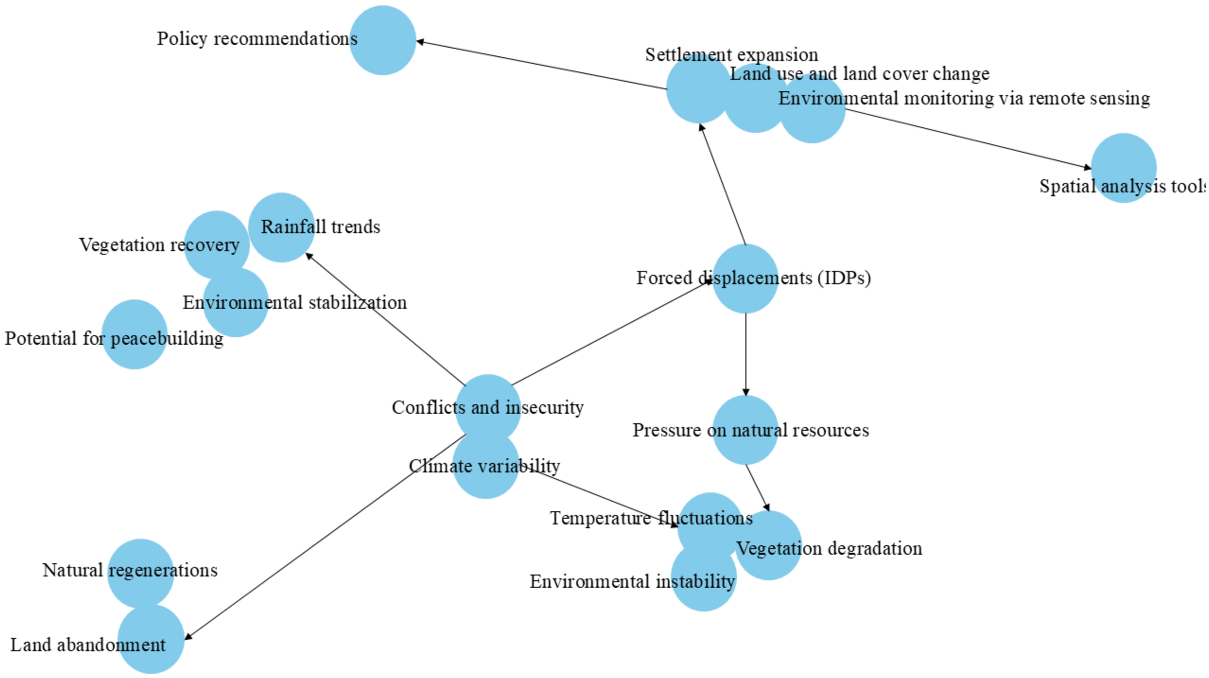

Conceptual framework mind map

Annex 5. Dynamics of Conflict

This flowchart illustrates the cascading effects of conflict and political marginalization leading to mass displacement, overexploitation of natural resources, environmental degradation, and feedback mechanisms that reinforce socio-ecological vulnerability.

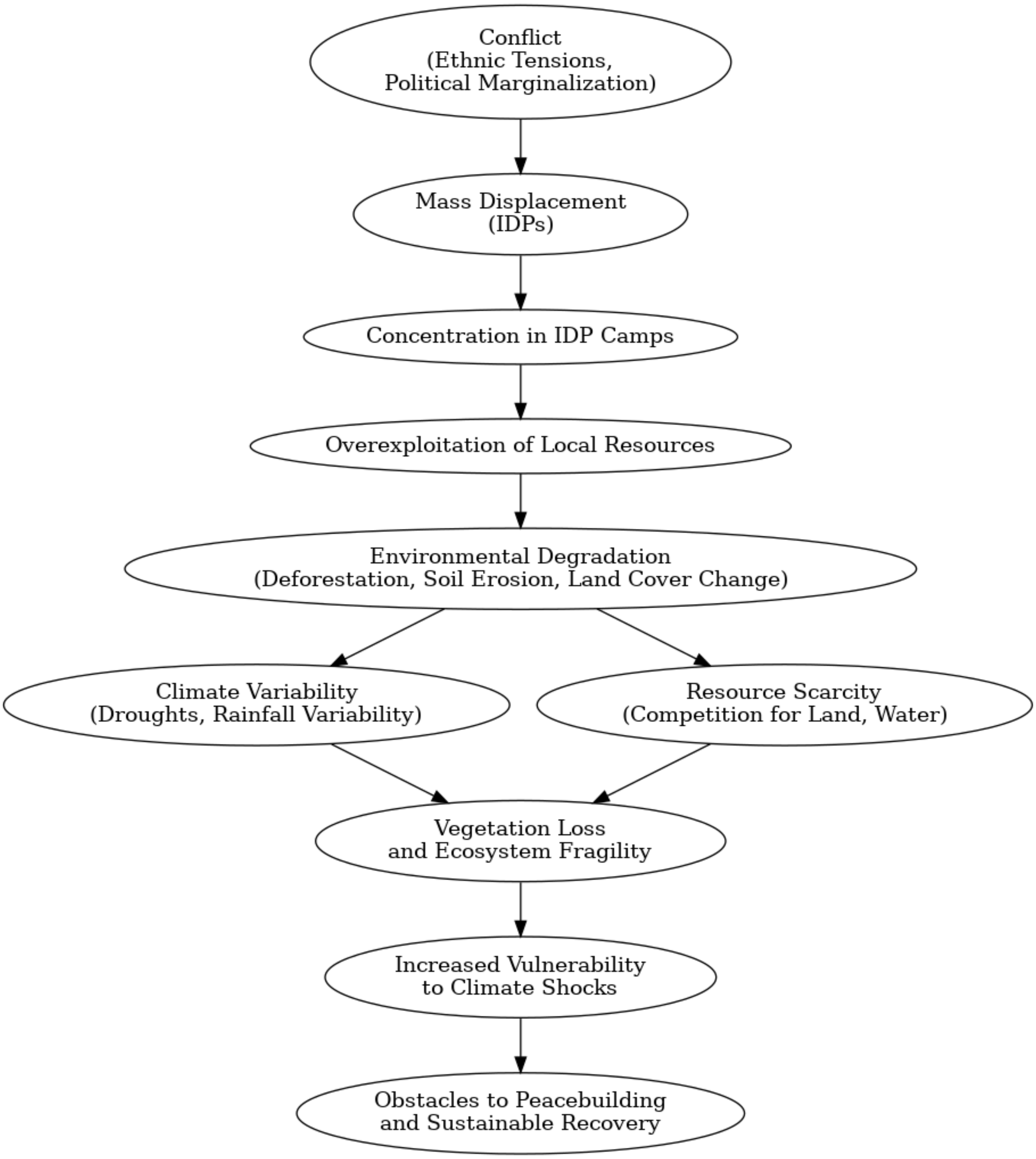

Dynamics of Conflict, Displacement, and Environmental Degradation in Darfur, Sudan.

Annex 6. Policy-Action Framework

This framework illustrates the interlinkages between conflict, climate variability, land degradation, strategic policy responses, and targeted resilience outcomes. It emphasizes integrated approaches for mitigating ecological risks and fostering recovery through community participation, sustainable practices, and institutional support.

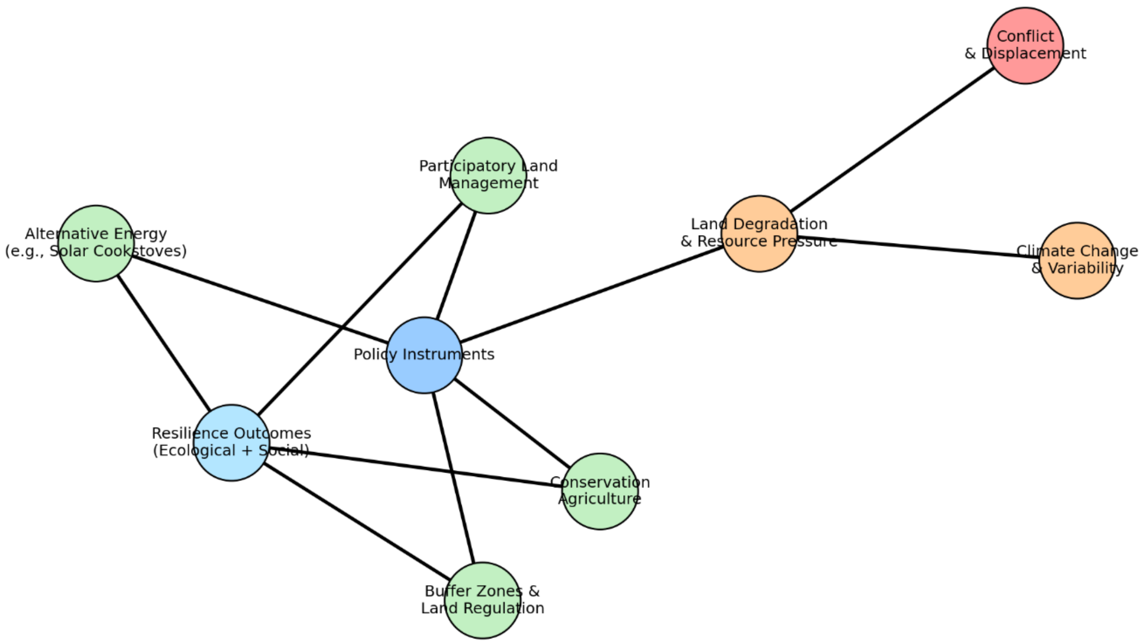

Policy-Action Framework for Enhancing Environmental Resilience in Conflict-Affected Regions.

Annex 7. Updated ESV coefficients (US$ ha^{-1} $year^{-1}$)

As referenced by (De Groot et al., 2020) the respective biomes were also considered for the identified LULC types (Table 25).

Updated ESV coefficients (US$ ha^{-1} $year^{-1}$) for the seven LULC types (De Groot et al., 2020).

ES group	ES	Forestland	Shrubland	Grassland	Cropland	Water features
Provisioning	Food	602	8		510	2,288
	Water	47,869		313	604	9,198
	Raw material	11,739	1	637	6	92
	Genetic resources	16				
	Medicinal resources	3	1			
	Ornamental resources					
Regulating	Air quality regulation	309	7	8	10	
	Climate regulation	658	89	73	10	251
	Moderation of extreme	108			993	18

	events					
	Regulation of water flows	442	71	43	17	4,221
	Waste treatment	12			40	50,760
	Erosion prevention	604			173	
	Maintenance of soil fertility	42			34	6,189
	Pollination	877			1,498	
	Biological control	14			621	142
Habitat	Maintenance of life cycles of migratory species	19				803
	Maintenance of genetic diversity	7				17,987
Cultural	Aesthetic information		38		395	2,276
	Opportunities for recreation and tourism	52,789	124	92	3,101	13,633
	Inspiration for culture, art, and design	5	214	284	16	310
	Spiritual experience					76
	Information for cognitive development		214	147		116
	Existence and bequest values	2,960	2			
	Total	**119,075**	**769**	**1,597**	**8,028**	**108,360**

Annex 8. Summary of accuracy assement table (West Sarfur 2000 – 2024)

Class	2000		
	User Accuray (%)	Producer Acuracy (%)	Overall Accuracy (%)
Forest Class	97.20	59.48	82.83
Non-Forest Class	80.99	99.56	
2005			
	User Accuray (%)	Producer Acuracy (%)	Overall Accuracy (%)
Forest Class	94.43	50.36	81.17
Non-Forest Class	59.94	99.35	
2010			
	User Accuray (%)	Producer Acuracy (%)	Overall Accuracy (%)
Forest Class	99.88	40.29	82.46
Non-Forest Class	81.08	99.98	
2015			
	User Accuray (%)	Producer Acuracy (%)	Overall Accuracy (%)
Forest Class	99.02	60.06	87.85
Non-Forest Class	86.81	100	
2020			
	User Accuray (%)	Producer Acuracy (%)	Overall Accuracy (%)
Forest Class	96.95	67.35	92.17
Non-Forest Class	91.28	99.38	
2024			
	User Accuray (%)	Producer Acuracy (%)	Overall Accuracy (%)
Forest Class	98.73	53.80	90.75
Non-Forest Class	89.79	99.83	